

LA-4193-MS

DOC-14 REPORT COLLECTION  
REPRODUCTION  
COPY

C-3

LOS ALAMOS SCIENTIFIC LABORATORY  
of the  
University of California  
LOS ALAMOS • NEW MEXICO

Quarterly Status Report on the  
Advanced Plutonium Fuels Program  
January 1 to March 31, 1969

LOS ALAMOS NATIONAL LABORATORY



3 9338 00368 8297

UNITED STATES  
ATOMIC ENERGY COMMISSION  
CONTRACT W-7405-ENG. 36

## LEGAL NOTICE

This report was prepared as an account of Government sponsored work. Neither the United States, nor the Commission, nor any person acting on behalf of the Commission,

A. Makes any warranty or representation, expressed or implied, with respect to the accuracy, completeness, or usefulness of the information contained in this report, or that the use of any information, apparatus, method, or process disclosed in this report may not infringe privately owned rights; or

B. Assumes any liabilities with respect to the use of, or for damages resulting from the use of any information, apparatus, method, or process disclosed in this report.

As used in the above, "person acting on behalf of the Commission" includes any employee or contractor of the Commission, or employee of such contractor, to the extent that such employee or contractor of the Commission, or employee of such contractor prepares, disseminates, or provides access to, any information pursuant to his employment or contract with the Commission, or his employment with such contractor.

This LA-MS report presents the status of the LASL Advanced Plutonium Fuels Program. Previous Quarterly Status Reports in this series, all unclassified, are:

LA-3607-MS

LA-3745-MS

LA-3933-MS

LA-3650-MS

LA-3760-MS

LA-3993-MS

LA-3686-MS

LA-3820-MS

LA-4073-MS

LA-3708-MS

LA-3880-MS

LA-4114-MS

This report, like other special-purpose documents in the LA-MS series, has not been reviewed or verified for accuracy in the interest of prompt distribution.

Advanced Reactor Technology (ART) Series.

Distributed: June 17, 1969

LA-4193-MS  
SPECIAL DISTRIBUTION

**LOS ALAMOS SCIENTIFIC LABORATORY**  
**of the**  
**University of California**  
LOS ALAMOS • NEW MEXICO

Quarterly Status Report on the  
**Advanced Plutonium Fuels Program**  
January 1 to March 31, 1969



LOS ALAMOS NATL LAB LIBS.  
3 9338 00368 8297

## FOREWORD

This is the eleventh quarterly report on the Advanced Plutonium Fuels Program conducted at the Los Alamos Scientific Laboratory. The work is centered around problem areas associated with LMFBR development, though some of it has a broader applicability to general reactor technology.

Most of the investigations discussed here are of the continuing type. Results and conclusions described may therefore be changed or augmented as the work continues. Published reference to results cited in this report should not be made without obtaining explicit permission to do so from the person in charge of the work.

TABLE OF CONTENTS

<u>PROJECT</u>	<u>PAGE</u>	
401	EXAMINATION OF FAST REACTOR FUELS	
	I. Introduction	5
	II. Hot Cell Equipment Development	5
	III. Hot Cell Applications of Methods of Analysis	7
	IV. Examination of Unirradiated Fuels	8
	V. Requests from DRDT	10
	VI. LMFBR/FFTF Mixed Oxide Analytical Studies	11
	VII. Publications	14
	VIII. References	14
462	SODIUM TECHNOLOGY	
	I. Introduction	15
	II. Materials Compatibility	15
	III. Study of Purification Methods for Nonradioactive Impurities	17
	IV. Fission Products in Sodium Systems	22
	V. On-Line Monitoring Methods	23
	VI. Sampling and Analysis - Laboratory Methods	28
	VII. Cover Gas and Maintenance Atmospheres	31
	References	32
463	CERAMIC PLUTONIUM FUEL MATERIALS	
	I. Introduction	33
	II. Synthesis and Fabrication	33
	III. Properties	35
	IV. Analytical Chemistry	41
	V. References	41
464	STUDIES OF Na-BONDED (U,Pu)C AND (U,Pu)N LMFBR FUELS	
	I. Introduction	43
	II. Synthesis and Fabrication of (U,Pu)C Pellets	43
	III. Loading Facility for Test Capsules	45
	IV. Carbide Fuel Compatibility Studies	45
	V. EBR-II Irradiation Testing	51
	VI. Gamma Scanning and Related Studies	55
	VII. Sodium-Bond Heat Transfer Studies	56
	VIII. Analytical Chemistry	57
	IX. References	58
466	FAST REACTOR METALLIC FUEL STUDIES	
	I. Introduction	59
	II. Fuel Preparation and Fabrication	59
	III. Metal Fuel Compatibility Testing	62
	IV. Irradiation Effects Studies	62
	V. Analytical Chemistry	63

TABLE OF CONTENTS  
(continued)

<u>PROJECT</u>		<u>PAGE</u>
465	REACTOR PHYSICS	
	I. Introduction	65
	II. Cross-Section Procurement, Evaluation and Testing	65
	III. Reactor Analysis Methods and Concept Evaluatlons	67
	References	70
471	OTHER ADVANCED SYSTEMS - RESEARCH AND DEVELOPMENT	
	I. Pulsed Reactor Neutronics	71
	II. <sup>3</sup> He Activation	73
	References	75
	SPECIAL DISTRIBUTION	76

## PROJECT 401

### EXAMINATION OF FAST REACTOR FUELS

Person in Charge: R. D. Baker  
Principal Investigators: J. W. Schulte  
J. A. Leary  
C. F. Metz

---

#### I. INTRODUCTION

This project is directed toward the examination and comparison of the effects of neutron irradiation on LMFBR Program fuel materials. Irradiated materials are examined as requested by the Fuels and Materials Branch of DRD & T.

Another phase of this project is the development of an analytical chemistry program designed to assure the high-quality well-characterized fuel required by the LMFBR/FFTF Program. In close cooperation with PNL, an analytical program has been developed which has the following objectives:

1. To evaluate the present capabilities of potential fuel producers for making the analytical measurements on FFTF fuel that are necessary to assure the uniformly high quality fuel required by the LMFBR/FFTF Program.
2. To provide technical guidance to fuel producers, as may be required, to assure these capabilities are established at the level required by FFTF reactor fuel specifications.
3. To establish and conduct a monitoring program that will assure continuing technical competence of fuel producers for the analysis of FFTF fuel at the level required by fuel specifications.

#### II. HOT CELL EQUIPMENT DEVELOPMENT

Argon Purification Systems  
(C. E. Court, R. F. Velkinburg)

The new Ar recirculation-purification unit, which was received in November, has undergone satisfactory proof testing. A few minor modifications are required in the unit, and plans for installing the unit in the basement are nearly completed. Designs for that portion of the system which goes inside the cell shielding are not complete. This system will provide inert gas for the two grinding-polishing boxes and the blister which houses the metallograph.

Extensive testing was carried out on the Ar unit which provides inert gas for the disassembly cell. It appears that massive in-leakage of air, as would occur with a large hole in the manipulator booting, tends to poison the oxygen absorbents in the purification system. However, since the manufacturer says this massive in-leakage should not cause such an effect, at present there is no explanation for the low rate of O<sub>2</sub> removal. Discussions with the manufacturer indicate that the absorbent should be replaced and further tests conducted.

A H<sub>2</sub>-He blender to provide more efficient and economical operation of the regenerant system was designed and installed.

#### Radiography Equipment and Methods

(M. E. Lazarus, C. D. Montgomery, J. F. Torbert, J. R. Trujillo)

A portable shield was designed, fabricated and tested for use during radiography with the Betatron. The shield, which contains an aperture through which the beam passes, reduces the exposure of the film to the radiation from the irradiated pin. Minimizing this

exposure decreases the general fogging of the film and provides better quality images.

Experiments were conducted to decrease the "beam hot spot" by varying the distances between source, object, and film. Preliminary results, with the PNL-X capsules which varied from 50-130 rhm, indicate that the above modifications provided improved images. In radiographing capsules which have an activity of about 1000 rhm, it may be necessary to provide the aperture on the portable shield with a remotely operated shutter-shield.

The containers in which the capsules are radiographed have been provided, on the outside, with a series of solder droplets in a repeating pattern along the length. These droplets serve as fiducial marks and are very helpful in studying the radiograph negatives.

The elevating mechanism was altered to permit the raising of the container with capsule in increments of 4 in. instead of 6 in. This change is expected to provide negatives which are of uniform focus and which can be more easily assembled for studying the entire length.

#### Shipping Casks

(C. D. Montgomery, J. W. Schulte)

Approval (DOT Permit No. 5885) was received from the Department of Transportation relative to the design of the Shipping Cask for transporting fuel elements from EBR-II. Expected delivery date for this depleted uranium cask is now August 1.

Two casks, with DOT approval (Special Permit No. DOT 5645), were obtained from LASL's Rover Program. These casks, which are rectangular, have 10 in. of Pb shielding and a cavity size of 62 in. long x 16 in. x 16 in. Five PNL-X series capsules and a mixed carbide LASL capsule were shipped from the EBR-II to Los Alamos in an unmodified Rover cask. The "poisoned" cask insert (also unmodified) was used as the inner container for these six capsules.

Designs are being considered for modifying this cask insert concept to accommodate both the BNW-1 type capsule and possibly the 61-in. long unencapsulated EBR-II fuel pins.

#### Transfer Cart for Microprobe Cask

(D. B. Court, L. E. Jones, C. D. Montgomery)

Design of this motorized cart for handling the transfer cask for the microprobe has been finished. A completion date of May 1 appears reasonable for this unit.

#### System for Processing Specimens for Microprobe Examination

The original target date for having irradiated mixed oxide samples available for examination in the microprobe was May 1, 1969, assuming that no abnormal delays would be encountered in procurement and fabrication. The procedure proposed for processing the specimens is as follows:

1. Selected, polished metallographic samples will be ultrasonically cleaned, and then rinsed. Transfer into a special purpose 7-in. alpha transfer can is to be made with clean tongs.
2. The special transfer can would be moved to the "DTA Cell" where efforts are made to maintain the area free of contaminated dust. The specimen will again be ultrasonically cleaned and dried. Non-conducting specimens such as  $(U, Pu)O_2$  will be coated in a carbon evaporator (to conducting specimens such as the carbides will be applied a stripe of silver-containing paint).
3. The coated specimen is then removed from the box via a modified alpha can (without hold-down spring) to the corridor where swipes of the specimen are taken and then measured to determine the contamination level. Additional ultrasonic cleaning will be carried out if required.
4. The clean specimen is next inserted into the "boat" of the transfer cask, which is then transported on the cart to the room in which the microprobe instrument is located.

#### In-Cell Equipment

(G. R. Brewer, D. B. Court, F. J. Fitzgibbon, M. E. Lazarus, C. D. Montgomery, T. Romanik, J. R. Trujillo)

1. Profilometer

A detailed study of two designs is being carried out in parallel. One design incorporates an electromechanical gauging sensor by Brown and Sharpe. The other design utilizes an electro-optical sensor by Physi-Tech Corporation, which may allow a simpler system, at least in terms of maintenance, if the required precision is attainable. The selection of the system to be used is pending receipt of more information and demonstrable performance from each of these suppliers.

#### 2. Gamma Scanning (DP West)

Shield wall penetrations have been provided in a hot cell at DP West. A "low headroom" hoist has been procured and the design completed for off-loading casks.

#### 3. Carbon Evaporator

The remotely-operated carbon evaporator for coating non-conducting specimens was designed and is being fabricated.

#### 4. Other Support Equipment

- a. Additional tests have been conducted on models of gastight containers for shipping or long-term storage in an inert gas environment.
- b. Designs of high-resolution photography equipment, in use on other LASL programs, are being adapted for use in the examination of fuel pins and specimens.
- c. An Aminco mercury porosimeter was received. Modification for remote operation will proceed following completion of work on the heat content equipment, since both determinations will be carried out in the same containment box.
- d. Modifications to the design of the alpha containment boxes were made in an attempt to improve the design from the standpoints of leak-tightness and cost.

#### Heat Content

(C. E. Frantz, R. F. Velkinburg)

The calorimeter was installed in an alpha containment box. Most of the required services have been connected, and the electronics and constant temperature systems are undergoing testing so that calorimeter calibrations can be made.

#### Differential Thermal Analysis

(D. B. Court)

This capability is essentially completed. The system has been tested and, in general, performs satisfactorily. Calibration runs have not yet been made because certain other equipment must be installed in the same cell. It is desirable not to make the cell hot until all of the equipment is installed. It is felt that only minor debugging of this system remains, and that operating experience is necessary to best determine any additional requirements.

#### Thermal Diffusivity Determination

(M. E. Lazarus)

All major equipment with the exception of the furnace is now on hand for the thermal diffusivity measuring system. Replies to bid requests are now being received for the required furnace.

### III. HOT CELL APPLICATIONS OF METHODS OF ANALYSIS

The development of capabilities to do various quantitative analyses on irradiated fuels was continued with the judicious selection of methods and equipment, modification (if necessary), and testing under hot cell conditions. The following capabilities were investigated or completed.

#### Measurement of U and Pu

(J. W. Dahlby and G. R. Waterbury)

In-cell testing of controlled-potential coulometric equipment for titrating U and Pu showed that the titration cells and associated equipment functioned properly. Titrations of volumetric aliquots of U and Pu solutions lacked the required precision. Repeated analyses of weighed aliquots containing known amounts of U or Pu showed that the precision (1  $\sigma$ ) for a single determination was 0.13 relative percent in titrating U and 0.11% in determining Pu. In these measurements, the titration current was integrated while U(VI) was coulometrically reduced at a Hg electrode to U(IV) following a preliminary reduction of more easily reduced impurities. Titration of Pu involved a quantitative reduction to Pu(III) at a Pt working electrode followed by an oxidation to Pu(IV) while the current was integrated.

Small positive biases in these measurements of 0.1 to 0.2 relative percent should be eliminated by using

chemical calibrations of the coulometer. As removal of the cause of the bias was a preferred solution, the purities of the reagents and of the Ar cover gas in the titration cell were investigated. A small leak in the Ar supply line was found and sealed. Further titrations of U and Pu were started to ascertain if the biases were eliminated by this change. A (U,Pu)O<sub>2</sub> fuel pellet, having undergone 1% burn-up was obtained to test the effects on the method of the highly radioactive fission products.

Shielded Electron Microprobe  
(W. V. Cummings and E. A. Hakdla)

Check-out and testing were essentially completed on the shielded electron microprobe (Materials Analysis Corporation) except for a few minor components on back order. The back-ordered items, which included camera support, stage traverse and drive assembly, unshielded specimen stage, and a spectrometer programmer, were to be shipped prior to May 1. The testing procedure showed unsatisfactory operation of a rate meter, two flow proportional counters, and a digital voltmeter-data coupler which were returned to the vendor for repair within warranty.

The effectiveness of the instrument shielding was tested by measuring external radiation while a 100 R/hr <sup>60</sup>Co source was in the sample chamber. The maximum surface reading was only 5 m R/hr. In addition, the intensely radioactive source did not adversely affect the precision of x-ray measurements.

The transfer cart for the sample cask is being fabricated, the vacuum evaporator and other sample preparation equipment are being installed, and modifications to the sample cask to permit remote loading operations compatible with local hot-cell equipment have been completed. Every possible effort is being made to have the electron microprobe capability operational within 1 or 2 months.

Measurement of O<sub>2</sub> and N<sub>2</sub>  
(G. C. Swanson and J. W. Dahlby)

Calibration and testing of a LECO Nitrox-6 Analyzer by making approximately sixty determinations of known amounts of N<sub>2</sub> between 9 and 65.6 μg showed that the

relative standard deviations were approximately 10% regardless of the quantity of N<sub>2</sub> measured. The unanticipated lack of dependence of the relative standard deviation on the quantity of N<sub>2</sub> measured cast some doubt on the accuracy of the commercial standards used. For this reason, working standards were carefully prepared by evaporation of weighed aliquots of a NH<sub>3</sub>Cl solution in tin capsules. These standards proved unsatisfactory, however, because one of the degradation products (presumably HCl) interfered with the measurement of N. Standards are now being prepared using a K<sub>3</sub>Fe(CN)<sub>6</sub> solution and will be analyzed.

Calibration of the analyzer for measuring O<sub>2</sub> is under way by making repeated analyses of commercial standards for O<sub>2</sub>.

Thermogravimetric Determination of O/M Atom Ratios  
(G. C. Swanson and J. W. Dahlby)

A micro thermobalance, partially modified to adapt it to hot-cell gravimetric measurements of O/M atom ratios, was tested using U metal as the starting material. Polished pieces of U metal weighing approximately 0.3 g were weighed accurately in Ar, oxidized in air, and then heated to 800°C in flowing moist Ar-8% H<sub>2</sub>. When the oxide weight became constant, the sample was cooled and reweighed in Ar. The O/M atom ratio of the product was calculated from the original metal weight and the final weight.

The reproducibility of the weighings of approximately ± 10 μg limited the precision of the O/M measurement to ± 0.0004. The average O/M ratio of the product was 2.013, which was significantly high. This ratio will be checked by making further determinations before changing the reaction temperature in an effort to produce stoichiometric UO<sub>2</sub>.

IV. EXAMINATION OF UNIRRADIATED FUELS

Examination of Westinghouse Atomic Power Department Carbides  
(J. A. Leary, M. W. Shupe, E. A. Hakdla, R. T. Phelps, G. R. Waterbury)

Pellets from ten batches of WARD carbides were evaluated. Document CMB-11-9492, describing the results, was transmitted to WARD and F & M/DRDT on April 11.

Examination of Pacific Northwest Laboratory Oxides

(J. A. Leary, M. W. Shupe, E. A. Hakkila, R. T. Phelps, G. R. Waterbury)

Four pellets of (U,Pu)<sub>2</sub>O<sub>3</sub> from batches used for the BNL and PNL irradiations were evaluated. The summary report was distributed to PNL and F & M/DRDT on March 6.

Examination of United Nuclear Corporation Oxides

(J. A. Leary, M. W. Shupe, E. A. Hakkila, R. T. Phelps, G. R. Waterbury)

Five (U,Pu)C pellets from UNC batches H and K were evaluated. Results were reported to UNC and F & M/DRDT in document CMB-11-9490 on April 1.

Thermal Conductivity

(K. W. R. Johnson)

Additional modifications have been made on the 3M Comparative Type Thermal Conductivity Apparatus to remove the components contributing to specimen oxidation. Using a stand-in specimen of hot pressed UC, measurements were extended to 800°C. At 1000°C, however, surface oxidation resulted in a low value for the thermal conductivity. Since the bulk of the material was unchanged it was possible to calculate a corrected value by measuring the decrease in the cross sectional area.

The thermal conductivity of a specimen of U<sub>0.8</sub>Pu<sub>0.2</sub>C was measured under similar conditions and pertinent data are listed in Table 401-I. As with the

Table 401-I  
Measured Thermal Conductivity of U<sub>0.8</sub>Pu<sub>0.2</sub>C

Temperature (°C)	Thermal Conductivity (cal./sec.cm.°C)
118	0.028
306	0.030
554	0.033
804	0.039
1001	0.039
1001	0.043*

\* corrected for 9.2% decrease in cross sectional area due to surface oxidation at 1001°C

	Specimen Description	
	Before Measurement	After Measurement
Composition	U <sub>0.79</sub> Pu <sub>0.21</sub> C <sub>0.99</sub>	U <sub>0.79</sub> Pu <sub>0.21</sub> C <sub>1.00</sub>
Oxygen (ppm)	410	180
Nitrogen (ppm)	225	215
Metallography	single phase	single phase
Percent theor. density	89.7	89.7

stand-in specimen, the measured value for the thermal conductivity at 1001°C was obviously too low. Surface oxidation had reduced the cross sectional area by 9.2%. Increasing the 1001°C measurement by 9.2% produced a value which fell on a smoothed line through the lower temperature data points.

Further equipment modifications are being made.

Compressive Creep

(M. Tokar)

Compressive creep measurements on mixed uranium-plutonium carbides are being undertaken using equipment described extensively in previous reports. Before committing this equipment to use with plutonium materials, uranium monocarbide and dicarbide specimens were used. Data on UC (but not UC<sub>2</sub>) are available in the literature<sup>(1-3)</sup> and can be readily compared to results obtained here, thus providing a check of the reliability of the test apparatus.

A graphical comparison of data obtained on UC at 1300°C is shown in Figure 401-1. The creep rates determined here at 1300°C, 4000 and 6000 psi are in reasonably good agreement with Norreys<sup>(1)</sup> and Stellrecht, et al.<sup>(2)</sup> The differences in creep rate shown in the figure appear to be due to differences in test specimen

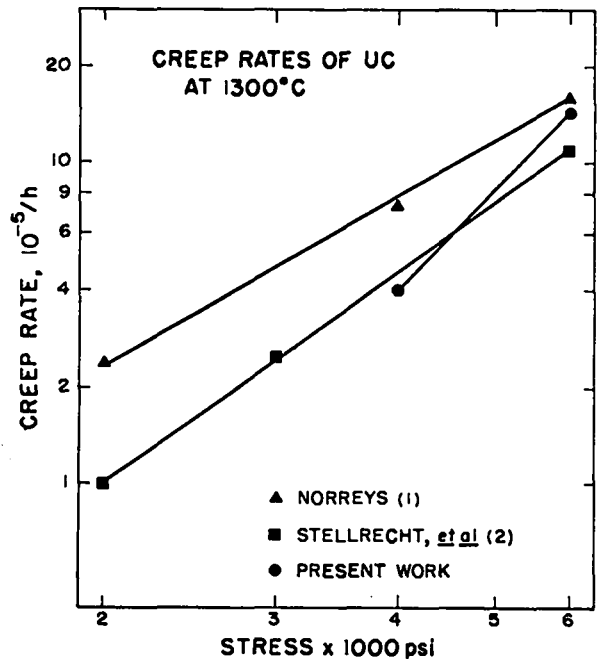


Figure 401-1

microstructure rather than to testing procedure or apparatus differences. The results reported here on UC are in good enough agreement with the literature to indicate that acceptable data will be obtained on the mixed carbides.

Hot Hardness  
(M. Tokar)

A microindentation hardness tester has been installed for use at elevated temperatures. The furnace is resistance-heated with a Mo wire heating element wound around an aluminum silicate muffle. The specimen, heating element, indenter (200 g load) and stainless steel radiation shields are all enclosed in a water-cooled stainless steel bell jar. The maximum use temperature is presently limited to about 1000°C, mainly due to the temperature limitations of the muffle, radiation shields, and indenter materials (sapphire or diamond). The use temperature may be raised, however, by substituting higher temperature materials (such as Ta and Al<sub>2</sub>O<sub>3</sub>) for the radiation shields and muffle and by using B<sub>4</sub>C for the indenter.

Before contaminating the apparatus with Pu-containing materials it has been used to test the hot-hardness of materials such as 347 stainless steel and Armco ingot iron. Armco iron is a particularly interesting material to test because of the BCC to FCC transition at 910°C. The diamond pyramid hardness versus temperature behavior from 500-1000°C is shown in Figure 401-2. These results are in good agreement with those of Hallerman and Gray, particularly with regard to changes in slope near the transformation temperature. The slight increase in hardness on cooling may be due to a refinement in grain size, as the carbon content of this material (~ 0.01%) is too low to permit hardening due to carbide formation.

V. REQUESTS FROM DRDT

Examination of Irradiated Material

(D. M. Holm (K-1), K. A. Johnson, J. W. Schulte, J. F. Torbert (GMX-1), G. R. Waterbury)

1. Battelle Northwest Laboratory Capsules and Pins

The following operations were carried out on specimens from PNL-1-15, -17, and -19, and from

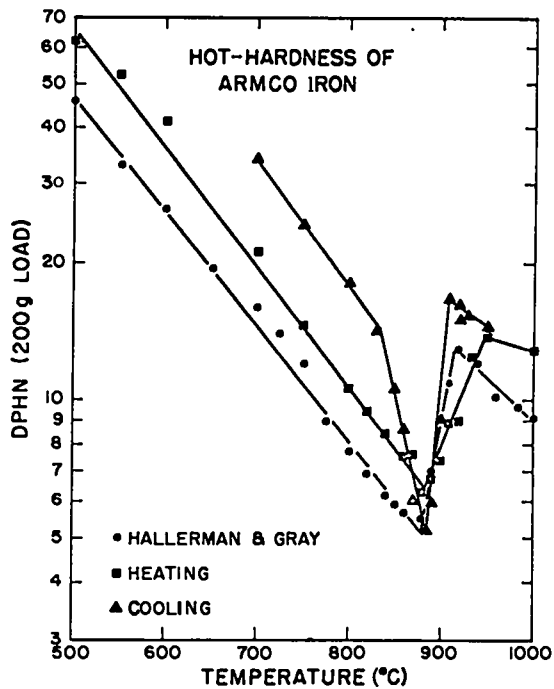


Figure 401-2

BNW-1-9 and -11:

- a. Metallography
- b. Alpha autoradiography
- c. Beta-gamma autoradiography
- d. Replication for electron microscopy

PNL-X-1, -3, -4, -6 and -7 were received on

February 7, and the following operations have been performed:

- a. Radiation measurements
- b. Viewing and photography
- c. Radiography with the Betatron
- d. Micrometer readings at 3-in. increments at 0° and 90°

2. LASL Mixed Carbide Capsule

LASL-42-B was received from the EBR-II on

February 7, and the following operations were performed:

- a. Radiography and gamma scanning
- b. Micrometer diameter measurements
- c. Temperature and radiation measurements

Negotiations are in progress by K Division to return this irradiated (U, Pu)C capsule to EBR-II for additional irradiation.

3. Westinghouse Capsules

Capsules W-1-G, W-2-G and W-3-G, containing

mixed carbide fuel, were received on February 19. The following operations have been completed on these capsules:

- a. Radiation and temperature measurements
- b. Visual inspection and photography
- c. Radiography
4. United Nuclear Capsules

The operations performed on these three (U, Pu)C pins during this quarter are as follows:

- a. Photography on UNC-89
- b. Profilometry on UNC-87, 89 and 90

All results have been forwarded to the sponsor.

5. Atomics International Fuel and Flux Monitoring Wires

The following operations have been performed on the UC (W-doped) pellets and flux wires:

- a. Contamination swipes and radiation level readings of three monitor wires.
- b. Gamma scan on one monitor wire; samples also taken for radiochemistry.
- c. Two of the 120 UC pellets were examined metallographically, and replicas made and sent to sponsor for evaluation.
- d. Four of the UC pellets packaged and shipped to Idaho Nuclear for burn-up analysis.

#### VI. LMFBR/FFTF MIXED OXIDE ANALYTICAL STUDIES

##### Visits to Laboratories of Potential FFTF Fuel Producers

(R. G. Bryan, C. F. Metz, and R. K. Zeigler)

Approximately three weeks were spent in visiting the laboratories of AI, B & W, GE (Sunnyvale), NFS, NUMEC, and UNC. PNL was included because of their responsibilities in the Pre-Qualification and Qualification Programs of their Fuel Procurement Program. AHRCO was included because of their role as a potential supplier of raw material. These visits were made in an attempt to obtain additional information concerning the capabilities of each laboratory for analyzing mixed oxide fuel. A summary trip report has been written and forwarded to RDT.

##### Phase II of the Analytical Program

This program is about to get under way. Instructions

were sent to the individual participating laboratories early in January. Sintered pellets have been made at PNL and will be forwarded as soon as contractual procedures are completed. Matrix material for spectrographic standards, four sets of spectrographic standards and "a common materials" consisting of ground sintered mixed oxides into which has been blended known quantities of halogens, carbon and nitride nitrogen have been prepared by LASL and will be distributed by April 15 to participating laboratories.

##### Determination of F in Sintered (U, Pu)O<sub>2</sub> (T. K. Marshall and G. R. Waterbury)

The fluoride ion specific electrode was shown to be applicable to measurement of F at trace concentrations in U<sub>3</sub>O<sub>8</sub>, used as a stand-in for sintered (U, Pu)O<sub>2</sub>, by making repeated determinations of 1 to 10 µg quantities as NaF to 1-g portions of the sintered oxide. In these analyses, the pyrohydrolytic separation of F<sup>-</sup>, that had been proved to be satisfactory in previous work, was coupled with the specific ion electrode measurement of the F<sup>-</sup> in the distillate.

First attempts to use the electrode were unsuccessful because the internal electrolyte had dried up, and very erratic readings were obtained. It was found that the electrode could be rejuvenated by disassembly, cleaning, and recharging with a solution 0.1 M in NaF and KCl. The electrode was then calibrated using six HF solutions containing known concentrations of F<sup>-</sup> between 0.010 and 0.206 µg/ml. The calibration curve was not linear, making the use of several concentrations mandatory.

The pyrohydrolysis was carried out in an all-nickel apparatus by passing steam, generated from slightly alkaline H<sub>2</sub>O containing KMnO<sub>4</sub>, over the sample until approximately 50 ml of condensate were collected. The F<sup>-</sup> was measured with the electrode, and then titrated with Th(NO<sub>3</sub>)<sub>4</sub> for comparison. The results obtained by the two measurement methods were approximately equal, and the less-sensitive titrations were discontinued. The average recovery of 1.9 to 9.3 µg of added fluoride was 97% and the precision (1 σ) was 4%, showing satisfactory operation of the method.

The effects on the F<sup>-</sup> recovery caused by use of a

SiO<sub>2</sub> boat and/or furnace tube in the pyrohydrolysis were investigated. Known quantities of F<sup>-</sup>, as NaF, between 0.9 and 9.3 μg were added to 1-g samples of U<sub>3</sub>O<sub>8</sub> to prepare test samples. Between thirteen and eighteen test samples were analyzed under each of the following conditions: (1) Ni furnace tube - SiO<sub>2</sub> boat, (2) SiO<sub>2</sub> furnace tube - Ni boat, and (3) SiO<sub>2</sub> furnace tube - SiO<sub>2</sub> boat. Average recoveries of F<sup>-</sup> were: (1) 94%, (2) 90%, and (3) 85%, under the respective conditions, showing that an all Ni system gave somewhat higher recoveries. Determinations of F<sup>-</sup> added to (U, Pu)O<sub>2</sub> are under way.

#### O/M Atom Ratio

(J. W. Dahlby, T. K. Marshall and G. R. Waterbury)

Two thermogravimetric methods, referred to here as Lyon's Method and Chikalla's Method, were tested under conditions that were stringently controlled to duplicate, except for atmospheric pressure, the conditions originally used. In these tests, the methods were applied repeatedly to analyses of oxides, made either from high-purity U metal or Pu metal in which the O<sub>2</sub> contents were accurately known.

For Lyon's method, the sample was oxidized by allowing air to back diffuse into the furnace at 750°C, the oxide was stirred in Ar at 750°C, and reduction (presumably to the stoichiometric dioxide) was accomplished at 700°C in He-6% H<sub>2</sub> atmosphere. Seven determinations on U<sub>3</sub>O<sub>8</sub> showed that the O/M ratio of the final oxide was 2.015 and the precision (1 σ) was 0.004. For twelve analyses of PuO<sub>2</sub>, the final O/M ratios averaged 2.010 and the standard deviation was 0.002. Both results were significantly high.

In the Chikalla Method, the oxide was heated in moist Ar-8% H<sub>2</sub> at 800°C to obtain the stoichiometric dioxide. At this temperature, the O/M ratios of the final oxides obtained from the U<sub>3</sub>O<sub>8</sub> samples ranged between 2.022 and 2.030. Samples of PuO<sub>2</sub> are to be analyzed next by this method.

Upon completion of the analyses of the U<sub>3</sub>O<sub>8</sub> and PuO<sub>2</sub> individually by each method, mixtures of the two oxides equivalent to 80% U and 20% Pu will be used as test samples.

#### Determination of Burn-up

(E. A. Hakkila and R. G. Hurley)

Considerations of recent proposals to determine burn-up by measuring the concentration of a non-radioactive fission product isotope indicated that <sup>148</sup>Nd offered promise as a burn-up monitor. As other fission product rare earth isotopes were abundant in irradiated fuel, a specific determination was required, and an x-ray fluorescence spectrometric method seemed appropriate.

For testing the proposed method, a solution was prepared that contained U, Ru, Rh, Mo, Zr, Nb, and Nd at relative concentrations that would be found in a U fuel having undergone 10% burn-up. The Nd, along with Y and Tb added as a carrier and an internal standard, respectively, was separated from U and fluoride-soluble elements by fluoride precipitation. Further purification of the rare earths was effected by adsorbing them from HCl-butanol solution onto cation exchange filter paper. Measurement of the intensities of the Lβ<sub>1</sub> x-ray for Nd and the Lα<sub>1</sub> x-ray for Tb on the paper permitted calculation of intensity ratios which were compared to ratios measured from discs containing known quantities of Nd and Tb. Repeated measurements under optimum conditions of 1 to 50 μg of Nd in aliquots containing 200 mg of U showed that the precision (1 σ) was 1 relative percent or less in measuring 20 to 50 μg of Nd, 5% in measuring 5 μg, and 16% at the 1 μg of Nd level. It was anticipated that the method would apply to measurement of burn-up in irradiated fuels such as the mixed oxide, and further, that it would be adaptable to hot cell operation.

#### Spectrochemical Methods

(W. M. Myers, C. B. Collier, and R. T. Phelps)

Determination of the metal impurity elements is planned to be done by emission spectrochemical methods. Analysis of test fuel pellets<sup>(4)</sup> indicated application of the carrier-distillation technique by using two substances as the carrier in order to obtain adequate detection sensitivity for all the impurity elements. With 6% Ga<sub>2</sub>O<sub>3</sub> as the carrier, most common elements (including Ag) could be adequately determined. For refractory elements such as Ti and W, use of AgCl as the carrier provided the sensitivity needed.

Use of the carrier-distillation technique requires standards having chemical and physical properties which match those of the sample. Usually, matching involves preparing the standards by the method used to prepare the sample; however, the sample may be altered (converting metal to oxide) in order to obtain similarity by less difficult treatments. Since the FFTF fuel consists of a single-phase solid solution of  $UO_2 - PuO_2$ , preparing a comparable matrix for standards would require sintering the pure constituents at high temperature without introducing contaminants. This is not readily done. Two alternatives offer less difficulties. One is to ignite the sample to form two-phase  $U_3O_8 - PuO_2$  and analyze with standards having a  $U_3O_8 - PuO_2$  matrix. Second is to use standards having a  $UO_2 - PuO_2$  matrix, but prepared as a mechanical mixture, and grind the sample to a fine powder.

Results previously reported<sup>(4)</sup> showed that test fuel pellets may be analyzed for the main impurities found -- Al, Cr, Fe, Ni, and Si -- by the method listed as the first alternative. Also shown was that the results for Al, Fe, and Si depend on whether the sample matrix was single-phase solid solution  $UO_2 - PuO_2$  or two-phase  $U_3O_8 - PuO_2$ .

Further analysis of test pellets<sup>(5)</sup>, but using the method described as the second alternative, yielded good precision results (< 20% relative standard deviation) for Al, Cr, Fe, Ni, and Si. Also, the results for Fe and Si were confirmed by independent chemical analyses. In this method, the fuel pellet is finely ground to pass through 200 mesh screen and analyzed with reference to standards having a  $UO_2 - PuO_2$  matrix. Ignition of the sample is avoided.

These evaluations indicate that reliable spectrochemical analysis may be made of the fuel pellets by using standards having a  $UO_2 - PuO_2$  matrix prepared as a mechanical mixture. The need to prepare a sintered matrix is obviated.

Plans made for Phase II of the evaluation of the analytical capabilities of potential fuel producers include supplying aid and materials by LASL. For spectrochemical analysis, matrix material for making standards and primary standards is to be furnished to the producers.

A batch of matrix material has been prepared and is ready for distribution to each of six potential fuel suppliers. This mixture of  $UO_2 - 22$  w/o  $PuO_2$  was made from high-purity  $UO_2$  and  $PuO_2$  by mechanical mixing including tumbling in a plastic bottle and grinding in a TaC mortar. The detectable impurities are Al and Si, each < 5 ppm, and 12 ppm of W.

Four primary A-standards have been prepared and analyzed. Three grams of each are ready for distribution to the potential fuel suppliers. These standards contain the following impurity elements:

Element	No. 2	No. 4	No. 6	No. 7
Al	12	65	250	500
Si	13	53	250	500
Cr, Fe, Ni	10	50	250	500
Ca, Mg, Mo, P	5	25	125	250
Cu, Mn, Na, Pb, Sn, Zn	2	10	50	100
Ag, B, Be, Bi, Cd, Li	0.5	2.5	12.5	25

Four primary B-standards containing impurity elements W, Nb, Ti, Zr, Mo, P, Co, V, Cd, Ba and Sr have been prepared but not analyzed. Eight B-standards for use by LASL have been prepared and are being studied to evaluate the spectrochemical procedure.

#### Electron Microprobe Examinations (E. A. Hakala and H. L. Barker)

The electron microprobe was used to identify inclusions and to determine if the matrix was homogeneous in a sintered  $(U, Pu)O_2$  pellet. Four types of inclusions were found: (1) P-Ni-Fe-W-Mo, (2) Mo-W-Ni, (3) P-Ni-W, and (4) P-Fe-Ni. Heterogeneous distributions of U and Pu were shown.

#### Miscellaneous Analytical Support

Controlled-potential coulometric methods, having relative standard deviations of 0.2 to 0.3%, were applied, without difficulty to measurement of U and Pu in three  $(U, Pu)O_2$  samples.

Spectrophotometric methods, each having a precision of  $(1 \sigma)$  of 2 relative percent, were used to measure W in one  $PuO_2$ , one Pu metal, and two  $(U, Pu)O_2$  samples; Fe in one  $PuO_2$  and sixteen  $(U, Pu)O_2$  samples; and Si in

sixteen (U,Pu)O<sub>2</sub> samples. In each case the concentration of the element determined was low, being no greater than 190 ppm. No difficulties were experienced.

A potentiometric titration method was used successfully to determine Pu in a PuO<sub>2</sub> sample. The relative standard deviation of the method was 0.06%. Dissolution of the PuO<sub>2</sub> was accomplished by heating at 300 to 325°C in 12 M HCl in a sealed silica tube. Pressures of 3000 to 4000 lb/sq. in. developed in the tube assisted in dissolving the PuO<sub>2</sub> in a minimum time of 1 to 2 hr.

#### VII. PUBLICATIONS

"Characterizing Compositions of Irradiated Fuel at Operating Temperatures -- Future Needs," G. R. Waterbury and C. F. Metz, Proceedings of the 16th Conference on Remote Systems Technology, American Nuclear Society, pp. 301-306, 1969.

"Gravimetric Determination of Oxygen in Refractory Oxide Materials," C. S. MacDougall, M. E. Smith, and G. R. Waterbury, Analy. Chem. **41**, 372 (1969).

"Radiographic Inspection of Irradiated Fuel Elements Using the 22-MeV Betatron," Proceedings of the 16th Conference on Remote Systems Technology, American Nuclear Society, pp. 22-27, 1969.

#### VIII. REFERENCES

1. J. J. Norreys, "The Compressive Creep of Uranium Monocarbide," Carbides in Nuclear Energy, Vol. 1, Harwell, 1963.
2. D. E. Stellrecht, M. S. Farkas, and D. P. Moak, "Compressive Creep of Uranium Carbide," J. Amer. Ceram. Soc., **51** (8), 455-8, 1968.
3. M. H. Fassler, F. J. Huegel, and M. A. DeCrescente, "Compressive Creep of UC and UN," October 1964, PWAC 482.
4. R. T. Phelps, et al., Quarterly Report, October 1, 1968, "Examination of Fast Reactor Fuels."
5. W. M. Myers, C. B. Collier, and R. T. Phelps, Quarterly Report, January 1, 1969.

PROJECT 462

SODIUM TECHNOLOGY

Person in Charge: D. B. Hall  
Principal Investigator: J. C. Biery

I. INTRODUCTION

For the successful operation of high temperature sodium systems contemplated for use in fast, central station reactor concepts, impurities in the sodium must be monitored and controlled. Nonradioactive impurities such as oxygen must be maintained at low concentration levels to limit corrosion processes. Radioactive impurities introduced into sodium from failed fuel elements should be removed to facilitate "contact maintenance" and to minimize safety and detection problems. To control the levels of these impurities, a knowledge of their behavior and interactions in sodium must be developed. Acquisition of this information has been subdivided in the LMFBR Program Plan into a number of task areas. The sodium technology program at LASL has projects which contribute to six of these areas. The broad tasks and current LASL projects within those areas are summarized below:

Task Area 1: Materials Compatibility

- A. Correlation of sodium and helium leaks.
- B. Study of carbon transport in thermal convection loops.

Task Area 2: Sodium Purification

- A. Study of sodium oxide kinetics in cold traps.
- B. Study of soluble getters for removal of impurities from sodium.
- C. Study of gas diffusion through metals into sodium.

Task Area 3: Fission Products in Sodium Systems

- A. Study of fission product distribution in loop experiments.
- B. Study of fission product gettering in capsule experiments.

Task Area 4: On-Line Monitoring Methods

- A. Plugging meter studies.

Task Area 5: Sampling and Analysis

- A. Vacuum distillation studies.
- B. Study of gamma ray activation analysis for C and O.
- C. Absorption spectrometry development for metal impurity analysis.
- D. Total carbon analysis development.
- E. Development of remotely operated distillation samplers for EBR-II.

Task Area 7: Cover Gas and Maintenance Atmospheres

- A. Development of a high temperature quadrupole mass spectrometer for cover gas analysis.

Details of the work in these programs are presented below.

II. MATERIALS COMPATIBILITY

A. Correlation of Sodium and Helium Leaks  
(D. C. Kirkpatrick, J. P. Brainard)

1. General

The correlation of sodium leak development with measured helium leak rates observed during acceptance testing provides information on the degree of component integrity which must be attained for safe, long-term sodium plant operation. No firm criteria now exist that establish acceptable levels of leak-tightness for various situations.

This study uses fabricated stainless steel leaks and leaks that occur naturally in stainless steel bar stock. Selected samples having a range of helium leak rates are incorporated into small sodium systems (cells) which are held at a predetermined temperature until sodium leakage occurs. From these observations it may be possible to establish, for

mass spectrometer acceptance tests on sodium system components, the maximum tolerable helium rate which is consistent with adequate long-term containment of sodium by that component.

An interesting side effect from this work has been observation of the elusiveness of what are considered to be large leaks ( $10^{-5}$  to  $10^{-6}$  atm cm<sup>3</sup>/sec). Normal contaminants such as grease, water and some solvents can completely mask leaks of this size and invalidate a leak test, unless proper pre-treatment of the component is performed; and in some cases this can involve firing of the component in a hydrogen atmosphere. If meaningful helium leak tests are to be performed on LMFBR components, procedures must be developed for treating and handling of the part prior to leak test.

## 2. Current Results

No leakage of sodium has been observed in Cells 1 through 4 (the 400°C cells) after 8000 h of operation. However, all the 650°C samples (Cells 5-8) known to have had helium leaks have leaked sodium. The sodium leakage of Cells 5 and 7 were reported last quarter. During this quarter Cell 8 began leaking sodium at low level ( $\sim 5 \times 10^{-2}$  cm<sup>3</sup>/day) after 93 days of operation. This cell is being allowed to continue in operation in order to observe leakage rate versus time. Cell 6, the control, had no helium leak and as expected has not leaked sodium. With data on sodium leakage from only eight experimental cells, it is very difficult to draw any general conclusions. However, it does appear that the higher the sodium system temperature, the greater the problem of sodium leakage through flaws in the container walls. A LAMS report (LA-4129-MS) has been written on the studies to date.

Weld adaptors were fabricated to place the fixed geometry leaks into the experiment. These leaks of known geometry will be used to test the mathematical model based on the theory of oxide buildup in the leak path and to determine additional temperature effects. The leak sizes are approximately  $10^{-3}$  atm cm<sup>3</sup>/sec.

## B. Study of Carbon Transport in Thermal Convection Loops

(J. C. Biery, C. R. Cushing)

### 1. General

Studies have indicated that the use of carbon beds may be useful in the gettering of <sup>137</sup>Cs in sodium systems. Carbon, however, is slightly soluble in sodium and can carburize austenitic stainless steels and refractory metals. Therefore, the purpose of this study is to determine the conditions under which carbon mass transfer rates are sufficiently low to allow the use of carbon beds in a sodium system.

The carbon transfer rates from carbon rods will be studied in thermal convection loops. The Type 304 or 316 stainless steel loop itself will serve as the carbon sink when these alloys are studied and vanadium alloy sleeves will serve as getter when vanadium is studied.

### 2. Current Results

The installation of the thermal harp to the steam generator sodium supply loop was completed, and sodium flow through the loop was started. Initially, sodium from the loop was passed through the harp to condition the internal surfaces to the oxygen concentration in the sodium. The cold trap temperature in the main loop was 150°C. The conditioning period continued 208 h. During 67 h of that time 250°C sodium from the supply loop was intermittently pumped through at 1 gpm. For 141 h the pumped flow was discontinued, and thermal convection at 500°C was allowed. The pumped and convection periods were alternated with the minimum period being 24 h in length.

On March 6, 1969, a graphite rod 1/4-in. diam and 2-9/16-in. long was submersed in the sodium at the top of the hot leg of the loop. As of March 28, 1969, the rod had been exposed to the thermally convecting sodium for 528 h. The temperature around the loop varies from a low of 485°C in the cool leg to a high of 525°C in the hot leg. The flow velocity as measured by a flowmeter is in the 2-3 cm/sec range.

Present plans call for continuation of the test for approximately 8000 h. At termination of the run the loop will be sacrificed and examined for carburization effects. Also, the graphite rod will be cleaned by heating under vacuum, weighed, and then burned and analyzed for sodium content.

### 111. STUDY OF PURIFICATION METHODS FOR NONRADIOACTIVE IMPURITIES

#### A. Study of Na<sub>2</sub>O Kinetics in Cold Traps

(C. C. McPheeters, J. C. Biery, W. W. Schertz, R. Martinez)

##### 1. General

In sodium coolant systems for future LMFBR's it will be necessary to use cold traps for removal and control of oxygen and other contaminants. These cold traps should be designed to handle adequately the impurity loads and to maintain the impurity concentration level below some specified upper limit. For economic reasons, cold traps must be the smallest and simplest designs which can meet the above requirements.

Knowledge of the mechanisms of impurity deposition in cold traps is necessary to reach the optimum design for a given sodium coolant system. The rate of mass transfer of impurity species to cold trap surfaces must be measured and the effect of various flow patterns, surface conditions, and temperature on the mass transfer rates must be determined. The purpose of this study is to determine the effect of the above variables on the mass transfer coefficient for removal of oxygen from sodium systems. Knowledge of the mechanisms involved and the mass transfer coefficients will allow calculation of the rate of oxygen removal and the location of deposited oxides in the cold trap for any given system size and cold trap geometry. Proposed cold trap designs could be evaluated in terms of total oxide capacity and expected system cleanup rates.

Cold trap tests are being conducted with a 60-gal sodium system which has analytical capabilities including a vacuum distillation sampler, a plugging indicator, and two UNC oxygen meters. The cold trap tests consist of measurement of the rates of change of oxygen concentration in the system. Various cold trapping conditions of temperature and flow rates are tested to determine the effect of these variables on the oxygen removal rates. When the rate of change of oxygen concentration, the cold trap temperatures and the deposition surface area is known, an overall mass transfer coefficient can be calculated.

##### 2. Current Results

##### a. Initial Runs with "Removable Core" Cold Trap

The cold trap test loop was started up after a four-month shutdown period during which the "removable core" cold trap was installed. The second cold trap design includes a feature which allows removal of a NaK-cooled section for direct observation and analysis of the cold trap deposits.

During initial operation of the cold trap test loop, after the shutdown period, the plugging indicator was operated in the partially plugged, oscillating mode, and two distinct impurity species were detected. The entire system including the cold trap was maintained at 450°C. One impurity was saturated at ~220°C, and the second impurity was saturated at ~270°C. Neither of these impurities had precipitation and dissolution characteristics indicative of the oxide. They exhibited very slow precipitation and dissolution rates while oxygen saturated at 220°C has very rapid mass transfer rates.

Two cold trapping runs were made in an attempt to determine the overall mass transfer coefficient of the 220°C impurity. These runs were made in the usual manner which consists of establishing a low cold trap temperature, then measuring the saturation temperature change with time. Mass transfer of oxygen in sodium has been found to be liquid phase diffusion controlled. Mass transfer of other species would also be expected to be liquid phase controlled; therefore, the mass transfer coefficient should have the same value for different impurities.

After the completion of the cold trap runs on this unknown impurity, the NaK-cooled section of the cold trap will be removed and examined visually as well as analytically. An attempt will be made to identify the compound present. Then the cold trapping data can be used to calculate the mass transfer coefficient associated with the impurity. If the specie has a known solubility curve, the coefficients will be calculated directly, and their size can be compared with oxygen coefficients obtained under similar conditions. Thus, the validity of the constancy of coefficients with specie variation can be partially tested. If the solubility curve is unknown, the curve will be estimated and adjusted to produce mass transfer coefficients of similar size to those obtained from similar oxygen precipitation runs.

b. New Computer Simulation Code

A computer code, COSIM, has been written which simulates the operation of the cold trap test loop with the "removable core" cold trap. First, the temperature profile in the cold trap is calculated and adjusted to agree with measured values, and then the cold trap mass transfer run is simulated as follows: The cold trap is divided into equal-volume sections, and the mass deposited in each section is calculated with the equation,

$$\Delta m = kA(C - C_e) \Delta t, \quad (1)$$

where  $\Delta m$  = the mass of impurity deposited in the section, g.

$k$  = mass transfer coefficient, g/cm<sup>2</sup>-sec-ppm.

$A$  = surface area on which deposition occurs, cm<sup>2</sup>.

$C$  = impurity concentration in the section, ppm.

$C_e$  = equilibrium concentration based on the surface temperature in the section, ppm.

$\Delta t$  = the time required for integrated flow rate to equal the volume of the section, sec.

The impurity concentration in each section is changed by the amount of mass deposited (or dissolved), and each section is advanced one step. The remainder of the system is simulated by storage allocations which represent slug flow and by a representation of the mixing tank. The computer code not only predicts the rate of change of impurity concentration in the system, but it also predicts the mass deposit distribution in the cold trap. This distribution can be measured by removal and analysis of the deposits on the NaK-cooled section of the cold trap.

c. Oxygen Addition System to Cold Trap Loop No. 1

The dynamics of adding oxygen to the sodium loop by connecting a volume of an oxygen-helium gas mixture to a space above flowing sodium in the vacuum distillation side loop have been calculated. It appears that an excessive time would be necessary to add a significant amount of oxygen, and that the quantity of oxygen added would not be well defined. The system has, therefore, been equipped with a controlled leak of pure oxygen into a gas space above a flowing sodium surface. This latter arrangement allows metering of known quantities of oxygen to the system under fast reaction rate conditions.

d. Kinetics of Impurity Precipitation at High Reynold's Number

The design of a sodium system to study impurity precipitation kinetics at high Reynold's number (up to  $5 \times 10^4$ ) has been initiated. The sodium system and the precipitation test section have been sized for the high Reynold's number operation, and equipment procurement and design are in progress.

B. Study of Soluble Getters for Removal of Impurities from Sodium  
(G. E. Meadows, L. A. Waldschmidt, D. N. Rodgers, O. E. Thomas)

1. General

For large sodium-cooled reactor systems, it may be desirable to use soluble getters for control of oxygen and other dissolved impurities in lieu of the more conventional hot and cold trapping techniques. The soluble getters of interest occur in the sodium coolant either naturally, as an impurity (calcium), or are produced during reactor operation (as with magnesium). The techniques for the controlled additions of these getters, maintenance of fixed getter levels, and the selective removal of depleted getter metals and other impurities from dynamic sodium systems must be developed if their usefulness is to be evaluated. The significant chemical reactions occurring in a sodium system containing these soluble getters must be understood and controlled. This mode of purity control has the potential for effectively controlling not only oxygen, but also carbon, hydrogen, nitrogen, and possible metallic impurities.

2. Current Results

a. Calcium Addition Run No. 2 in Analytical Loop No. 1

On January 6, 1969, 1.15 g of calcium metal were added to Analytical Loop No. 1. The addition was done in the same way as previous additions, i.e., a lump of calcium was put inside a wire screen basket which was lowered into the bulk tank. The calcium was weighed and loaded into the charger while inside a helium inert box; thus, it was not exposed to the atmosphere. The cold trap temperature was 225°C, and the bulk tank temperature was 350°C. If the calcium were evenly distributed throughout the system, the sodium would contain 45 ppm calcium, by weight.

No change in the system behavior was observed

after the calcium addition. A vacuum distillation sample taken 1-1/2 h after the addition contained 29.0 ppm oxygen and 0.17 ppm calcium in the residue. A second distillation 4-1/2 h after the addition indicated 29.0 ppm oxygen and 0.14 ppm calcium. Five samples analyzed before the addition had a range of 24-34 ppm oxygen (average 28.6) and 0.10-0.14 ppm calcium (average 0.11). Thus, the calcium addition did not significantly alter the bulk sodium analysis.

The basket used to add the calcium was then pulled from the loop to determine how much calcium had dissolved. Out of 9.845 g of metallic substance recovered from the basket, 0.238 g (21% of the calcium added) of calcium were found. The sodium was removed from the basket by distillation. When the residue in the distillation cup was dissolved in 0.01N HCl as per the normal procedure, an extremely strong odor of phosphine (PH<sub>3</sub>) was noticed. Apparently, there was a phosphorus compound in the basket when it was pulled from the loop. The compound was not identified. The phosphorus compound may have precipitated the calcium and may have made it unavailable for oxygen getting.

b. Calcium Addition Run No. 3 in Analytical Loop No. 1

Between Runs 2 and 3, the old cold trap was cut out of the loop, and a new clean cold trap was installed. The change was made in an attempt to remove all impurities from the system before the next calcium addition.

After establishing the oxygen and calcium levels for Loop No. 1, assuming that sodium in the distillation residue was Na<sub>2</sub>O, 1.06 g of calcium metal were added to the loop using a procedure similar to addition No. 2. A summary of the oxygen and calcium backgrounds before addition of the calcium is presented in Table 462-I. The loop temperature at the time of the addition was an isothermal 350°C. The calcium added was sufficient to make a 45 ppm solution if no precipitation or adsorption occurred.

Upon addition of the calcium the oxygen level of the system showed an immediate decrease, as expected. The average of thirteen samples taken over a two-week period was 0.125 ppm oxygen. The lowest oxygen level recorded was 0.066 ppm.

Table 462-1

Loop No. 1 Background Before Third Calcium Addition

Sample No.	Cold Trap	ppm O*	ppm Ca* Residue	Date
119	125°C	1.58	0.15	2/28
120	125°C	1.62	0.094	3/3
121	By pass	1.54	0.31	3/4
122	By pass	1.5	0.36	3/5
123	By pass	1.77	0.11	3/7
124	By pass	1.34	0.14	3/10

\* Referred to sodium sample weight.

The calcium level in the distillation residue of the sample taken 1 h after the calcium addition was 7.15 ppm. Subsequent samples ranged from 8.5 to 3.2 ppm with an average of 5.8 ppm. The trend appeared to be toward lower concentrations at longer times. The techniques used to determine the residue calcium content (atomic absorption) did not allow a distinction to be made between calcium metal and calcium oxide. No correlation was observed between the minor variations in calcium and oxygen levels, and no calcium ( $\pm 0.5$  ppm) was detected in the sample distillates. The calcium and oxygen sample results are summarized in Table 462-II and in Fig. 462-1.

Table 462-II

Distillation Sample Analysis After Addition of Calcium

Sample No.	Oxygen* ppm	Calcium in Residue* ppm	Calcium on cup Exterior mg	Date
125	0.21	7.15	0.216	3/11
126	0.10	3.2	0.045	3/11
127	0.10	8.5	0.035	3/12
128	0.066	7.4	0.024	3/12
129	0.069	8.0	0.046	3/13
130	0.12	6.1	0.024	3/13
131	0.20	5.15	0.047	3/14
132	0.19	5.1	0.035	3/17
134	0.07	4.1	0.056	3/18
135	0.14	4.9	0.038	3/19
136	0.12	7.1	0.050	3/20
138	0.14	5.6	0.053	3/24
140	0.09	3.2	0.039	3/26

\* Referred to sodium sample weight.

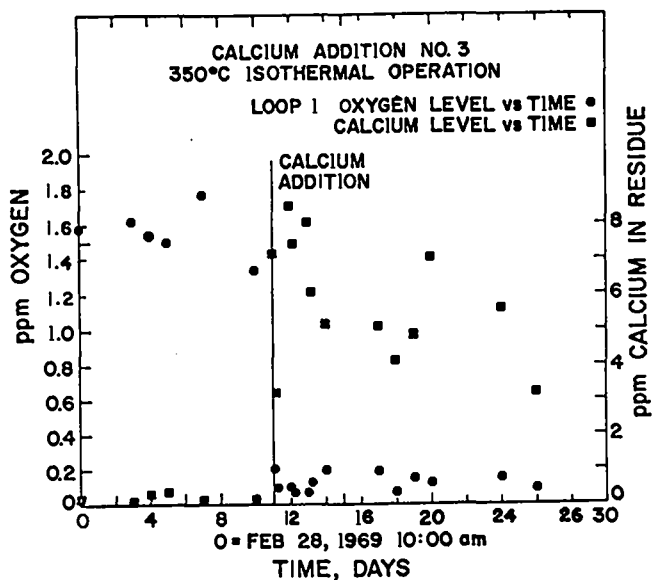


Fig. 462-1. Summary of Oxygen and Calcium Sodium Concentrations after Calcium Addition No. 3 as Determined by Distillation.

Calcium was found not only in the distillation residue but also on the outside of the distillation cup. The amount of calcium was determined by washing the outside of the cup with 0.01N HCl and analyzing the resulting solution by atomic absorption. The amounts of calcium found varied from 0.035 to 0.056 mg which would be equivalent to 8.6 to 12.8 ppm based on the total sample weight. To see whether the amount of calcium deposited would change, the sample cup was submerged for up to 2 h (normal submergence time is 15-20 min) in the sodium flowing through the sample pot. No increase in calcium deposition was observed.

A length of 3/4-in. nickel suspended inside the sodium bulk tank when the calcium was added was subsequently removed and analyzed for calcium deposition on the outside wall. Considerably more calcium was found on the nickel tubing than was found on the outside of the sample cup. For comparison, 0.050 mg calcium on the outside of the distillation cup is equivalent to 0.0016 mg/cm<sup>2</sup> which is a factor of 3-5 lower than that found on the nickel tubing. The calcium deposition found on the tubing is given in Table 462-III.

The calcium basket was pulled out of the loop eight days after it had been put in. The excess sodium was distilled from the basket in preparation for analysis. Inside the basket was a lump of

black, porous-looking material of approximately the same size and irregular shape of the calcium originally added. However, the material weighed 0.1048 g, only 10% of the original calcium weight. The material proved to be extremely pyrophoric.

Table 462-III

Calcium Deposition on Outside of Nickel Tube

No.	Length mm	Area Outside cm <sup>2</sup>	Calcium mg/cm <sup>2</sup>
1	12.0	7.30	0.0815
2	11.5	6.96	0.0805
3	15.0	9.07	0.0557

Part of the material was quickly transferred to a beaker of hexane. Water was slowly added to the hexane until the material was completely dissolved. There was no insoluble black material remaining. Thus, little, if any, elemental carbon was present. Atomic absorption analysis showed that of the 63.0 mg of material, 35.0 mg were calcium (55%) and 13.8 mg were sodium (22%).

Another piece of the material was partially hydrolyzed with a small amount of wet helium in a glass reaction chamber. Analysis by mass spectrometer showed the product gas to be mostly hydrogen with amounts of helium, water vapor, and air. Traces of methyl acetylene and phosphine were also detected.

The one remaining piece of material will be sent out for x-ray diffraction and qualitative spectrochemical analysis.

#### C. Study of Gas Diffusion Through Metals Into Sodium (J. P. Brainard, D. C. Kirkpatrick)

##### 1. General

Very little quantitative information is available on the diffusion of gases in reactor system containment materials, although the phenomenon has been observed in several high temperature, liquid-metal-cooled systems. Diffusion of nitrogen through stainless steel in such systems may be misinterpreted as evidence of an air leak in the plumbing. If quantitative information on diffusion were available, the expected rate of nitrogen influx could be estimated, and the existence of small hard-to-find leaks might be substantiated or dismissed by comparing the expected and observed rates of nitrogen accumulation in the system.

A program for determining the diffusion rate of nitrogen in stainless steels has therefore been undertaken. In later phases of the program the diffusion of O and H in stainless steels will be studied.

## 2. Current Results

The diffusion oven heaters and insulation have been completed. The system is shown in Figs. 462-2 and 462-3.

The fore vacuum, electrical, water, and liquid nitrogen plumbing are nearly complete. Liquid nitrogen level controllers were modified from two-level probes to a one-level probe and timer.

Weld adaptors have been designed and fabricated to weld the thin wall stainless steel tubing of the diffusion cell to the diffusion oven system. The adaptors have been welded to two diffusion cells. The cells are now being radiographed to

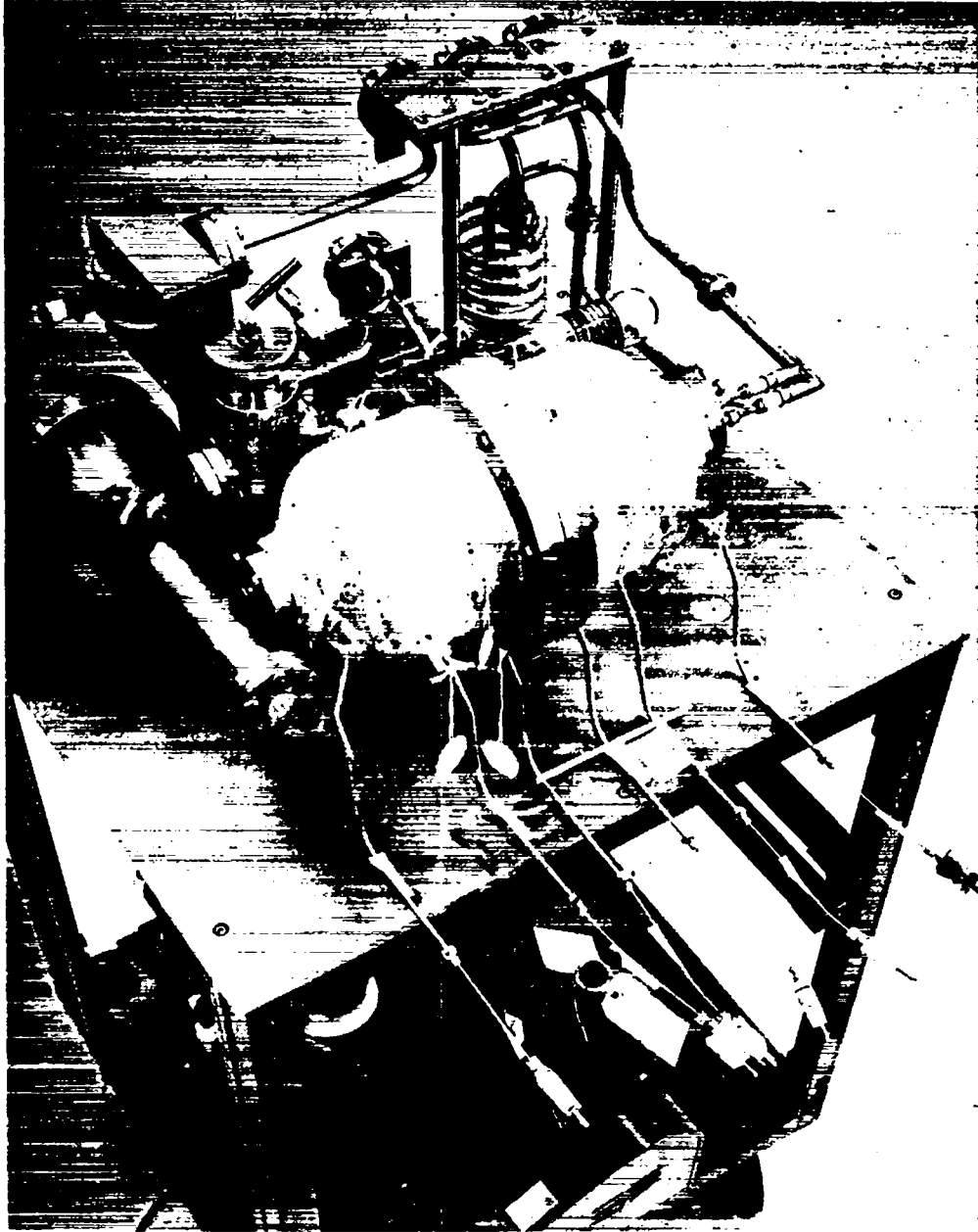


Fig. 462-2. Gas Diffusion Equipment.

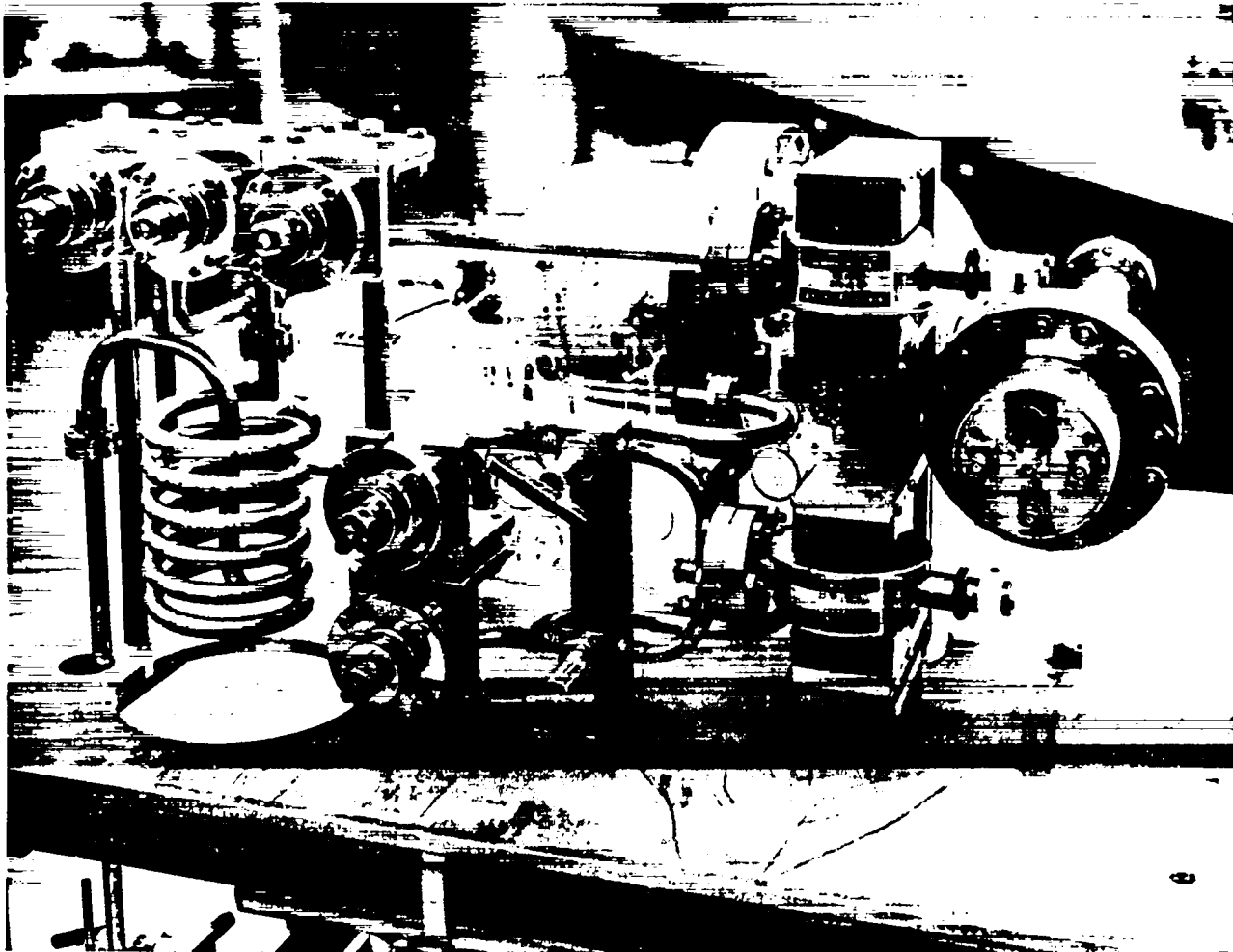


Fig. 462-3. Gas Diffusion Equipment.

determine variation in wall thickness.

The high pressure handling facility for the nitrogen and helium is now in fabrication.

#### IV. FISSION PRODUCTS IN SODIUM SYSTEMS

##### A. Study of Fission Product Gettering in Capsule Experiments

(H. A. O'Brien, C. R. Cushing)

##### 1. General

Capsule experiments have been designed to determine the distribution of gamma-active isotopes in the sodium/stainless steel/helium/adsorber system as a function of time and temperature. Gamma ray scanning permits a study of transport rates, adsorption and desorption phenomena, and the equilibrium distribution between phases to be made.

The isotope  $^{137}\text{Cs}$  is the first radioisotope to be studied in these experiments because it is a major

fission product released from irradiated nuclear fuels, and its long (27.7-yr) half-life simplifies measurements. Other candidates for study, using these experimental techniques, are  $^{131}\text{I}$  and  $^{140}\text{Ba}$ - $^{140}\text{La}$ .

In the present series of experiments, the  $^{137}\text{Cs}$  gettering and adsorption capacities of carbon and various oxides are being determined. In each test capsule a basket containing one of the materials being studied is introduced into the sodium after the cesium and sodium have come into equilibrium. The capsule is then scanned with a collimated NaI(Tl) crystal in order to determine the  $^{137}\text{Cs}$  distribution and the amount of pickup by the getter.

## 2. Current Results

### a. Gettering Behavior of Various Oxides

In the last report, it was shown that  $Al_2O_3$  and  $Cr_2O_3$  were ineffective as gettering agents for cesium in sodium. Since that time the behavior of  $Fe_2O_3$ ,  $MgO$ , and  $ZrO$  was studied and was found similar to that of the other oxides. It is concluded that none of these oxides would be useful as gettering agents for cesium in sodium.

Perhaps because of scatter in the data, no noticeable difference was observed in the effects of these oxides on the rate of cesium movement from the sodium to the vapor region. In general, it was observed that, after a slight adsorption of cesium on these oxides during the first 24 h of the experiments, which were conducted at  $500^\circ C$ , the cesium began to accumulate in the vapor region in appreciable quantities. Although there had been a noticeable accumulation of  $^{137}Cs$  in the vapor region during the preliminary equilibration period, the apparent acceleration of cesium distillation after the introduction of the oxides into the sodium suggested that either these oxides were acting to some extent as reducing agents for cesium ions, or the increased surface area of the stainless steel baskets which contained the oxides was the cause for the accelerated distillation. An additional experiment is planned in which only an empty basket will be lowered into the sodium. The result of this experiment should permit a decision to be made between the two postulated mechanisms.

### b. Behavior of Cesium Metal Versus Cesium Chloride

A question has arisen concerning the effect of cesium's valence state on its behavior in these systems. In an attempt to resolve this question, 10-mg samples of  $CsCl$  and  $Cs$  metal were irradiated in the OWR reactor. Following the irradiation, the samples were introduced into separate capsules which contained only sodium.

The distribution of  $^{134}Cs$ , both throughout the sodium and in the vapor region above the sodium, was observed by scanning the capsule with a  $NaI(Tl)$  crystal. The scanning was initiated while the capsule was at room temperature. The capsule was then heated to  $500^\circ C$  and maintained at that temperature for about 400 h.

By plotting the natural logarithm of the fraction of cesium remaining in the sodium vs time, it was observed that the resultant curves were similar to a two-component radioactive decay curve. Both components of the curve could be expressed by a first-order kinetic equation of the type,

$$A = A_0 e^{-\lambda t},$$

where  $A_0$  and  $A$  are the fractions of  $Cs$  in the sodium at times  $t_0$  and  $t$ , respectively. The term  $\lambda$  represents the first-order rate constant in units of  $sec^{-1}$ , while  $t$  is time, expressed in seconds, after the experiment was initiated.

During the first 24 h of the experiment, both  $Cs$  metal and  $CsCl$  left the sodium and entered the vapor region at a relatively rapid rate. The calculated rate constant for  $Cs$  metal during this period was  $4.3 \times 10^{-5} sec^{-1}$ , while that for  $CsCl$  was found to be  $2.0 \times 10^{-5} sec^{-1}$ . Thus, the rate for  $Cs$  metal was a factor of two greater than that for  $CsCl$ . However, at the end of the first 24 h of the experiment, the concentrations of  $Cs$  from both the metal and the  $CsCl$  in the vapor region were approximately equal, i.e., about 25%. From this point until the termination of the experiments, the rates of cesium elimination from both the metal and chloride solutions were approximately equal. The calculated rate constants during this period were  $2.2 \times 10^{-7} sec^{-1}$  for the metal and  $1.8 \times 10^{-7} sec^{-1}$  for the chloride.

Based on the fact that both metal and chloride capsules reached essentially the same cesium concentration in the vapor region after the first 24 h, and that, from that point to the end of the experiments, the rate constants for both capsules were about equal, it was concluded that the initial valence state of the cesium has little effect on its behavior in these sodium systems.

## V. ON-LINE MONITORING METHODS

### A. Plugging Meter Studies (C. C. McPheeters, J. C. Biery)

#### 1. General

Plugging meters have been used on sodium systems for many years. They are relatively simple to design, install, and operate; however, the meaning of the data obtained from these instruments has not always been clear, and as a result, the value of

the instrument has sometimes been questioned. Work previously reported<sup>1</sup> indicates that the plugging meter is a valuable instrument and that it can be used with confidence. The three areas of investigation indicated below are continuing in order to better understand the meter.

- (a) Studies of the bare orifice meter.
- (b) Observations of the operating characteristics of the oscillating plugging meter.
- (c) Determination of mass transfer coefficients from plugging meter data.

## 2. Current Results

### a. Computer Program for Processing Plugging Indicator Data

Mass transfer coefficients can be calculated from the flow and temperature traces obtained from plugging meter runs. These coefficients may be characteristic of the orifice and the flow Reynold's number in the case where the mass transfer is liquid phase controlled or of the impurity precipitating on the orifice in the case where the transfer is reaction rate controlled. Even in the situation where the coefficient is determined by the liquid flow patterns in the orifice, the actual calculation depends upon a solubility curve for the precipitating impurity and is, therefore, dependent upon the impurity. Therefore, by investigating the variations of mass transfer coefficients with flow, impurity, and orifice characteristics, a method might possibly be developed whereby the type of impurity and its concentration can be determined from its plugging meter traces.

Large quantities of data from the plugging meter traces must be analyzed to determine these functional variations. To help expedite this job, a computer program, PLUGIN, has been written to process data from the temperature and flow traces. The mathematics and processing characteristics of the program are summarized below.

#### (1) Mathematical Characteristics

The calculational procedure contains two major steps. First, the plug fraction must be calculated from the change in measured flow. Second, from the plug fraction and the sodium time-temperature plot, the mass transfer coefficients can be calculated. The double orifice effect produced by upstream throttling has been previously described<sup>1</sup> and can be represented mathematically by Eq. 2.

$$\frac{G}{G_{BO} \text{ (Valve open)}} = \frac{(1 - P_f)}{[(1 - P_f)^2 K_{OV}^2 + 1]^{1/2}} \quad (2)$$

- $G$  = Flow rate, gpm, through orifice and throttling valve.
- $G_{BO}$  (Valve open) = Flow through the bare orifice with the throttling valve wide open, gpm.
- $P_f$  = Fraction of the orifice cross sectional area covered by the plug.
- $K_{OV}$  = Orifice-throttling valve constant.
- $\frac{G_{BO} \text{ (Valve open)}}{G_V \text{ (Orifice removed)}}$  = Flow through throttled valve if orifice were removed, gpm.

Once  $P_f$  has been calculated, the rate constant can be determined from Eq. 3 for any segment of the plugging run. The derivation of Eq. 3 is presented in Reference 1.

$$k_i = \frac{\rho r_o \left[ (1 - P_{f_{i-1}})^{1/2} - (1 - P_{f_i})^{1/2} \right]}{\int_{t_{i-1}}^t (C - C_e) dt} \quad (3)$$

- $k_i$  = Mass transfer coefficient for the  $i^{\text{th}}$  time segment, g O/(cm<sup>2</sup>-h,pp.).
- $\rho$  = Density of impurity (oxygen) in the precipitate on the orifice, g O/cm<sup>3</sup>.
- $r_o$  = Radius of the bare orifice, cm.
- $P_{f_i}, P_{f_{i-1}}$  = Plug fraction at end and beginning of the  $i^{\text{th}}$  time segment.
- $C$  = Concentration of impurity (oxygen) passing through the orifice, ppm.
- $C_e$  = Equilibrium saturation concentration of impurity (oxygen) calculated from a solubility curve at the temperature of the orifice, ppm.
- $t_i, t_{i-1}$  = Time at end and beginning of time segment, h.

To calculate  $k_i$ , a solubility curve must be selected for determination of both  $C$  and  $C_e$  in the integral of Eq. 3. For all of the calculations reported here for oxygen, the semi-log linear curve of Rutkauskas<sup>2</sup> has been utilized. That curve is given as Eq. 4.

$$\log_{10} \text{ppm}(\text{oxygen}) = 8.25 \cdot \frac{3500}{T(^{\circ}\text{K})} \quad (4)$$

(2) Program Characteristics

The initial data required are  $G_{B0}$  (Valve open), initial  $P_f$ , diameter of bare orifice, number of orifice holes, saturation temperature of impurity, and density of precipitate. For each time segment of the run the following data are required: initial and final flow rate; initial and final sodium temperature; and length of time segment. From these data  $K_{OV}$  is first calculated from the initial conditions and then  $P_{f_i}$  is determined from the change in flow rate. To determine  $k_i$  the time-concentration integral must be calculated from the saturation temperature, sodium temperatures, and solubility curve. Because of the nonlinear nature of the solubility curve, the integral is calculated numerically. With the plug fractions and the concentration-time integral,  $k_i$  can be calculated directly from Eq. 3.

b. Mass Transfer Coefficients Calculated from Plugging Meter on General Electric Loop 8 at San Jose, California

Number of holes in orifice plate: 4  
 Diam of holes: 0.035 in.  
 Length of holes: 0.035 in.

Type of meter: Regenerative, flow down outside, up inside, orifice plate at bottom of inside tube.

Data from the General Electric plugging indicator runs<sup>3</sup> were processed through the computer program described above. The data from Loop 8 were divided into two runs. In both runs a plug was precipitated on a bare orifice; was partially dissolved off; and then repeatedly precipitated on and partially dissolved off in the oscillating mode. This type of run allowed changes in mass transfer coefficient to be determined as a function of Reynold's number and time. The results from both runs indicate that time has an effect on the mass transfer coefficient in that the plug appears to approach the cylindrical shape of the postulated model with repeated precipitations and dissolutions. Also, the velocity dependence observed earlier at LASL<sup>3</sup> seems to be evident in the middle portions of the precipitation run. Large deviations from the postulated model seem to be indicated early in a precipitation run when the plug may not be uniformly distributed and late in a run at

high plug fractions when bridging across the cylindrical hole may occur. Figures 462-4 through 462-7 show the mass transfer coefficient both as a function of Reynold's number and time for the two G. E. runs on Loop 8.

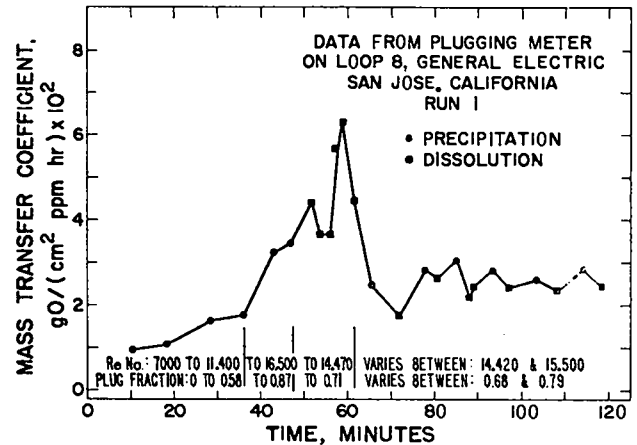


Fig. 462-4. Plugging Indicator Mass Transfer Coefficient vs Time from Run 1 on Loop 8, General Electric, San Jose, California.

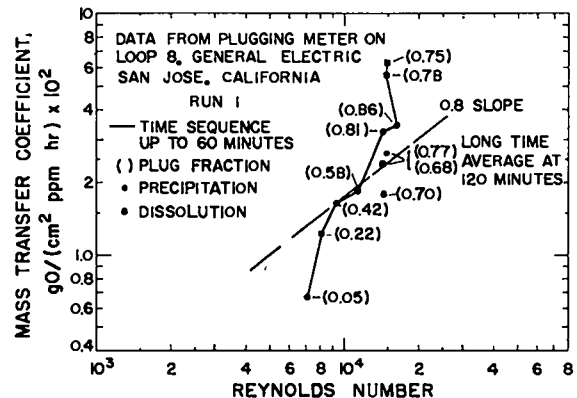


Fig. 462-5. Plugging Indicator Mass Transfer Coefficient vs Reynold's number from Run 1 on Loop 8, General Electric, San Jose, California.

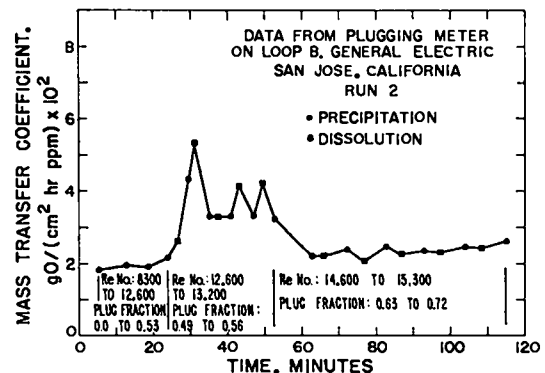


Fig. 462-6. Plugging Indicator Mass Transfer Coefficient vs Time from Run 2 on Loop 8, General Electric, San Jose, California.

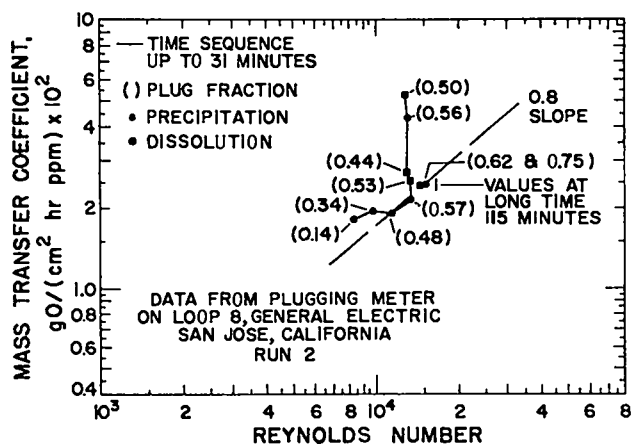


Fig. 462-7. Plugging Indicator Mass Transfer Coefficient vs Reynold's number from Run 2 on Loop 8, General Electric, San Jose, California.

The mass transfer coefficients from two runs seem to indicate that the original nucleation characteristics of the two plugs were somewhat different. In Run 1 the coefficients started below the 0.8 slope  $k(v)$  line and then approached it as the plug grew. In Run 2 the coefficients started above the 0.8 slope line and then approached it as the Reynold's number increased. An analysis of nucleation characteristics (number of nuclei initially precipitated) and their effect on the mass transfer coefficient was previously presented.<sup>3</sup> That analysis indicated that for a few initial nuclei the mass transfer coefficient should start below the 0.8 slope line (as much as a factor of 3.5 below for 1 nucleus) and then approach the line as the plug increased in size and possibly go above the line and then drop back to it. For a single nucleus, the line should be crossed at a plug fraction of 0.55 and go 29% above it and then drop back at a plug fraction of 0.75. For 16 or more nuclei, the coefficient should initially be above the 0.8 slope line and then drop back to it as the cylindrical precipitate surface is formed. In the case of 16 nuclei the coefficient could be a factor of 2.8 too large as the plug increases and should drop back to the 0.8 slope line at a plug fraction of 0.5. With 113 nuclei, the coefficient could be a factor of 3.0 too large and could be expected to drop back at a plug fraction of 0.1 to 0.2.

The two runs may be examples of the two types of cases, i.e., a few and many initial nuclei. In Run 1, the coefficient started a factor of 2 below

the 0.8 slope line and came up to it at a plug fraction of 0.4. The previous analysis suggests that the number of nuclei initially precipitated was 3-5 per hole. In Run 2 the initial coefficients started above the 0.8 slope line by a factor of 1.3 and approached the line at a plug fraction of 0.35 to 0.45. In this case 20-25 nuclei per hole are indicated.

If the nucleation characteristics were in fact different, then the initial precipitation  $\Delta C$  driving force should have been greater in Run 2 than in Run 1. This condition appears to have existed. In Run 2 the  $\Delta C$  driving force at the first noticeable flow change was 1.1 ppm while in Run 1 the driving force was 0.6 ppm.

#### c. Plugging Meter Studies at MSA Research, Evans City, Pennsylvania

A trip was made by McPheeters and Biery to MSA Research Laboratory in Evans City, Pennsylvania. A study of the behavior of plugging indicators on three sodium systems at MSA Research Laboratories was made during a visit by LASL personnel. The three loops consisted of a "high carbon" loop, a "high oxygen" loop and a "clean" loop. The results of operating the plugging indicators on these three loops are summarized below:

##### Loop 1 - (High Carbon Loop)

The cold trap was operated continuously at 250°F. Three distinct precipitable impurities were detected at three different temperatures. The three saturation temperatures were ~750, ~550, and ~320°F.

##### Loop 2 - (High Oxygen Loop)

The cold trap had been operating continuously at 440°F up to two weeks prior to these tests. Two distinct precipitable impurities were detected which had different saturation temperatures. The temperatures were ~550 and ~440°F.

##### Loop 3 - (Clean Loop)

The cold trap was operating continuously at 250°F. Only one impurity was detected in this loop, and its saturation temperature was 285 ± 5°F.

The highlights of the above studies were the detection and measurement of kinetics of as many as three impurities in a single loop. In Loop No. 1, each impurity nucleated quite readily; however, the concentrations were sufficiently low so that only a slow growth of the plug occurred. Therefore, the

temperature could be lowered sufficiently to nucleate and grow the impurities with lower saturation temperatures. Kinetic behavior of each of the lower temperature impurities were studied by oscillating the sodium temperature about the individual saturation temperatures and causing each impurity to dissolve and precipitate. Mass transfer coefficients from these data are now being calculated.

The high temperature impurities in Loops 1 and 2 (550 and 750°F) exhibited kinetics of dissolution and precipitation typical of impurities in the 1-2 ppm range. Since these impurities are precipitable in the sense that they precipitate in the plugging indicator, the question arises - why are the saturation temperatures not controlled by the cold trap temperature since the cold trap also operates by precipitating impurities? Unusually high impurity saturation temperatures in the presence of low cold trap temperatures were observed also at G. E. - San Jose, on corrosion Study Loop 9, as well as the MSA loops.

The basic difference between plugging indicators and cold traps as precipitation devices is the relative sodium velocities and degree of turbulence. Flow conditions in cold traps may be too nearly stagnant to cause nucleation and growth of the low concentration-high saturation temperature impurities which have been observed. In order to effectively remove these impurities, it may be necessary to operate a small, high-velocity cold trap at a temperature above the oxygen saturation temperature but below that of the high temperature impurities. Velocity and turbulence comparable to that found in

plugging indicators would remove these impurities because of the better nucleation and mass transfer conditions.

d. Unknown Impurities in LASL Cold Trap Loop - Kinetic Studies on Plugging Indicator

Two unknown impurities have been detected in the Cold Trap Loop after startup with the new "removable core" cold trap. (See Section III-A) The oscillating plugging indicator tended to operate initially on the impurity with a saturation temperature near 195°C but at longer times indicated a saturation temperature in the 260-270°C range for the second impurity. Dissolution and precipitation runs for the 195°C impurity were analyzed kinetically by calculating mass transfer coefficients. The impurity was assumed to be NaH, and the Addison solubility curve was used. (The oxygen level in the loop appeared to be low, with a saturation temperature below 150°C.) The results of the mass transfer coefficient calculation are tabulated in Table 462-IV.

The mass transfer coefficients on the precipitation cycle were in the range of  $1.1 \times 10^{-2}$  to  $1.5 \times 10^{-2}$  g H/(ppm(H) cm<sup>2</sup>·h). These numbers are almost identical with similar coefficients calculated for Na<sub>2</sub>O precipitation. The inference from the agreement is that the assumed species is NaH and that the solubility curve is correct since the mass transfer rate appears to be liquid phase controlled and, as a result, mass transfer coefficients for various species should be of a similar size. The quantity of data does not prove the inference; however, the process of guessing at the identity of

Table 462-IV

Mass Transfer Coefficient Data

LASL - Cold Trap Loop No. 1 - 3/13/69 - Plugging Run 1 - Unknown Impurity  
 Flow Valve Open, gpm, = 0.6550. Initial Plug Fraction = 0. Diameter 8are Orifice, in. = 0.0520  
 Saturation Temperature, °C = 195.0  
 Temperature °C = 195.0 H<sub>2</sub> Concentration, ppm = 0.303, Log<sub>10</sub> ppm = 10.211 - 5021.0/T(K) (Addison)  
 Density of Impurity in Precipitate, g/cm<sup>3</sup> = 0.0581, No. of Holes in Plate = 4

Inc No.	Reynold's Number	Velocity, cm/sec	Plug Fraction at End of Time Segment	Concentration at End of Time Segment, ppm	Concentration-Time Integral, ppm·min	Mass Transfer Coefficient gH/(ppm cm <sup>2</sup> ·h)	Average Mass Transfer Coefficient for Two Time Segments	Cumulative Time, Min
1	6719	301.9	0.7017	0.02657	4.268	0.02448	-----	15.0
2	10400	467.2	0.7466	0.02831	1.381	0.00714	0.02024	20.0
3	11760	528.3	0.8088	0.01580	1.410	0.01079	0.00898	25.0
4	13430	603.3	0.8652	0.01580	0.9597	0.01684	0.01324	28.3
5	14430	648.5	0.8772	0.03640	0.4641	0.00829	0.01405	30.0
6	14940	671.2	0.9010	0.08974	0.6102	0.01349	0.01124	32.5
7	15470	695.0	0.9166	0.3036	0.3156	0.01884	0.01531	35.0

an impurity, and then using its solubility curve to determine whether the mass transfer coefficient has a reasonable value, may be valuable in identifying impurities and verifying their solubility curves.

These data from the Cold Trap Loop may also give some insight into the  $\text{Na}_2\text{O}$ ,  $\text{NaOH}$ ,  $\text{NaH}$  system. When the  $\text{Na}_2\text{O}$  concentration is very low, the precipitation data in Table 462-IV seem to indicate that  $\text{NaH}$  was the specie precipitating. However, in other runs previously reported<sup>4</sup> at LASL, when the  $\text{Na}_2\text{O}$  plugging temperature was above  $200^\circ\text{C}$ , the plugging indicator curves for the impurity believed to be  $\text{NaH}$  behaved considerably different. For the high oxygen condition the precipitation cycle was approximately five times slower than the dissolution cycle and the mass transfer coefficients calculated by using  $\text{NaH}$  solubility data was a factor of 10 too low for the precipitation. The slowed rate may indicate that a reaction is occurring at the surface of the plug. Possibly,  $\text{NaH}$  is the first specie to precipitate. However, since  $\text{O}$  is present, a reaction on the surface may occur to produce  $\text{NaOH}$ , and the conversion to  $\text{NaOH}$  may be the rate limiting step. Data from the G. E. precipitate collection device at San Jose, California, have shown that both  $\text{NaH}$  and  $\text{NaOH}$  are present in the precipitate collected and that the ratio can vary from 100%  $\text{NaH}$  to 50%  $\text{NaH}$  - 50%  $\text{NaOH}$ .

e. Plugging Indicator Test Facility

The construction of the facility is 95% complete. (The title and purpose of the facility has been changed; it was titled Analytical Loop No. 2 previously and was to be used in the soluble getter program.) The plugging indicator, distillation sampler, and cold trap have also been fabricated, leak checked, and installed. Also the side loops for these instruments have been welded and helium leak checked. Installation of trace heaters and insulation are proceeding. Work remaining includes wiring of heater and thermocouple leads, construction of the vacuum system (from assembled parts) and system outgassing and cleanup.

The loop will be utilized in the plugging indicator program as a test unit to supply various impurities to the indicators being investigated. The kinetic behavior of a variety of impurities will be studied to characterize behavior with the impurity. Removable orifice units will be tested

to verify that the suspected specific impurity is in reality precipitating. The ultimate goal is to be able to identify and determine concentrations of a multiplicity of impurities with the plugging indicator from the kinetics of precipitation and dissolution.

VI. SAMPLING AND ANALYSIS - Laboratory Methods

A. Vacuum Distillation Studies

(G. E. Meadows, L. A. Waldschmidt, D. N. Rodgers)

1. General

The vacuum distillation technique has been shown to be a valuable method for analyses of oxygen in sodium.<sup>2</sup> As a result, the method is routinely used on many of the experimental loops at LASL. The determination of oxygen using this technique is an indirect method. The assumption is made that the sodium in the residue is  $\text{Na}_2\text{O}$  and the  $\text{O}$  concentration is computed from the residual sodium concentration. The presence of other compounds of sodium and materials capable of reducing  $\text{Na}_2\text{O}$  can influence oxygen values obtained by this technique. Distillation studies are directed toward understanding these interactions.

2. Current Results

a. Effects of Calcium on Distillation Results

Using the vacuum distillation sampler which has been installed on the sodium chemistry inert glove box, some of the effects of metallic  $\text{Ca}$  on sodium residues have been studied. A supply of solid sodium was used as the source of sodium; the concentration of oxygen in it was determined by vacuum distillation to be  $18 \pm 8$  ppm  $\text{O}$ . Known amounts of  $\text{Ca}$  metal were added to the individual sodium samples, and the distillations were carried out in the usual manner with an initial distillation temperature of  $\sim 300^\circ\text{C}$ , end of cycle temperature of  $400^\circ\text{C}$ . It was found that the oxygen concentrations as determined from sodium in the residues were substantially lowered ( $< 2$  ppm  $\text{O}$ ) when the  $\text{Ca}$  was 5-30 times the amount needed for stoichiometric reduction of the  $\text{Na}_2\text{O}$ . The following reaction perhaps explains the reduction of  $\text{Na}_2\text{O}$  in the residues:

$$\text{Na}_2\text{O} + \text{Ca} = 2\text{Na} \uparrow + \text{CaO}.$$

It was also found that 17-30 w/o of the  $\text{Ca}$  added to the  $\text{Na}$  samples was carried over with the distillate. Ninety-five percent material balances

for Ca were obtained when the Ca in the distillate and in the residues were recovered. Ca metal without sodium when heated in a similar manner was not found to distill nor exhibit a detectable weight change during the distillation cycle.

b. Off Gas From Distillation

The pressure peak previously observed at the end of the distillation did not change noticeably in tests performed after the new cold trap was installed in Analytical Loop No. 1. However, the shape of the peak has been observed to vary with the total vacuum system pressure. With the cold trap at 125°C and a system pressure of  $\sim 1 \mu$  (measured at the distillation chamber), the peak duration is one minute and the height is 2.5  $\mu$ . At a system pressure of  $\sim 0.5 \mu$ , the peak duration is 30 sec and the height is 1.5  $\mu$ . The narrower peak seems more reproducible. In an effort to run future distillations at the lower pressure, a diffusion pump was connected to the vacuum system.

B. Study of Gamma Ray Activation Analysis for C and O

(D. M. Holm, G. E. Meadows, W. J. Heyman, D. N. Rodgers, B. K. Barnes, J. L. Parker)

1. General

Many analytical techniques for the analysis of oxygen such as vacuum distillation and amalgamation methods are not specific for a given compound and give oxygen concentrations by assuming the form of the final residue being extracted or analyzed by flame photometry. Thus, analytical techniques are required which can give concentrations of oxygen and other impurities such as carbon directly without making assumptions about the chemical form of the impurity.

Photon activation of oxygen and carbon may be used to determine total impurity concentration regardless of its chemical nature. The sodium sample is irradiated by high energy photons ( $\sim 20$  MeV); the sodium is extruded from its container and then is transported pneumatically to the counter where positron annihilation radiation is detected in a very large segmented NaI crystal. The resulting count rate vs time curve is decomposed by computer analysis into O, C, and K decay curves. Thus, O and C can be determined from one sample if the K and Na interferences are kept at low levels.

2. Current Results

a. Photon Activation Run

A sodium sample drawn from a barrel of Reactor Grade Sodium was irradiated at the Los Alamos Electron Prototype Accelerator and analyzed for carbon content. The results indicated that there was not sufficient photon energy to activate carbon.

Therefore, work was done to determine the electron beam energy of the accelerator as a function of the normal operating parameters. There is no provision at the present time for monitoring electron energy during operation of the accelerator; however, a bending magnet is being designed for this purpose.

The beam energy can be determined to  $\sim 5\%$  by using simple techniques and readily available instruments. From data published by a French physicist,<sup>5</sup> a curve was constructed relating the ratio of oxygen to carbon  $^{15}\text{O}/^{11}\text{C}$  activation in Lucite (poly-methyl methacrylate) to the electron beam energy for a 300-sec irradiation time.

Several pieces of 1-1/2 x 1-1/2 x 1/8-in. Lucite were irradiated for 5 min each and then counted for 20 min with an environmental survey meter. Since the half life of  $^{15}\text{O}$  is 2.1 min and  $^{11}\text{C}$  is 20.4 min, the initial slope of the decay curve can be extrapolated back to zero time (when the irradiation stops) to give the oxygen activation. Likewise, the final slope can be extrapolated back to give the carbon activation. The ratio of these numbers determines the electron beam energy. Because of the curve's steep slope, an error of 30% in the  $^{15}\text{O}/^{11}\text{C}$  ratio corresponds to an error of only 1.6% in the beam energy (at 19 MeV).

The Lucite irradiations showed that the beam energy was considerably lower than expected. When operating at full power, the actual energy was about 17.1 MeV as compared to an expected 24-25 MeV. Further calculations by MP-Division staff have confirmed the results of the Lucite irradiations. Efforts are being made to increase the beam energy at least to 20 MeV which is a desirable energy for sodium activation analysis.

b. Sodium Shear Extruder

Since the shear extruder was not working properly, modifications were made to improve its performance. Limit switches were relocated on the sodium extruder so the extruded sodium samples would be

deposited deeper into the plastic container. A new shear block was made which seems to work much better. Also, the stroke on the shear cylinder was reduced by 1/4 in. on the down stroke. Air inlet and exhaust fittings on the extruder cylinder were relocated from the top to the side to eliminate interference with the sodium-filled tube being installed in the shear.

C. Absorption Spectrophotometry Development for Metal Impurity Analyses  
(G. E. Meadows, L. A. Waldschmidt, R. D. Gardner, R. L. Carpenter)

1. General

Soluble getter and corrosion studies require that various metal impurity concentrations be known as a function of operating conditions. One technique for determining these concentrations is absorption spectrophotometry. Refinement of this technique is being made to detect low level concentration (~1 ppm) both in vacuum distillation residues and in bulk sodium samples. The impurities to be studied are Ca, Mg, K, Fe, Ni, and Cr.

2. Current Results

a. Calcium Determination

The atomic adsorption analysis procedures have been used extensively in analyzing for Ca in both distillation residues, distillation condensates, and in sodium bulk samples in support of the calcium soluble getter and the vacuum distillation studies. Those results are presented elsewhere in this report. (See section III-B.)

b. Determination of Cesium in Sodium

A procedure has been developed for the determination of Cs in Na metal in the 20-200 ppm range using atomic absorption spectrophotometry. The sample is dissolved in ethanol and diluted with water. The maximum sensitivity is achieved at a pH of 5 in HNO<sub>3</sub> solution. Nitric acid was chosen for the neutralization after testing the effects of chloride, nitrate, acetate, sulfate, and phosphate on the absorbance of Cs. The light source is an Osram lamp, and the absorbance of Cs is measured at 8521 Å with a red-sensitive photomultiplier tube. At a sample concentration of 1 g/25 ml the Na has no absorbance, but it does reduce the sensitivity for the Cs. The absorbance-concentration curve for 0-200 ppm Cs in the presence of Na was found to be

a straight line. The procedure, applied to prepared samples containing 24, 50, 100, and 180 ppm of Cs, gave recoveries of 25 ± 1, 52 ± 1, 104 ± 1, and 184 ± 2 ppm, respectively.

D. Total Carbon Analysis Development  
(K. S. Bergstresser)

1. General

The low temperature combustion technique for total carbon analysis is being refined. By using a high sensitivity gas chromatograph for quantitative measurement of the CO<sub>2</sub> produced, it is hoped that carbon concentrations in the 1 ppm range can be determined.

2. Current Results

Several modifications were made in the proposed method and in the apparatus for the determination of C at concentrations between 1 and 10 ppm in metallic Na. The basic operations remained unchanged: low temperature combustion of the Na in O<sub>2</sub> in a Ni chamber, dissolution of the combustion product in H<sub>2</sub>O, acidification with H<sub>2</sub>SO<sub>4</sub>, collection of evolved traces of CO<sub>2</sub>, and measurement of the CO<sub>2</sub> with a sensitive gas chromatograph. Modifications included: (1) addition of the Na sample directly to the Ni chamber, without the previously used heavy Ni crucible, in order to reduce the combustion time, (2) transfer of the alkaline solution from the Ni chamber to a small glass flask before acidification so that the volume from which the CO<sub>2</sub> was swept was smaller, and (3) use of an unpacked collection trap to increase the rate of the subsequent transfer to the gas chromatograph and reduce tailing of the chromatogram.

Modifications also were made to the inert-atmosphere drybox system for handling Na and to the Na supply system to (1) prevent H<sub>2</sub>O leaks from a water-cooled heat exchanger into the drybox system, and (2) provide more heat to the compartment from which samples were dipped and thus eliminate cold-trapping of Na<sub>2</sub>O in this area. The Na supply system was dismantled and thoroughly cleaned.

The analysis system was tested by measuring known quantities of CO<sub>2</sub> added as CO<sub>2</sub> gas (equivalent to 1-4 ppm of C in 5 g of Na) or as dilute Na<sub>2</sub>CO<sub>3</sub> solution. Some satisfactory results were obtained, but occasional erratic behavior of the gas chromatograph indicated instrumental problems that remained to be corrected.

- E. Development of Remotely Operated Distillation Samplers for EBR-II  
(W. R. Wykoff, D. N. Dunning, J. R. Phillips,  
H. M. Ruess, E. O. Swickard, J. M. Reilly,  
E. L. Duran)

1. General

At the request of the AEC, part of the effort directed to a study of in-line sampling associated with the vacuum distillation analytical method has been redirected to the design and construction of remotely operated, integral sampling and distillation units for installation on the primary coolant loop of EBR-II. A version of the sampling system is also being developed for the nonradioactive secondary sodium system of EBR-II. The sampling system design is a modified engineering loop version of the laboratory model integral full-flow vacuum distillation sampling system currently in use on the Analytical Loop No. 1 and cold trap experimental facilities at the LASL. The entire sampling system will be fabricated of Type 304 stainless steel, and separation of sodium from the nonvolatile impurities will be accomplished by induction heating. The work coil of the induction heater is located within the metal envelope surrounding the distillation zone.

2. Current Results

a. Transfer Machine

The mock-up transfer machine has been built and tested. It performed satisfactorily, except that the cup transfer speeds were not optimum, and the model S0 Slo-Syn motors were marginal in torque output. The gear-box of the mock-up is being modified to provide the desired transfer speeds, and to accept Model 250 Slo-Syn motors. With these changes, the mock-up will become Unit 1, (the unit to be retained by LASL).

Design of the electronic circuitry for control of the transfer machine is completed. Fabrication of the prototype unit is in progress (printed circuitry is being used).

b. Vacuum-Inert Gas System

Three complete systems have been built and tested and are ready for use.

c. Control and Instrumentation

A control system has been designed which will permit semi-automatic operation of the entire sam-

pling procedure. Twenty-two distinct steps are involved in the procedure. Manual mode of operation is also provided, with key-lock control. Mock-up systems have been built and tested and modified until satisfactory operation was achieved. Unit 1 is now being fabricated.

VII. COVER GAS AND MAINTENANCE ATMOSPHERES

- A. Development of a High Temperature Quadrupole Mass Spectrometer for Cover Gas Analysis  
(J. P. Brainard, D. C. Kirkpatrick, C. R. Winkelman)

1. General

The purpose of this research is to develop a method for continuous on-line analysis of high temperature (up to 650°C) cover gas in an LMFBR. The analyzer must be capable of detecting impurities such as nitrogen, oxygen, hydrogen, carbon dioxide, methane, and fission products in the cover gas with a sensitivity varying from the part-per-million range to the percent range. A response time of about 1 min is necessary if the analytical data are to serve as an error signal for activating devices for continuous control of cover gas composition.

A quadrupole mass spectrometer was obtained in order to meet the above requirements. It is believed that reasonably representative sampling can be accomplished by transporting the sample gas in sodium loop containment materials and at sodium loop temperatures until it has passed through the spectrometer for analysis.

2. Current Results

A paper is being prepared for an American Vacuum Symposium in April, 1969, on the gas beam studies. The gas beam flux distribution has been measured for three different collimated hole structures (bundles of a few thousand tubes) and for a single 7-mil i.d. tube.

The 7-mil i.d. long tube with a 7-mil aperture about 0.1 in. away has been chosen for the initial gas beam source for the gas analyzer. The target for the molecular beam is a small opening in the ionization chamber of the mass spectrometer. The closer the gas source is to this opening, the greater the beam divergence that can be accepted and hence, the less total gas flow that would be needed for a fixed beam flux. The aperture must be far enough away from the gas source to make it appear a point source (~15 times the diameter of

the source). This means the large diameter of the collimated hole structure must be much farther away from the ionization chamber than does the 7-mil i.d. tube. For this reason the 7-mil tube can place a given molecular beam in the ion source with less than half the total gas flow of the collimated hole structure source even though the collimated hole structures have a more resolved flux distribution. Another consideration is the diameter of the aperture. The aperture must be about the diameter of the gas source for efficient gas beam formation. Too large an aperture will allow effusion of random gas from the collimation region of the gas analyzer system into the ionization chamber. The small aperture of the 7-mil tube will reduce this problem.

A gas flux distribution was obtained from the 7-mil i.d. tube and 7-mil aperture to give an 8° divergence from the beam axis. This divergence is approximately the amount necessary for the gas analyzer beam.

More work on the precise alignment of the gas beam with the ion source of the mass spectrometer is in progress. The quadrupole residual gas analyzer will be placed in a bellows on the cover gas

analyzer system to help align the cover gas beam with the ion source. Variations in welds and copper seals were felt too much to maintain tolerances without this flexibility.

The system vacuum envelope has been designed. Only design of the gas beam source installation remains.

#### REFERENCES

1. "Quarterly Status Report on the Advanced Plutonium Fuels Program," April 1 - June 30, 1968, Report LA-3993-MS, Los Alamos Scientific Laboratory.
2. V. J. Rutkauskas, "Determination of the Solubility of Oxygen in Sodium Using the Vacuum Distillation Analytical Technique," Report LA-3879, Los Alamos Scientific Laboratory, 1968.
3. "Quarterly Status Report on the Advanced Plutonium Fuels Program," October 1 - December 31, 1968, Report LA-4114-MS, Los Alamos Scientific Laboratory.
4. "Quarterly Status Report on the Advanced Plutonium Fuels Program," July 1 - September 30, 1968, Report LA-4073-MS, Los Alamos Scientific Laboratory.
5. C. Englemann, "Emploi de Particules Antres Que Les Neutrons en Analyse Par Activation," CEA-R-2559, Centre D' Etudes Nucleaires de Saclay, 1964.

## PROJECT 463

### CERAMIC PLUTONIUM FUEL MATERIALS

Person in Charge: R.D. Baker

Principal Investigator: J.A. Leary

#### I. INTRODUCTION

The principal goals of this project are to prepare pure, well characterized plutonium fuel materials, and to determine their high temperature properties. Properties of interest are (1) thermal stability, (2) thermal expansion, (3) thermal conductivity, (4) phase relationships by differential thermal analysis, (5) structure and phase relationships by x-ray diffraction, high temperature x-ray diffraction, neutron diffraction and high temperature neutron diffraction, (6) density, (7) hardness and its temperature dependence, (8) compatibility including electron microprobe analysis, (9) compressive creep (deformation).

In addition to phase equilibria and general properties, specific thermodynamic properties such as free energy of formation by vaporization equilibria in the 1000-2000°C temperature range with mass spectrometer identification of vapor species, free energy of formation by electromotive force measurements in the 450-1200°C temperature range, and heat capacity and heat of transition are being determined.

#### II. SYNTHESIS AND FABRICATION

(R. Honnell, M.W. Shupe, R. Nance, D. Kelley, C. Gilley, J.A. Leary)

##### 1. Carbides

To meet the material needs of the physical property measurement program, a number of different carbide

compositions were synthesized and fabricated into useful forms for testing. Compositions made were: plutonium, uranium, and plutonium substituted uranium dicarbides (plutonium replacing approximately 1.6 to 16.5 a/o of the uranium in the substituted dicarbides); plutonium carbides of a composition  $\text{PuC}_x$  where  $1 \leq x \leq 1.5$  and plutonium substituted uranium monocarbide (plutonium replacing from 5 to 25 a/o of the uranium). Previously described synthesis procedures were employed with these exceptions: Since PuC melts at 1655°C, the sintering and annealing temperatures of 1800 and 1600°C, respectively, were lowered to 1500°C or less; and the 850°C hydrogen treatment cycle was omitted for those materials having a carbon to metal atom ratio greater than one.

It can be shown theoretically that in an equilibrium mixture of either metal and monocarbide or monocarbide and sesquicarbide, the plutonium will preferentially be depleted in the monocarbide phase. This was evaluated experimentally by preparing sample pellets of the following types:

Sample 68-0369 consisted of a pellet from lot 7-60-3D having the composition  $\text{U}_{0.802}\text{Pu}_{0.198}\text{C}_{1-13}$  after heat treatment 24 hr at 1500°C.

The volume fraction of  $\text{M}_2\text{C}_3$  phase was approximately 28 percent by point count analysis. In this

specimen, the plutonium x-ray intensity in the  $M_2C_3$  phase was approximately 100 percent greater than that from the MC phase. The uranium x-ray intensity was approximately 25 percent less than from the MC phase. The carbon x-ray intensity in the  $M_2C_3$  phase was approximately 45 percent greater than that from the MC phase.

Sample 68-0225 consisted of a pellet of single phase MC having the composition  $U_{0.8}Pu_{0.2}C_{0.99}$  after heat treating for  $1800^\circ - 4 \text{ hr} + 1400^\circ - 2 \text{ hr}$  (normal sintering cycle, lot 7-26-1, pellet no. 926).

Using this specimen as a reference, the intensities of the constituents in sample 68-0369 were as follows:

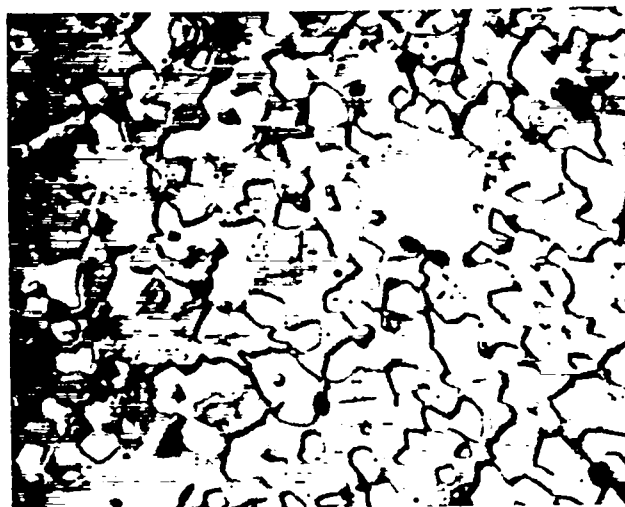
- (a) In the  $M_2C_3$  phase, the plutonium intensity was 42 percent greater than that in sample 68-0225
- (b) In the  $M_2C_3$  phase, the uranium intensity was 16 percent less than in sample 68-0225
- (c) In the MC phase, the plutonium intensity was 27 percent less than in sample 68-0225
- (d) In the MC phase, the uranium intensity was 10 percent greater than in sample 68-0225.

Photomicrographs of these specimens are shown in Figure 463-1. Chemical purity is shown in Table 463-I.

Table 463-I

Spectrochemical Analysis on  $(U, Pu)C_{1.13}$  Pellets

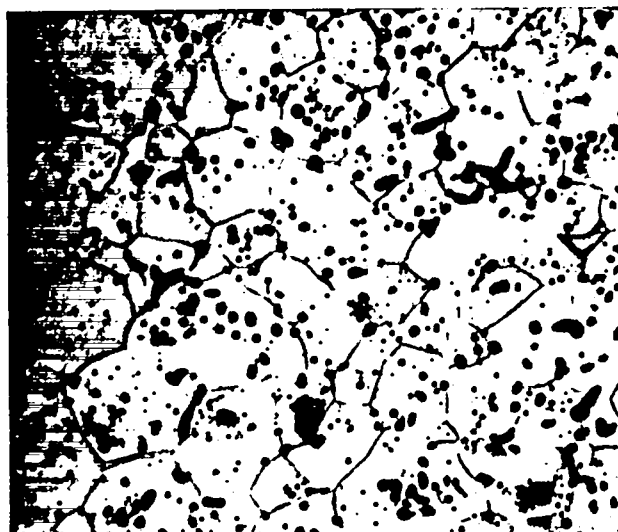
Element	ppm	Element	ppm
Li	< 2	Co	10
Be	< 1	Ni	< 10
B	2	Cu	2
Na	< 5	Zn	< 10
Mg	< 5	Zr	< 100
Al	< 10	Nb	< 100
Si	95	Mo	15
P	< 100	Cd	< 10
Ca	< 5	Sn	< 5
Ti	< 50	Ta	< 1000
V	< 5	W	< 1000
Cr	20	Pb	< 10
Mn	< 5	Bi	< 2
Fe	170		



Mount No. 68-0369

1:1:1 Etch

380X



Mount No. 68-0225

1:1:1 Etch

380X

Figure 463-1. Photomicrographs of Carbide Samples

From these results, the compositions of the two phases in sample 68-0369 are calculated to be  $(U_{0.70}Pu_{0.30})_2C_3$  and  $U_{0.85}Pu_{0.15}C$ . Theoretically, the compositions in equilibrium at  $1500^\circ C$  should be approximately  $(U_{0.66}Pu_{0.34})_2C_3$  and  $U_{0.85}Pu_{0.15}C$ . In view of the estimates used for some of the thermodynamic properties, these results are in good agreement. Similar results were obtained on mixed carbide pellets produced by carbothermic reduction of the oxides; these

samples contained approximately 0.3 percent by wt. oxygen.

## 2. Nitrides

The preparation of pure single phase PuN pellets for the UK was reported last quarter (LA-4114-MS).

Companion pellets had the following properties:

### Chemical composition

Pu (Theor = 94.5 w/o)	94.5
N (Theor = 5.55 w/o)	5.49
O, ppm by wt	330
U, ppm by wt	26
Th, ppm by wt	<75
Spectrochemical Analysis	(Table 463-II)

### X-ray powder diffraction analysis

Single phase PuN.  $a = 4.9046 \pm 0.0004 \text{ \AA}$

### Density:

12.2 g/cc

## 3. Oxides

Reference pellets of (U, Pu)O<sub>2</sub> are needed for an exchange with the UK. Pure UO<sub>2</sub> and PuO<sub>2</sub> powders were blended and ball milled to -325 mesh for 24 hr. This powder mixture was then pressed and sintered at 1600°C for 6 hr in Ar - 6% H<sub>2</sub> that contained 0.4 mm H<sub>2</sub>O to adjust the O/M ratio. A total of 160 pellets were prepared. X-ray powder diffraction analysis indicated that the pellets contained two solid solution phases.

Table 463-II

### Spectrochemical Analysis of PuN Pellets for UK

Element	ppm by wt.	Element	ppm by wt.
B	< 0.5	Zr	< 300
Si	10	Nb	< 300
Ti	< 50	Mo	< 30
Cr	< 2	Cd	< 3
Mn	< 0.5	Sn	< 1
Fe	< 5	Ta	< 1000
Ni	< 5	W	< 30
Cu	1	Pb	1
Zn	< 5	Bi	< 0.5

Therefore additional experiments were conducted to develop a procedure for producing single phase mixed oxide. Results are summarized in Table 463-III. Apparently the best procedure is to form the solid solution by sintering in CO<sub>2</sub>, followed by adjusting the O/M ratio.

## III. PROPERTIES

### 1. X-ray Powder Diffraction Studies

(M. W. Shupe, C. W. Bjorklund, R. M. Douglass)

A series of compositions in the plutonium-carbon system were prepared (mainly by powder metallurgy methods), heat treated, and analyzed by conventional x-ray powder techniques. The results, which are summarized in Table 463-IV, clearly indicate that both PuC and Pu<sub>2</sub>C<sub>3</sub> have a range of composition. In addition, the lattice dimension of Pu<sub>2</sub>C<sub>3</sub> in the presence of PuC is constant at an average value of 8.1287 Å from a C/Pu

Table 463-III

### Effect of Sintering Conditions on U<sub>0.75</sub>Pu<sub>0.25</sub>O<sub>2</sub> Solid Solution Formation

First Firing Conditions	X-ray Diffraction Analysis	Second Firing Cycle	X-ray Diffraction Results
1. 1600°C - 12 hr. 6% H <sub>2</sub> - Ar - 0.4 mm H <sub>2</sub> O	Multiphase	[1600°C - 4 hr. - CO <sub>2</sub> ] + [6% H <sub>2</sub> - Ar (Tank) - 4 hr.]	Single Phase $a = 5.4529 \pm 0.0004 \text{ \AA}$
2. 1600°C - 15 hr. 6% H <sub>2</sub> - Ar (Tank)	Multiphase	[1600°C - 4 hr. - CO <sub>2</sub> ] + [4 hr. 6% H <sub>2</sub> - Ar (Tank)]	Single Phase $a = 5.4544 \pm 0.0002 \text{ \AA}$
3. [1650°C - 4 hr. - CO <sub>2</sub> ] + [4 hr. 6% H <sub>2</sub> - Ar (Tank)]	Single Phase	(none)	Single Phase $a = 5.4531 \text{ \AA}$
4. [1650°C - 4 hr. - CO <sub>2</sub> ] + [4 hr. 6% H <sub>2</sub> - Ar (Tank)]	Single Phase	[1625°C - 8 hr. - 6% H <sub>2</sub> - Ar (Dried)]	Multiphase
5. [1625°C - 3.5 hr. Ar] + [4.5 hr. 6% H <sub>2</sub> - Ar (Moist)]	Multiphase	[1625°C - 8 hr. 6% H <sub>2</sub> - Ar (Dried)]	Multiphase
6. 1625°C - 8 hr. 6% H <sub>2</sub> - Ar (Dried)	Multiphase		

Table 463-IV

Effect of Changing Composition on Lattice Dimensions of Plutonium Carbides

Specimen	Composition	Heat Treatment	Phase	Lattice Dimension Å
7-37-1	$\text{PuC}_{0.381}\text{O}_{0.001}\text{N}_{0.000}$	as melted	$\alpha$ Pu PuC	minor $4.9501 \pm 0.0007$
7-37-2	$\text{PuC}_{0.705}\text{O}_{0.000}\text{N}_{0.000}$	as melted	$\alpha$ Pu PuC	minor $4.953 \pm 0.002$
6-123-1	$\text{PuC}_{0.847}\text{O}_{0.003}\text{N}_{0.004}$	$1300^{\circ}\text{C}$ -2 hr. -Ar	PuC	$4.953 \pm 0.002$
6-123-2	$\text{PuC}_{0.992}\text{O}_{0.003}\text{N}_{0.004}$	$1300^{\circ}\text{C}$ -2 hr. -Ar	PuC $\text{Pu}_2\text{C}_3$	$4.9776 \pm 0.0005$ $8.1283 \pm 0.0003$
6-123-3	$\text{PuC}_{1.228}\text{O}_{0.004}\text{N}_{0.004}$	$1300^{\circ}\text{C}$ -2 hr. -Ar	PuC $\text{Pu}_2\text{C}_3$	$4.9785 \pm 0.0004$ $8.1289 \pm 0.0003$
6-123-4	$\text{PuC}_{1.343}\text{O}_{0.003}\text{N}_{0.003}$	$1300^{\circ}\text{C}$ -2 hr. -Ar	PuC $\text{Pu}_2\text{C}_3$	$4.9804 \pm 0.0009$ $8.1289 \pm 0.0002$
7-5-1	$\text{PuC}_{1.485}\text{O}_{0.001}\text{N}_{0.002}$	$1600^{\circ}\text{C}$ -6 hr. + $1400^{\circ}\text{C}$ -2 hr. -Ar	$\text{Pu}_2\text{C}_3$ $\text{Pu}_2\text{C}_3$	$8.1306 \pm 0.0006$
7-19-2	$\text{PuC}_{1.500}\text{O}_{0.001}\text{N}_{0.002}$	$1700^{\circ}\text{C}$ -3 hr. + $1600^{\circ}\text{C}$ -2 hr.	$\text{Pu}_2\text{C}_3$	8.1313
7-19-1	$\text{PuC}_{1.58}\text{O}_{0.001}\text{N}_{0.000}$	$1700^{\circ}\text{C}$ -3 hr. + $1600^{\circ}\text{C}$ -2 hr.	$\text{Pu}_2\text{C}_3$	8.1317
7-21-1	$\text{PuC}_{2.12}\text{O}_{0.001}\text{N}_{0.001}$	$1700^{\circ}\text{C}$ -3 hr. + $1600^{\circ}\text{C}$ -2 hr.	$\text{Pu}_2\text{C}_3$	$8.1324 \pm 0.0002$
7-11-1	$\text{PuC}_{1.678}\text{O}_{0.001}\text{N}_{0.002}$	$1700^{\circ}\text{C}$ -3 hr. + $1600^{\circ}\text{C}$ -2 hr.	$\text{Pu}_2\text{C}_3$	$8.1324 \pm 0.0004$

ratio of 0.992 to 1.343. This value increases significantly at  $\text{PuC}_{1.485}$ , which indicates that this substoichiometric composition is in the single phase " $\text{Pu}_2\text{C}_3$ " region. The upper limit of the " $\text{Pu}_2\text{C}_3$ " region apparently lies between  $\text{PuC}_{1.58}$  and  $\text{PuC}_{2.12}$ .

## 2. Differential Thermal Analysis (J.G. Reavis, L. Reese)

Samples of single phase  $\text{U}_{0.8}\text{Pu}_{0.2}\text{C}$  have been observed by use of differential thermal analysis techniques and have been quenched for metallographic examination to determine solidus and liquidus temperatures.

(U, Pu) $\text{C}_2$  compositions containing 0 to 50%  $\text{PuC}_2$  have been observed by DTA during preparation of quenched samples for x-ray powder diffraction analysis. Transition temperatures observed were generally in good agreement with those previously reported. X-ray analyses are in agreement with but do not prove identities tentatively assigned to the various regions of the  $\text{MC}_2$  isopleth.

### Transition Temperatures of (U, Pu) Monocarbides:

Previous observations of near-single phase  $\text{U}_{0.8}\text{Pu}_{0.2}\text{C}$  led to the assignment of  $2285 \pm 20^{\circ}$  and  $2485 \pm 20^{\circ}$  as

solidus and liquidus temperatures, respectively. DTA observations of single phase materials show gradual heating arrests becoming detectable at  $2305^{\circ}$  and metallographic analysis of quenched samples shows what is believed to be the beginning of liquid phase formation at  $2275^{\circ}$ . The liquidus temperature determined in this series was  $2475^{\circ}$ . Taking all measurements into account, best solidus and liquidus temperatures for single phase  $\text{U}_{0.8}\text{Pu}_{0.2}\text{C}$  should remain  $2285 \pm 20^{\circ}$  and  $2485 \pm 20^{\circ}$ , respectively.

### Identification of Species in the (U, Pu) $\text{C}_2$ System:

Previous observations led to the plot of thermal arrests in the (U, Pu) $\text{C}_2$  system shown by Fig. 463-2, which was previously reported and is included here for ready reference. More recently, samples containing 0-5 m/o  $\text{PuC}_2$  (excess C) have been quenched from selected temperatures in an attempt to identify phases existing at these temperatures. Incidental to these sample treatments, thermal arrests were observed by DTA and were found to be in generally good agreement with Fig. 463-2. Results of phase identification by x-ray powder diffraction methods is given in Table 463-V. The

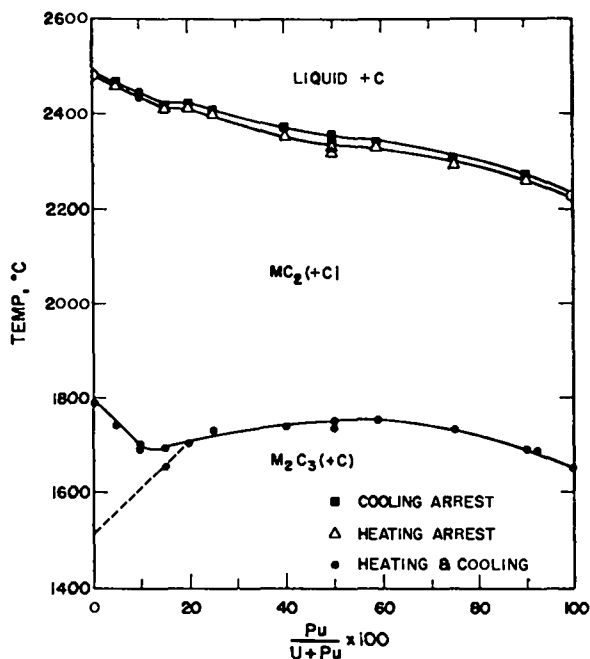


Figure 463-2. Major Phase Fields in the High Temperature - High Carbon Region of the U-Pu-C System

results listed here can be misleading if reaction rates are ignored, but they also give some indication of reaction rates. It has been reported<sup>(1)</sup> that tetragonal  $UC_2$  decomposes to  $U_2C_3 + C$  at  $1515^\circ$  and lower temperatures but that the decomposition is extremely slow, requiring many days for detectable  $U_2C_3$  to form. The results shown in Table 463-V are in agreement with this and also show the acceleration of this decomposition by the addition of  $PuC_2$ . The degree of acceleration appears to be progressive as the  $PuC_2$  concentration is increased from 5 to 50 m/o.

Other investigators have shown that  $UC_2$  is cubic above  $1795^\circ$ <sup>(1)</sup> and  $PuC_2$  is cubic above  $1700^\circ$ ,<sup>(2)</sup> but that cubic  $MC_2$  cannot be "quenched in" because of the extreme rapidity of the diffusionless cubic to tetragonal transition. The stable form of  $UC_2$  between  $1515$  and  $1795^\circ$  was found to be tetragonal.

The present results are consistent with these observations and lead to tentative assignment of identities to the phase fields of Fig. 463-2. It appears that the region labelled " $MC_2 (+ C)$ " contains cubic solid solution  $MC_2 + C$ . The region labelled " $M_2C_3 + C$ " contains body

Table 463-V  
Identity of Phases in (U, Pu) $C_2$  Samples Quenched from Selected Temperatures

Composition	Annealing or Quench Temp., °C	Annealing Time at Quench Temp.	Phases Found <sup>(a)</sup>
$UC_2$	1800	< 1 min.	tet. $UC_2$
$UC_2$	1460	63 hr.	tot. $UC_2$
$U_{95}Pu_5C_2$	1800	< 1 min.	tot. $MC_2$
$U_{95}Pu_5C_2$	1690	< 1 min.	tot. $MC_2$
$U_{95}Pu_5C_2$	1460	18 hr.	major b. c. o. $M_1C_2$ , minor tet. $MC_2$
$U_{90}Pu_{10}C_2$	1730	- 1 min.	tot. $MC_2$
$U_{90}Pu_{10}C_2$	1650	10 min.	major tet. $MC_2$ , trace b. c. o. $M_1C_2$
$U_{80}Pu_{20}C_2$	1650	1 hr.	major tet. $MC_2$ , minor b. c. o. $M_2C_3$
$U_{70}Pu_{30}C_2$	1800	3 min.	major tet. $MC_2$ , trace b. o. o. $M_2C_3$
$U_{50}Pu_{50}C_2$	1675	4 min.	b. o. c. $M_1C_2$

(a) Graphite lines were also observed in the diffraction patterns.

centered cubic solid solution  $M_2C_3 + C$ . At least part of the triangular region near  $1700^\circ$  reaching out to about 20 m/o  $PuC_2$  contains tetragonal  $MC_2 (+ C)$  as the stable phase.

### 3. X-ray Powder Diffraction (C. W. Bjorklund, R. M. Douglass)

The results of x-ray powder diffraction analyses of plutonium fuel materials are incorporated in other sections of this report.

The lattice dimensions of several of the plutonium compounds for which self-irradiation damage is being studied as a function of time were remeasured approximately 6 mos. after the previous set of measurements. The compounds  $PuO_2$ ,  $PuN$ , and  $Pu_2C_3$ , all with normal Pu isotopic composition, are now 5.7, 5.3, and 3.6 years old, respectively, and their lattices have expanded to within 94%, 97%, and 81%, respectively, of the saturation values predicted by a least squares fit of each set of data to the equation

$$\frac{\Delta a_t}{a_0} = A (1 - e^{-Bt}) \quad (1)$$

( $\Delta a_t$  is the lattice expansion measured at time  $t$ ,  $a_0$  is the lattice dimension at time 0, and A and B are constants.)

The lattice expansion of a 5 yr. old sample of  $PuO_2$  enriched with 3.75 a/o  $^{238}Pu$  has now been saturated for almost 4 yrs.

Measurements of the lattice expansion of enriched  $PuO_2$  as a function of time and temperature have been applied to the equation derived previously

$$\frac{\Delta a_t}{a_0} = \frac{P_1 P_2}{P_2 + P_3 e^{-P_4/T}} \left[ 1 - e^{-(P_2 + P_3 e^{-P_4/T}) t} \right] \quad (2)$$

in which the constants  $P_1$ ,  $P_2$ ,  $P_3$ ,  $P_4$ , and  $a_o$  were evaluated by a least squares technique. The  $\text{PuO}_2$  used in this study was enriched with 3.75 a/o  $^{238}\text{Pu}$ . In order to apply Eq. 2 the normal  $\text{PuO}_2$  for which the lattice expansion was measured at only one temperature, the values of  $P_2$  and  $P_3$  were recalculated for normal  $\text{PuO}_2$ . These calculations were based on the experimental observation that the lattice expansion of  $\text{PuO}_2$  at saturation is independent of the dose rate which, in turn, is proportional to the average disintegration constant  $\lambda$  of the material. It can be shown that the parameters  $\underline{P}_2$  and  $\underline{P}_3$  in Eq. 2 contain the disintegration constant  $\lambda$  as a factor, whereas the parameters  $\underline{P}_1$  and  $\underline{P}_4$  do not. The resultant equation for normal  $\text{PuO}_2$  was

$$\frac{\Delta a_t}{a_o} = \frac{3.22_1 \times 10^{-3} \times 1.15_1 \times 10^{-3}}{1.15_1 \times 10^{-3} + 6.27_6 \times 10^{-3} e^{-1321/T}} \left[ 1 - e^{-(1.15_1 \times 10^{-3} + 6.27_6 \times 10^{-3} e^{-1321/T}) t} \right] \quad (3)$$

The agreement between the experimental data obtained for normal  $\text{PuO}_2$  at room temperature and the values calculated by means of Eq. 3 was quite reasonable, indicating that the same technique might be applied to  $\text{PuO}_2$  of any isotopic composition.

As the time  $t$  approaches infinity, Eq. 2 reduces to

$$\frac{\Delta a_{\text{sat.}}}{a_o} = \frac{P_1 P_2}{P_2 + P_3 e^{-P_4/T}} \quad (4)$$

An annealing curve for  $\text{PuO}_2$  was calculated by means of Eq. 4 and compared with annealing data in the literature.<sup>(3)</sup> Satisfactory agreement was obtained over the range  $-198^\circ$  to  $\sim 500^\circ\text{C}$ , but the calculated curve leveled off too soon at higher temperatures. Attempts were made to extend the temperature range by including arbitrary data showing a negligible lattice expansion at  $1000^\circ\text{C}$  in keeping with experimental observations without success. The constant  $P_4$  in Eq. 4 is proportional to an average annealing activation energy, and apparently cannot be adjusted to accommodate a larger temperature range. Annealing undoubtedly occurs by several processes with different activation energies, particularly at the higher temperatures. More than one activation energy term may be required in Eq. 4 to match the experimental data above  $500^\circ\text{C}$ .

#### 4. High Temperature X-ray and Neutron Diffraction (J. L. Green, K. L. Walters)

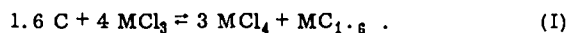
During the time that the neutron diffraction work was done on the  $^{240}\text{PuC}_{1-x}$  target, oxygen and nitrogen analyses of the sample material were not done. These analyses involve the unrecoverable loss of the analytical samples. It was later decided that the uncertainties introduced by the possible effect of oxygen and nitrogen contamination on the magnetic properties of  $\text{PuC}$  were sufficient to justify the material losses. The diffraction target was, therefore, broken open and sampled in an inert atmosphere box. The target had been stored for a considerable length of time, therefore, the results should probably be regarded as upper limits. The

analyses showed that the target material contained 240 ppm  $\text{N}_2$  and 1000 ppm  $\text{O}_2$ . This is equivalent to approximately 2 at % of the total carbon content. It is felt that it is unlikely that contamination levels of this magnitude would result in significant magnetic perturbations.

Most of the computer programs used for crystallographic calculations have been adapted for use on the CDC 6600, which is now the primary computing machine. In addition, a linear least squares fitting program has been set up specifically for fitting crystallographic thermal expansion data.

#### 5. Thermodynamic Properties of Plutonium Compounds by Electromotive Force Techniques (G. M. Campbell)

Sufficient data has now been obtained on the systems  $\text{PuC}_{1.6}$ ,  $\text{UC}_{1.6}$ , and  $\text{U}_{0.8}\text{Pu}_{0.2}\text{C}_{1.6}$  so that an unambiguous interpretation can be made. In the absence of the pure metal, Pu or U as the case may be,  $\text{M}^{+4}$  is generated in the  $\text{LiCl-KCl}$  electrolyte through the mechanism



In the presence of  $\text{M}^{+4}$  the reaction



at the electrode surface competes with reaction (I) preventing thermodynamic information from being gained from reaction (I) alone. Although the reactions result

in a mixed potential which is dependent on the activities of  $M^{+4}$  and  $M^{+3}$ , no dissolution occurs and the potentials are stable over long periods of time. One cell containing  $PuC_{1.6}$  electrodes was operated for a period of 1006.4 hr at temperatures ranging between 644 and 744°C. The  $Pu^{+4}$  activity increased as the temperature was raised. This was indicated by the chronopotentiometric trace.

Cells containing the pure metal vs one of the electrodes undergo metal enrichment at the  $MC_{1.6}$  electrode due to the reduction of  $M^{+4}$  in Eq. (I) by the pure metal. These cells are unstable after 100 hr operation.

The theory necessary for obtaining thermodynamic information from the mixed potential has now been formulated and the experimental technique is being checked out. Results so far indicate that it will be successful. It appears certain that reliable thermodynamic data on the  $PuC_{1.6}$  and  $UC_{1.6}$  can be obtained. Additional instrumentation will be required for successful studies to be made on the solid solution system. One experiment was carried out on this system which indicated conclusively that both U and Pu are involved in the metal-electrolyte equilibrium.

#### 6. Thermodynamic Properties from Vaporization Studies

(R. A. Kent)

Mass Spectrometric Studies of the Vaporization of Plutonium Compounds. Manuscripts detailing the completed investigations of the vaporization behavior of Pu metal and  $PuN_{0.98}$  have been accepted for publication in the Journal of High Temperature Science.

The study of the vaporization behavior of the Pu-C system as a function of both composition and temperature is being continued. These studies indicate that, above the solid mixture  $Pu-C-Pu_2C_3$ , the  $Pu(g)$  pressure is  $4.6 \times 10^{-6}$  atm at 1800°C, and above the solid mixture  $Pu_2C_3-C$  the value is  $1.0 \times 10^{-7}$  atm at the same temperature. When the  $Pu(g)$  pressure data above  $Pu-C-Pu_2C_3$  and above  $Pu_2C_3-C$  are combined with thermodynamic functions published for  $PuC^{(4)}$  and estimated for  $Pu_2C_3$  one obtains:

	$\Delta H_f^{298}$ kcal mole <sup>-1</sup>	$\Delta S_f^{298}$ eu
$PuC_{0.87}(s)$	- 10.2	+ 3.0
$PuC_{1.50}(s)$	- 12.2	+ 5.3

At  $1660 \pm 15^\circ C$ , the sesquicarbide transforms to the dicarbide. Above this temperature, a detailed knowledge of the Pu-C phase diagram is lacking. The vapor above the solid mixture  $PuC_{2-x}-C$  contains both gaseous Pu and  $PuC_2$ . The study of this region of the phase diagram will be completed when the new Hitachi-Perkin Elmer magnetic mass spectrometer is installed. This unit is now scheduled for delivery to LASL on May 1, 1969.

#### 7. High Temperature Calorimetry (A. E. Ogard, G. Melton)

In a continuing effort to determine the high temperature physical and chemical properties of plutonium-containing materials the high temperature heat content of these materials is being determined.

During this reporting period, several features of aneroid calorimeters have been investigated that greatly affect the experimental accuracy obtainable. These features should not be peculiar to this particular calorimeter but should apply to all Cu block calorimeters used for high temperature drop calorimetry (higher temperatures than 1400°C).

A large error (1-2%) is introduced into the results if the temperature sensing device is not permanently attached to the Cu block calorimeter. The calorimeter was described at the 1967 Vienna Thermodynamics Meeting.<sup>(5)</sup> The important features are a 6" dia Au plated Cu block weighing ~ 28 kgs., a constant temperature (25.0°C) surface at 2.5 cm from all surfaces of the Cu block and an Al radiation and convection shield positioned ~ 1 cm from all surfaces of the Cu block. The cylindrical surface of the Cu block is grooved for placement of a resistance thermometer. If the resistance thermometer is wound on the Cu block without any adhesive the calibration constant of the calorimeter was found to be dependent on the gas surrounding the Cu block. The difference in calibration constant can be as large as  $\pm 1-2\%$  between calibrations

in Ar and vacuum although the precision for calibration in a particular atmosphere is better than  $\pm 1\%$ . This difference in calibration constant is also dependent on the total amount of heat supplied to the calorimeter during calibration. The calibration constant can be made reproducible and almost independent of the atmosphere surrounding the Cu block by permanently attaching the resistance thermometer to the Cu block. This was done by spraying 3 coats of a clear acrylic coating on the thermometer wire and Cu block after installation of the thermometer. Although it has not been tested, this problem could equally exist with the use of thermocouples as with the resistance thermometer. A permanent bond between calorimeter block and temperature sensing device is needed.

The high temperature calorimeter must be operated in vacuum if an accuracy of better than  $\pm 1\%$  is desired. The calibration constant of the calorimeter is independent of the difference in temperature ( $\Delta T$ ) between the Cu block and constant temperature surface only if vacuum separates them. In the  $\Delta T$  range of 1 to  $10^\circ\text{C}$  the calibration constant increases at the rate of  $\sim 0.1\%$ / $^\circ\text{C}$  of  $\Delta T$  if the calorimeter is surrounded by Ar. In vacuum, the calibration constant is independent of this  $\Delta T$ .

A large  $\Delta T$  capability is needed in high temperature drop calorimetry ( $> 1400^\circ\text{C}$ ) since only a single sample is normally used over a large range of drop temperatures. The crucibles are difficult and expensive to fabricate so a minimum of samples are used. Ideally, a separate sample should be used at each drop temperature. This sample should be of a size that would give the same amount of heat to the calorimeter at each drop temperature.

The calibration constant of the calorimeter has been determined with vacuum surrounding the calorimeter. A  $\Delta T$  covering the range 1 to  $9.2^\circ\text{C}$  and a heating rate over a factor of 2 have been studied. The calibration factor of  $2582.6 \text{ cal/min} \pm 0.3\%$  was obtained. The least accurate part of the calibration presently is the recording system and chart paper. An all electronic integrating system with an accuracy of better than  $0.1\%$

is being built to replace the recording system.

The apparent heat content of three W crucibles has been determined as a function of temperature from 1500 to  $2550^\circ\text{C}$ . The results are listed in Table 463-VI and are not corrected for any heat loss during drop.

In this set of results there is no apparent systematic relationship of heat content with sample size or weight. These results when plotted on a graph show an experimental precision of  $\sim \pm 1\%$  at all temperatures. Included as causes of this error are the  $\pm 0.3\%$  calibration accuracy and  $\pm 0.5\%$  calibration of the optical pyrometer used for temperature measurements.

Pellets of  $\text{PuO}_2$  weighing 56 g have been loaded into a crack free W crucible and welded. A thin spot in the weld was found in the x-ray radiographs of the completed crucible. The weld cannot be repaired so a new crucible is being fabricated and the  $\text{PuO}_2$  will be reloaded. The heat content of  $\text{PuO}_2$  will be determined up to  $\sim 2650^\circ\text{C}$  including the heat of fusion.

#### 8. Medium Temperature Drop Calorimeter (A. Ogard, D. Clifton, G. Melton)

A drop calorimeter covering the temperature range of 300 to  $1100^\circ\text{C}$  is being assembled. The design is similar to the high temperature drop calorimeter but with a smaller Cu calorimeter block. This will permit the use of the same sample in both calorimeters.

In this temperature range accurate thermocouples can be used for determination of the temperature of the crucible before dropping. The accuracy of these heat content measurements should be  $\sim 0.1\%$ . It has been demonstrated in other laboratories that accuracies of  $\pm 0.1\%$  can be obtained and therefore it will be legitimate

Table 463-VI  
Apparent Heat Content of Tungsten Vacuum Drop Calorimeter

Temp., $^\circ\text{C}$	$\Delta H$ , cal/g	Crucible	Temp., $^\circ\text{C}$	$\Delta H$ , cal/g	Crucible
1510	51.6	A	2260	81.9	B
1510	51.3	A	2265	82.2	A
1832	51.1	B	2345	84.8	A
1827	54.7	C	2345	86.3	C
1832	54.2	B	2358	86.4	B
1840	64.6	B	2447	89.3	B
1840	66.0	A	2453	90.4	A
1843	54.7	B	2462	92.8	C
2160	77.5	B	2480	91.4	B
2163	78.6	C	2546	94.2	A
2163	78.0	A	2545	95.7	B
2260	81.0	C			

A - 103 g. -  $17.1 \text{ cm}^2$  surface area  
B - 54.5 g. -  $17.1 \text{ cm}^2$  surface area  
C - 98.0 g. -  $36.1 \text{ cm}^2$  surface area

to take the derivative of the heat content equation to obtain an equation for the heat capacity.

The calorimeter has been assembled and tested, including the constant temperature surrounding bath, vacuum system and Marshall furnace assembly. The dropping mechanism is now being fabricated.

#### 9. Adiabatic Calorimeter (D. G. Clifton)

The adiabatic calorimeter and its associated vacuum system and instrumentation have been completely assembled and partially tested.

A set of experiments to determine power settings for the sample heater which are necessary to obtain various rates of temperature rise for a Ta sample weighing 31.25 gms have been completed.

Calibration of the integrating circuitry which is used to give a digital read-out of the integral of current through the sample heater times time has been accomplished. These tests were performed using a standard resistor load, standard resistor voltage dividers, a timer and potentiometric readings. The power ranges covered were from about 0.03 watts to 5.6 watts and the calibration showed the integrator to be accurate to about 0.07%, which is adequate. Other data which has been acquired are the necessary power settings for the main heater power supply to attain various steady state operating temperatures of the calorimeter. The maximum temperature reached to date has been about 1150°C.

The control circuitry, which is used to maintain a minimum  $\Delta T$  across the shields surrounding the sample and thereby minimizing heat losses, has been tested several times and has been found to need adjustments in the control parameters.

#### IV. ANALYTICAL CHEMISTRY

##### 1. Electron Microprobe Examinations (E. A. Hakkila, H. L. Barker)

Homogeneity of the matrices and mottled areas of eight (U, Pu)C samples and of the matrices of three (U, Pu)O<sub>2</sub> samples was examined. The matrices of the (U, Pu)C samples were homogeneous but the mottled areas were not. Higher carbide phases in the mixed carbides contained more Pu and C but less U than the matrices.

##### 2. Miscellaneous Support

(N. L. Koski, W. W. Wilson, T. K. Marshall)

Controlled-potential coulometric methods were applied without difficulty to determination of U and/or Pu in nine PuC, two PuN, six (U, Pu)C, and one PuO<sub>2</sub>. The precision ( $1\sigma$ ) of the method was 0.2 to 0.3 percent in determining either metal. The PuO<sub>2</sub> was dissolved in HCl at 325°C and 4000 psi pressure by the sealed-tube method for the measurement of Pu and N.

A Kjeldahl-spectrophotometric method was used in measuring N concentrations at the ppm level in one UC, one PuC, one PuO<sub>2</sub>, and ten (U, Pu)C samples. The relative standard deviation of the method was 2 percent. A method utilizing the Kjeldahl distillation separation with a titrimetric finish was applied to measurement of N in two PuN samples. At the 5.50 percent N concentration level found, the precision ( $1\sigma$ ) of the method was 0.2 relative percent.

A combustion-gravimetric method, having a relative standard deviation of 0.2 to 0.3 percent, was applied successfully to determination of C in nine PuC and eight (U, Pu)C. A combustion-micromanometric method was used to measure C at ppm concentrations in four PuO<sub>2</sub> samples. The precision ( $1\sigma$ ) of this method was 10 relative percent.

Measurements of Pt concentrations in the ppm range in four PuO<sub>2</sub> samples were accomplished without difficulty by a spectrophotometric method having a relative standard deviation of 3 percent. The sealed-tube method was used to dissolve these samples.

Spectrophotometric methods also were used in determining U and Th in two PuN samples. The precisions ( $1\sigma$ ) of the methods were 5 relative percent for the measurement of U and 2 relative percent for the Th at low (ppm) concentrations.

#### V. REFERENCES

- (1) A. L. Bowman, et al., Acta Cryst., 21, 670 (1966).
- (2) E. A. Harper, et al., Nature, 219, 151 (1968).
- (3) C. S. Griffin, et al., "Self-Irradiation Damage in Transuranic Elements and Compounds," Paper No. 10 in Kay and Waldron "Plutonium 1965" (1967).
- (4) M. H. Rand, IAEA, Vienna (1968).

- (5) A. E. Ogard, J. A. Leary, "High Temperature Heat Content and Heat Capacity of Uranium Dioxide and Uranium Dioxide-Plutonium Dioxide Solid Solutions," Thermodynamics of Nuclear Materials, with Emphasis on Solution Systems, IAEA, Vienna (1967).

PROJECT 464

STUDIES OF Na-BONDED (U,Pu)C AND (U,Pu)N LMFBR FUELS

Person in Charge: D. B. Hall  
Principal Investigators: R. H. Perkins  
G. H. Best

I. INTRODUCTION

(U,Pu)C and (U,Pu)N are regarded as attractive alternates to mixed oxides as fuels for commercial LMFBR application. The high heavy-atom densities and thermal conductivities of the mixed carbide and nitride make it possible for these fuels to outperform mixed oxides. Full exploitation of carbides and nitrides dictates the use of a gap between fuel and clad to accommodate fuel swelling (with minimal fuel-cladding mechanical interactions) and a high thermal conductivity path across the gap to limit fuel temperature. The conditions can be met by filling an annulus between fuel and clad with sodium.

Before a satisfactory sodium-bonded fuel element can be developed, however, information is required that will identify the number and severity of problems associated with sodium bonding and will suggest solutions to these problems. Problem areas that are being studied in this experimental program are:

1. The mechanisms and kinetics of carbon transfer to claddings through the sodium bond.
2. The significant fuel and sodium variables that affect compatibility.
3. The consequences of exposing fuel to coolant sodium.
4. The behavior of sodium-bonded fuel elements under irradiation.
5. The performance limitations of the sodium bond under high-heat-flux conditions.

Efforts are now concentrated on the mixed car-

bide fuel. Type 316 stainless steel is the base cladding material being studied, though vanadium alloys are also being tested.

As prerequisites for this compatibility program, a number of developmental efforts have been undertaken. These include establishment of (1) techniques for the production of single-phase monocarbide pellets of known composition and dimensions, (2) techniques and equipment for fuel pin loading, bonding, and inspection, and (3) techniques and equipment for determining the distribution of fission products in irradiated fuel pins.

II. SYNTHESIS AND FABRICATION OF (U,Pu)C PELLETS  
(M. W. Shupe, J. A. Leary, A. E. Ogard,  
R. W. Walker, S. McClanahan, R. E. Honnel,  
H. G. Moore, C. Gilley)

A. General

Standardized procedures for producing single-phase monocarbide pellets of known composition and dimensions have been developed. These pellets will be utilized in EBR-II irradiation experiments and compatibility testing. Basic process steps are:

1. Multiple arc melting of a physical mixture of  $^{235}\text{U}$ , Pu, and C on a 60-g scale using a graphite electrode.
2. Solution treatment of the arc melted ingot for 24 h at 1600°C.
3. Crushing and grinding of the ingot in a WC vibratory mill, followed by screening of the resulting powder to  $\leq 62 \mu$  size.
4. Blending of several powder batches.
5. Elimination of excess carbon by reaction with  $\text{H}_2$  at 850°C.
6. Cold compaction at 20 tsi into pellets

without the use of binders and sintering aids.

7. Sintering of the pellets in Ar at 1800°C.
8. Characterization of the pellets by linear dimensioning, weighing, density (by immersion technique), metallography, x-ray powder diffraction analysis, chemical analysis including U, Pu, C, N, O, H, and spectrochemical analysis for trace impurities, electron microprobe analysis, x-ray radiography for determination of possible internal cracks, and isotopic analysis of the uranium and plutonium.

#### B. Current Results

Carbide pellets are needed with a nominal composition of  $U_{0.8}Pu_{0.2}C$  and a density 95% of theoretical. Pellets are presently being fabricated with measured densities  $\geq 12.7 \text{ g/cm}^3$  or 94.4% of theoretical, the theoretical density being  $13.44 \text{ g/cm}^3$  as calculated from lattice constant and chemical composition values of similar material.

Process procedures for the denser material are similar to those referenced previously; however, the 1800°C sintering time was increased from 4 to 8 h, and a 12-h ball milling cycle was added to supplement the oscillatory grinding. Particle size distribution of the milled powder before sintering is shown in Fig. 464-1. Metallographic evaluation of

both electrolytically etched and stained pellets have shown them to be single phase with intergranular porosity. A typical photomicrograph of an electrolytically etched pellet is shown in Fig. 464-2.

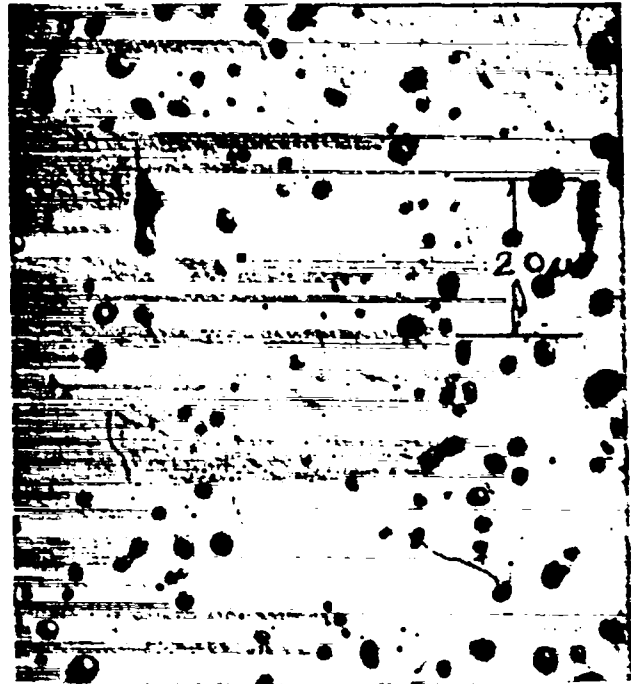


Fig. 464-2 94.4% T.D. single-phase  $(U_{0.8}Pu_{0.2})C$  at 900X (electrolytically etched with a 1:1:1 acetic:lactic:nitric acid at a current density of  $90 \text{ mA/cm}^2$ )

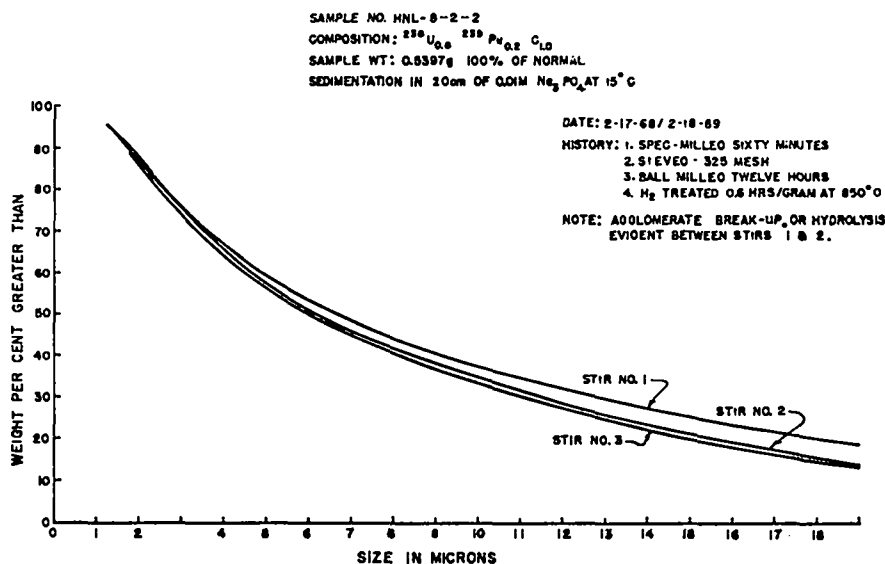


Fig. 464-1. Particle size distribution of  $(U_{0.8}Pu_{0.2})C$  powder after ball milling and hydrogen treating.

It should be noted that process procedures for the 94.4% T.D. pellets are not optimum. In fact, radiographs have revealed that approximately 30 per cent of the sintered pellets are capped; i.e., microcracks are present usually near the end of the pellet which seats against the short punch during pressing. Consequently, work will continue to be directed toward determining the effect of process parameters on pellet integrity.

Approximately 900 single-phase pellets with a nominal composition of  $(^{235}\text{U}_{0.8}^{239}\text{Pu}_{0.2})\text{C}$  and a 95% T.D. are required for a planned series of compatibility and nuclear evaluation tests. To date 200 pellets have been prepared, and further details on these pellets will be reported upon completion of all the characterization tests. Buttons of  $(\text{U,Pu})\text{C}_{1+x}$  have also been prepared and are being processed into pellets for use in compatibility tests.

### III. LOADING FACILITY FOR TEST CAPSULES (D. N. Dunning)

#### A. General

A prerequisite to a compatibility program involving  $(\text{U,Pu})\text{C}$  and sodium is a satisfactory capsule loading and bonding facility. There is little point to obtaining well-characterized materials for testing if these materials are contaminated before they are placed in test. Sodium and  $(\text{U,Pu})\text{C}$  are sufficiently reactive that all operations must be performed either in vacuum or in a high-quality inert atmosphere. The loading facility for handling these materials has been constructed; it consists of inert-atmosphere gloveboxes equipped with inert-gas cleanup systems to provide an environment for handling fuel pellets and bonding sodium with a minimum of contamination.

#### B. Current Results

During this reporting period, the loading facility was shut down and general maintenance on the gloveboxes was performed. The complete system, including the inert-gas cleanup system, was checked with a helium leak detector; several leaks were detected and corrected. The pressure switches used as box pressure controls were leaking through neoprene diaphragms; these were replaced with switches utilizing stainless steel bellows. Mass spectrom-

eter analyses of gas samples from the boxes after maintenance gave the results shown in Table 464-I.

Table 464-I

#### Analyses of Gas from Loading Facility Gloveboxes

	Fuel Glovebox (ppm)	Sodium and Weld Glovebox (ppm)
H <sub>2</sub> O	Not detectable	Not detectable to 2
H <sub>2</sub>	3-6	Not detectable
N <sub>2</sub>	1-3	6-7
O <sub>2</sub>	1	Not detectable

Several different types of test capsules containing fuel and sodium were loaded during this reporting period. These included OWR and EBR-II irradiation assemblies as well as out-of-pile compatibility test capsules.

### IV. CARBIDE FUEL COMPATIBILITY STUDIES (F. B. Litton, H. A. O'Brien, Jr., L. A. Geoffrion, J. H. Bender)

#### A. General

The objectives of this program are to study the interactions among single-phase mixed  $(\text{U,Pu})\text{C}$ , a sodium bond, and potential cladding materials, i.e., to investigate the technology related to sodium-bonded fuel elements. There are two approaches to the experimental work. One approach is to determine the reactions occurring between  $(\text{U}_{0.8}\text{Pu}_{0.2})\text{C}$  and potential cladding materials, using Type 316 stainless steel and a high strength vanadium-base alloy as the first and second choices of cladding material, respectively. A second concurrent set of experiments is designed to study the mechanism of carbon transport through sodium, the effect of impurities such as oxygen, and the carburizing potential of sodium in mutual contact with carbides and the preferred cladding materials.

Capsules containing sodium-bonded, single-phase  $(\text{U,Pu})\text{C}$  are tested in sodium loops at 750°C for periods up to 10,000 h. High purity, thoroughly-characterized sodium is used for the studies. Fuels of known composition are used in all tests. Most of the testing is performed on single-phase  $(\text{U,Pu})\text{C}$  fuel in which the Pu/U ratio is maintained at 0.25, but some experiments are being carried out on material containing a second phase (either metallic or carbon-rich). Other experiments are being carried out on stoichiometric and hyperstoichiometric UC to determine the effect of plutonium

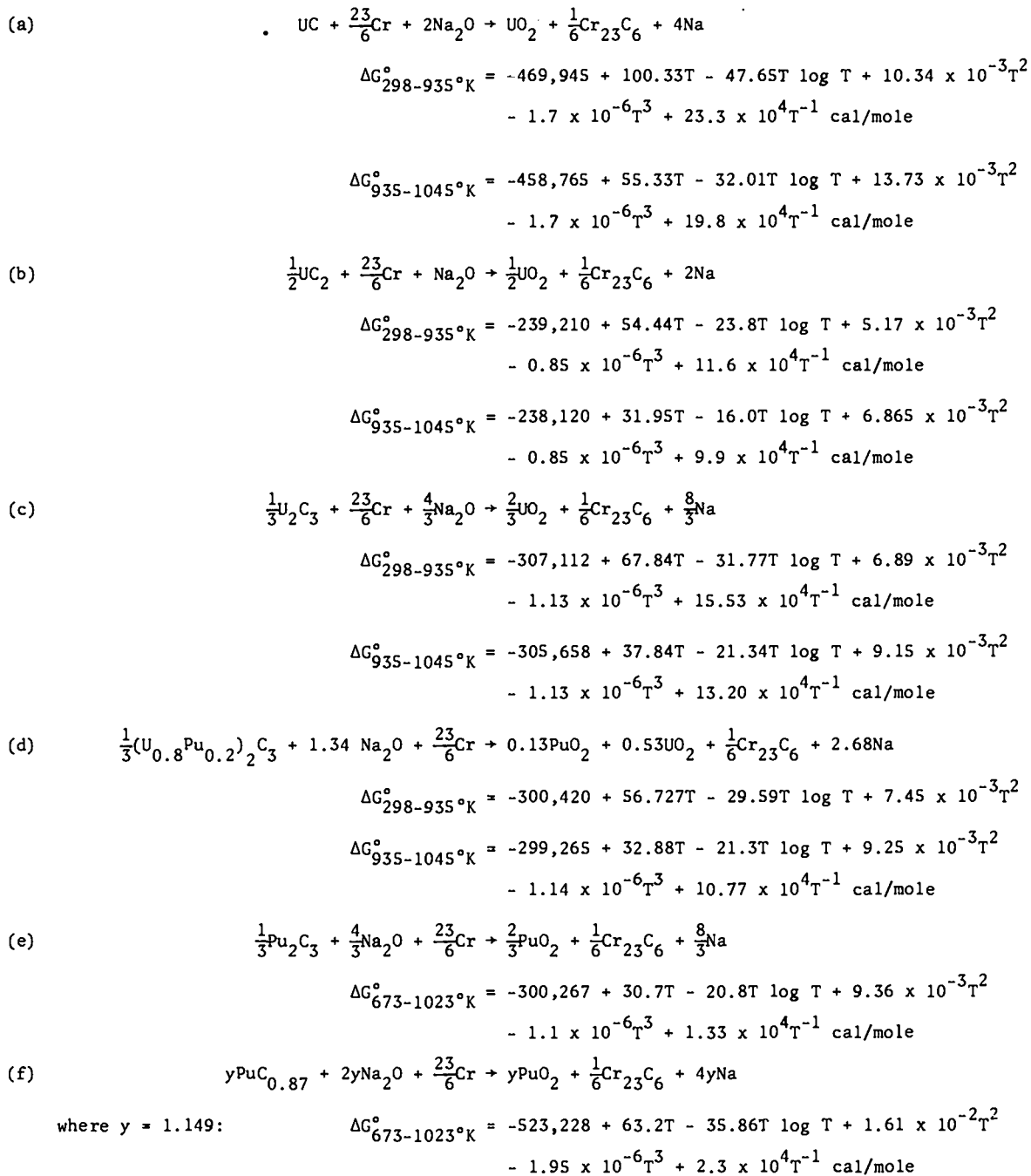
addition on the behavior of the carbide fuel.

## B. Current Results

### 1. Thermodynamic Calculations

As part of the program to determine the compatibilities of various fuel carbides and structural materials, calculations were made of the thermodynamic equilibrium constants for the reactions of

fuel carbides with sodium oxide and the resultant transfer of carbon from the fuel to chromium. The calculations were based on reported standard free-energy equations which are applicable over the temperature range of interest. The reactions, together with the appropriate standard free-energy equations, that were studied are:



The results of the calculations indicate, in all cases, a strong thermodynamic potential for the carbide fuel to react with sodium oxide and chromium. However, these calculations give no information about the kinetics of these reactions or about the effect of oxygen concentrations in sodium below the solubility limit.

## 2. Studies of Carbon Transfer in Sodium

Carburization of potential cladding alloys in sodium is thought to be a diffusion-controlled process in which the difference in chemical activities between the carbon source and the product of reactions is the primary driving force. It is apparent that relatively long periods of time may be required to establish equilibrium in a given system, and that the activities of the carbon and metals in the source and the cladding alloy change during the carburizing process. This, of course, implies that the rate-controlling step also may change. Carbon is assumed to be soluble in sodium to some small but finite amount. While the transfer mechanism is contingent on the formation of a particular species in the sodium, the end products of the reaction are independent of the transferring species. Carburization of cladding alloys using carbon sources of different activities are being studied in an attempt to determine the rate-limiting step in the reaction.

Type 316L stainless steel tabs were carburized in zirconium-gettered sodium at 650°C for periods from 2 to 116 h using eutectoid (0.85 w/o C) iron-carbon alloy as the carbon source. The sodium (229.36 g) was held in a magnesia crucible under a purified helium atmosphere. Four 1/2-in.-square Type 316L stainless steel tabs were suspended by nickel wires with the carburizing source at the center of the assembly. The depth of carburization of the tabs and decarburization of the source was measured metallographically. The metallographic measurements were confirmed by microhardness determinations. Chemical analyses of the tabs will be used for determining the carbon flux. The carburizing/decarburizing data are recorded in Table 464-II.

Other Type 316L stainless steel tabs were immersed in sodium after the initial carburization experiment had been completed and the carbon source had been removed. No carburization was observed in

the sodium when no source was present, showing that the activity of the residual carbon in the sodium, or the amount of available carbon, was insufficient to carburize the stainless steel.

The structure of the source after decarburization consisted of an iron case, a relatively thin transition zone, and a core of eutectoid iron-carbon alloy. The cementite ( $Fe_3C$ ) tended to spheroidize, and after prolonged heating (116 h test) converted to nodular graphite. Spheroids of cementite were occasionally observed in the grain boundaries of the case. A typical metallographic structure of the iron-carbon alloy source is shown in Fig. 464-3.

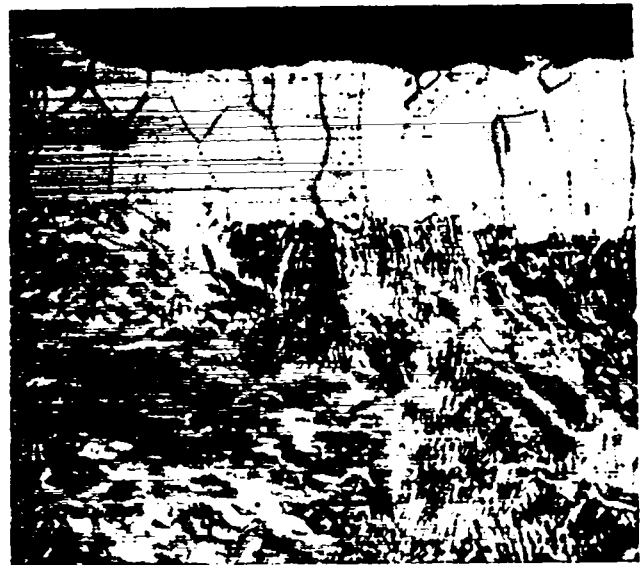


Fig. 464-3. Typical metallographic structure at the surface of iron-carbon alloy source after immersion in sodium with Type 316L stainless steel for 2 h at 650°C. Etched, 300X.

The initial phase of carbon penetration into Type 316L stainless steel is shown in Fig. 464-4. After a 2-h immersion in 650°C sodium with iron-carbon alloy source, grain boundary penetration occurred to a depth of 40  $\mu m$  and bulk penetration occurred to a depth of 18  $\mu m$ . In all of the tests, which included exposure times up to 116 h, the structure at the surface of heavily carburized Type 316L stainless steel consisted of four zones: a thin layer at the surface, uniform in appearance (presently unidentified); a zone characterized by massive carbide precipitation, resembling a hyper-eutectoid structure; a zone characterized by carbide precipitation throughout the grains; and a zone in

Table 464-II

Diffusion of Carbon from  $\text{Fe}_3\text{C}$  Source to Type 316L Stainless Steel in Sodium at 650°C

Reaction Time (sec)	Area of $\text{Fe}_3\text{C}$ Source ( $\text{cm}^2$ )	Area of Stainless Steel ( $\text{cm}^2$ )	Weight Loss of Source (mg)	Weight Gain of Stainless Steel (mg)	Depth of $\text{Fe}_3\text{C}$ Removal (microns)	Depth of Carburization (microns)		Rate of Decarburization of $\text{Fe}_3$ Source ( $\text{g}/\text{cm}^2\text{-sec} \times 10^{-9}$ )	Rate of Carburization of Type 316L Stainless Steel* ( $\text{g}/\text{cm}^2\text{-sec} \times 10^{-9}$ )
						Bulk	Bulk plus Grain Boundary		
7,200	2.415	14.796	1.90	1.34	70	18	40	109.7	12.5
22,200	4.031	14.783	3.67	3.19	125	25	58	40.9	9.9
76,200	3.612	14.782	7.29	7.25	260	66	150	26.5	6.4
163,800	2.967	14.764	9.36	8.72	500	133	216	19.2	3.6
418,200	4.979	14.783	18.87	15.93	675	150	230	9.1	2.6

\*Based on weights gained; rates will also be obtained from chemical analyses.



Fig. 464-4. Bulk and grain boundary penetration of carbon at the surface of Type 316L stainless steel after immersion in sodium with iron-carbon alloy source for 2 h at 650°C. Etched, 1200X.

which grain boundary carbide precipitation was predominant.

In a series of capsule tests for studying the transfer of carbon through a sodium bond to Type 316 stainless steel containers, metal carbides were selected which possess thermodynamic stabilities lower than, approximately equivalent to, and higher than the stability of single-phase mixed uranium-plutonium carbide. The capsule loading information is recorded in Table 464-III. The capsules were heated for 1000 h at 750°C.

Capsule 1685 containing  $\text{Cr}_{23}\text{C}_6$  developed a

sodium leak during testing and was discarded. Inasmuch as this phase is the primary reaction product resulting from carburization of Type 316 stainless steel, further tests on its stability in sodium are planned.

Metallographic examination of heat-treated  $\text{UC}_{1.04}$  (capsule 1680) showed that a zone at the surface was depleted in the dicarbide phase. The structure is shown in Fig. 464-5. The surface

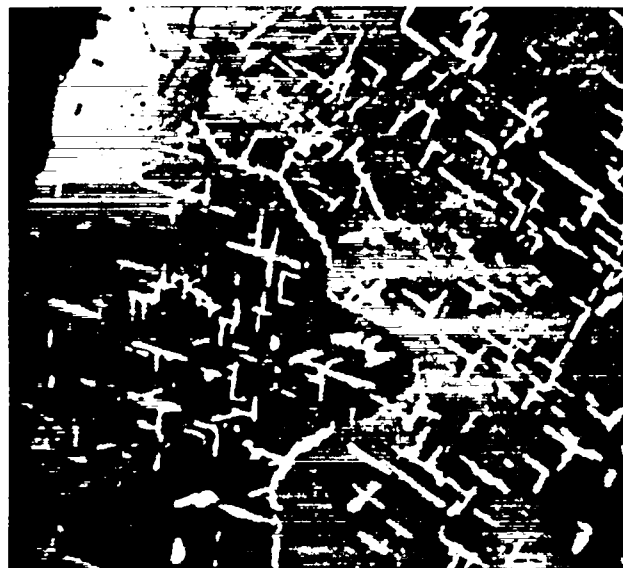


Fig. 464-5. Structure at the surface of  $\text{UC}_{1.04}$  carbon source in capsule 1680. The surface in contact with sodium was depleted in the dicarbide phase, and consisted of sesquicarbide distributed in a monocarbide matrix. Etched, 300X.

structure consisted of sesquicarbide distributed in the monocarbide matrix. The structure away from

Table 464-III  
Capsule Loading for Studying the Relative Stability  
of Sodium-Bonded Metal Carbides

Capsule No.	Carbide Material	Carbide Weight (g)	Form	Sodium Weight (g)	Weight of Type 316L Stainless Steel Tab (g)
1680	UC <sub>1.04</sub> - heat treated 116 h at 1350°C to convert UC <sub>2</sub> to U <sub>2</sub> C <sub>3</sub> Both phases were present in the heat-treated structure	4.6479	Granular -10+14 mesh	4.50	1.17584
1681	UC <sub>1.04</sub> - as cast; UC <sub>2</sub> in UC matrix	4.4429	Granular -10+14 mesh	4.52	1.17223
1683	Cast iron - Fe <sub>3</sub> C and graphite in Fe matrix	3.0140	1/8" x 1/8" x 3/4"	4.98	1.18083
1685	Cr <sub>23</sub> C <sub>6</sub> - essentially single phase	3.9152	Granular -10+14 mesh	4.59	1.17978

this zone, which is shown in Fig. 464-6, was unaffected by the test conditions. The stainless steel tab gained  $1.8 \times 10^{-5}$  g/cm<sup>2</sup> in weight, and showed a general precipitation of chromium carbide throughout the cross section. The tab structure is shown in Fig. 464-7.

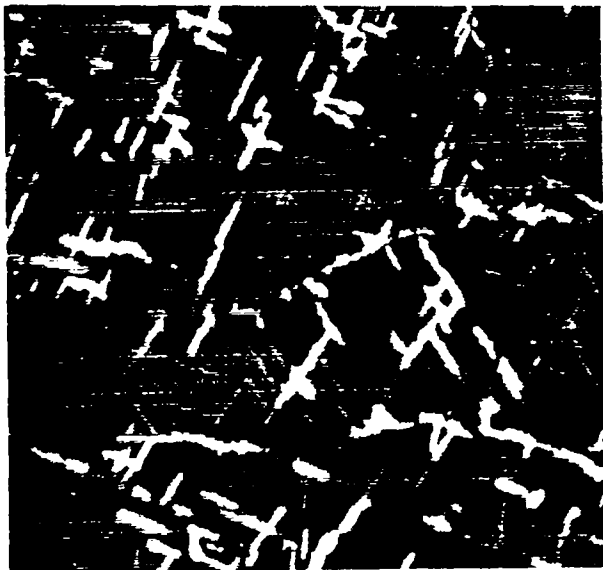


Fig. 464-6. Core structure of UC<sub>1.04</sub> carbon source in capsule 1680. The structure consisted of the dicarbide and sesquicarbide phases distributed in the monocarbide matrix.

The structure of as-cast UC<sub>1.04</sub> (capsule 1681) after test was single-phase monocarbide throughout. Cracks developed in the granules permitting more rapid diffusion of carbon from the dicarbide phase



Fig. 464-7. Distribution of chromium carbide precipitates in Type 316L stainless steel after carburizing for 1000 h at 750°C from heat-treated UC<sub>1.04</sub> source. Tab from capsule 1680. Etched, 300X.

out of the granules. The stainless steel tab gained  $4.4 \times 10^{-5}$  g/cm<sup>2</sup> in weight and showed a more pronounced chromium carbide precipitation gradient than occurred in capsule 1680.

The cast iron source (Fe, Fe<sub>3</sub>C, C phases) in capsule 1683 was depleted in the Fe<sub>3</sub>C phase. However, graphite remained in contact with sodium. The stainless steel tab gained  $58 \times 10^{-5}$  g/cm<sup>2</sup> and was extensively carburized throughout its 0.036-in. cross section.

### 3. Behavior of Vanadium Alloys in Hot-Trapped Sodium

Vanadium alloys have been proposed as a back-up cladding material for Type 316 stainless steel for the liquid-metal fast breeder reactor. The information being developed in this experimental work will aid in the screening of vanadium alloys for this application.

Weight changes of vanadium alloys tested in hot-trapped sodium were summarized in Fig. 464-6 in the Quarterly Report dated March 4, 1969 (LA-4114-MS). The curve included data as a function of temperature on V, V-10Ti, V-20Ti, V-40Ti, and V-15Ti-7.5Cr immersed in sodium from 500 to 4000 h. The test samples were analyzed for oxygen. The oxygen contents versus test temperatures for V, V-20Ti, V-15Ti-7.5Cr, and V-15Cr-5Ti alloys are shown in Fig. 464-8. The data for V-10Ti and V-40Ti overlap the curves for V-20Ti and V-15Ti-7.5Cr and are not shown in the figure.

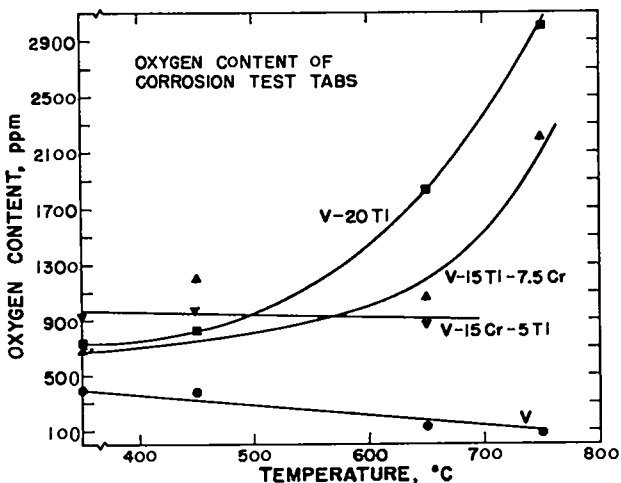


Fig. 464-8. Oxygen content of corrosion test tabs immersed in hot-trapped sodium from 500 to 4000 h.

The oxygen contents of these alloys indicate that relatively pure vanadium and the V-15Cr-5Ti alloy are stable (as far as oxygen pickup is concerned) in hot-trapped sodium, though not necessarily in cold-trapped sodium. These data confirm the thermodynamic calculations shown in Fig. 464-5 of the referenced report.

Using the technique previously described, additional carburization experiments were conducted

on Type 316L stainless steel and on V-15Cr-5Ti alloy in sodium utilizing a magnesia crucible and iron carbide-graphite sources of carbon. The sodium did not carburize the Type 316L stainless steel prior to immersing the carbon source. In the experiments, one-half-in.-square tabs of either potential cladding alloy material and an iron carbide-graphite carbon source of approximately equivalent surface were immersed in sodium for 72 h at 650°C.

Metallographic examination of the Type 316L stainless steel showed bulk penetration of 85  $\mu\text{m}$  and grain boundary carburization for an additional 200  $\mu\text{m}$ . Microhardness measurements indicated a hardened surface layer of 262  $\mu\text{m}$  (0.0105 in.) thickness. Using the metallographic data, a diffusion constant of  $1.96 \times 10^{-10} \text{ cm}^2/\text{sec}$  was calculated for carbon in Type 316L stainless steel. Compared to the stainless steel tab, carburization of the V-15Cr-5Ti alloy was much less extensive. Metallographic examination did not reveal bulk penetration of carbon at the surface. The structure is shown in Fig. 464-9. Microhardness measurements, however, indicated a depth of carbon penetration of 75  $\mu\text{m}$  (0.003 in.). From these microhardness measurements, a diffusion constant of  $1.06 \times 10^{-11} \text{ cm}^2/\text{sec}$  was calculated.



Fig. 464-9. Microstructure of V-15Cr-5Ti alloy after carburizing in sodium from Fe-Fe<sub>3</sub>C-C alloy source for 72 h at 650°C. Etched, 300X.

The carbon diffusion coefficient of  $1.96 \times 10^{-10}$  cm<sup>2</sup>/sec in stainless steel is consistent with the value of  $1.75 \times 10^{-10}$  cm<sup>2</sup>/sec calculated by Campbell and Tyzack.<sup>1</sup> The value of  $4.12 \times 10^{-11}$  cm<sup>2</sup>/sec reported by Anderson and Sneesby<sup>2</sup> for Type 304 stainless steel appears to be low. The diffusion coefficient in unalloyed iron is reported as  $\sim 10^{-9}$  cm<sup>2</sup>/sec.<sup>3</sup>

V. EBR-II IRRADIATION TESTING  
(J. O. Barner)

A. General

The purpose of these irradiations is to evaluate candidate fuel/sodium/clad systems for the LMFBF program. In the reference design, pellets of single-phase (U,Pu)C are separated by a sodium bond from a cladding of Type 316 stainless steel or other high temperature alloy. Seven fuel-element tests are planned in the initial group of a continuing series of EBR-II irradiation experiments.

The capsules are to be irradiated under the following conditions:

1. Lineal power: 29.15 to 30.20 kW/ft (max).
2. Fuel composition: (U<sub>0.8</sub>Pu<sub>0.2</sub>)C (single-phase, sintered, fully enriched).
3. Fuel density: 90% of theoretical.
4. Smear density: 80%.
5. Clad size: 0.300 in. o.d. x 0.010 in. wall.
6. Fuel size: 0.265 in. diam x 0.25 in. high.
7. Clad type: 316 SS
8. Maximum clad temperature: 1250°F.
9. Maximum fuel centerline temperature: 2130°F.
10. Burnup: 0.22 to 0.66 g fissioned per cm<sup>3</sup>.

B. Current Results

In addition to the first seven tests described above, approval-in-principle has been received for irradiation of three capsules which are to operate at  $\sim 42$  kW/ft. In the three capsules tested at high power the <sup>235</sup>U will be replaced by <sup>233</sup>U. The purpose of these experiments is to investigate the effect of high thermal stresses on clad behavior. Proposals for approval-in-principle have also been submitted for reirradiation of LASL-42B (nondestructive test results are described below) and for the irradiation of six capsules fueled with 95% dense fuel.

LASL-42B is a doubly encapsulated, doubly

sodium-bonded (U<sub>0.8</sub>Pu<sub>0.2</sub>)C-fueled EBR-II capsule from the first set of reference capsules. The uranium is fully enriched. LASL-42B has operated in EBR-11 in the X039 subassembly at an estimated lineal heat rating of 29-30 kW/ft. It has accumulated a maximum burnup of approximately 1.4 a/o. The maximum fuel centerline temperature was estimated to be 2230°F (1220°C), while the maximum inner Type 316 stainless steel clad temperature was 1250°F (677°C). The nondestructive testing of LASL-42B has been completed. Nothing unexpected was observed from the initial irradiation. The following paragraphs describe the nondestructive test results.

1. Initial Hot Cell Evaluation

Upon arrival at the LASL hot cell, LASL-42B was examined visually. Contamination swipes, radiation readings, surface temperature readings, and micrometer measurements were taken. The capsule was clean with no apparent discolorations. Contamination swipes read 20 mR/h beta + gamma with no detectable alpha contamination. The gross beta + gamma reading was 300 R/h at one meter. The temperature of the outer Type 304 stainless steel surface of the capsule varied from 3.6°C to 15.3°C above the ambient air temperature. Diametral micrometer measurements of the outer Type 304 stainless steel clad indicated that along the majority of the length the diameter was the same as that determined by the preirradiation measurement,  $0.375 \pm 0.001$  in. At one point 20 in. from the bottom of the capsule, the indicated diameter was 0.377 in. Because the measurement accuracies before and after irradiation were no better than  $\pm 0.001$ , this apparent increase may not be real.

2. Neutron Radiography from TREAT

Neutron radiographs of LASL-42B with one orientation were taken at TREAT utilizing indium and dysprosium foils. These radiographs confirmed that the pellets in the first four positions from the bottom were depleted UC pellets. However, the top pellet, which was supposed to be a depleted UC pellet, was found to be a (U<sub>0.8</sub>Pu<sub>0.2</sub>)C fuel pellet. The fact that this was a fuel pellet increased the capsule heat generation by about 2%. A small fuel chip was observed resting on the lower end cap in the annulus between the bottom UC pellet and the

clad. Another small chip was observed resting on the shelf formed by the top of the third UC pellet from the bottom (Note: The fourth UC pellet is misaligned with respect to the third, thus forming a shelf.) These chips will not affect the further operation of LASL-42B. An apparent large chip was located in the annulus at pellet number 36 (all pellets including the UC pellets are numbered from the bottom of the capsule). This apparent chip is so large that it is believed to be a piece of pellet number 36 which has remained in place with respect to its origin. Several pellets were observed to be split longitudinally. The split pellets resulted from the high thermal stresses encountered during operation. Observations concerning split pellets are tabulated in Table 464-IV. Pellet number 4, a UC pellet, which was in immediate contact with a fuel pellet appeared to have a higher density of fissionable material than the other three UC pellets. This may be due to contamination during manufacture. However, it is much more likely that the fissionable material is  $^{239}\text{Pu}$  from breeding because it is located at the bottom of the EBR-II core.

### 3. Betatron X-Radiography

LASL-42B was x-radiographed utilizing a betatron machine. Resultant radiographs illustrated 6-in. sections of the capsule (at a magnification of 1.5). The total length of the capsule was radiographed in successive shots taken at both  $0^\circ$  and  $90^\circ$ .

The resolution of the capsule components and split pellets in the x-radiographs was better than that in the neutron radiographs. Information obtained on split fuel pellets and annular gaps is tabulated in Table 464-IV. The sodium level was observed to be 3 in. above the fuel, which is identical to that observed prior to irradiation.

All components, except some of the pellets, appeared to be intact. The inner can was not bowed with respect to the outer capsule and was in the same position as prior to irradiation. The possible chip in the fueled region observed in the neutron radiograph was not observed in the x-radiographs.

### 4. Gamma Scanning

LASL-42B was gamma scanned for total gamma

activity over the majority of its length, and diametral scans were taken at selected points. (See Section VI for additional information on gamma scanning of this fuel element.)

Total gamma scans over the fueled length were taken in 0.003-in. steps and 0.010-in. steps. Over approximately the lower 2/3 of the fueled length, counting statistics were good enough to measure fuel pellet lengths to  $\pm 0.003$  in. Over the upper 1/3 of the fueled length, the 0.010-in.-step scan had to be relied upon, so the pellet-to-pellet interfaces were measured to  $\pm 0.010$  in. Heights of selected stacks of pellets were also measured to  $\pm 0.003$  in. and  $\pm 0.010$  in. Preirradiation and postirradiation lengths of individual pellets are tabulated in Table 464-V. Obviously, error in any one measurement affects the measurements of the two pellets on either side of the pellet under consideration.

The total fuel stack height, as measured by gross gamma activity, was 13.631 in. The total length of the original stack, based upon the sum of the preirradiation pellet lengths, was 13.570 in. The preirradiation stack height was also determined from contact radiographs; a value of approximately 13.63 in. was obtained. The average axial pellet expansion during irradiation, based upon the sum of pellet lengths, is 0.45%. Therefore, the average axial expansion is 0.36% per a/o burnup (see next paragraph for average burnup results). If the pellet expansion of the fuel is isotropic, a value for the average volume expansion is 1.1 v/o per a/o burnup. If the preirradiation stack height obtained from contact radiographs is used instead of the sum of the individual pellet height, a somewhat smaller value for fuel expansion during irradiation is obtained.

Analysis of the gross gamma activity in the fuel region (not corrected for clad activation products) resulted in a peak-to-average burnup ratio of 1.12. The minimum-to-average ratio was 0.85 at the top of the element and 0.87 at the bottom of the element. The peak burnup was observed at about 3/4 in. below the EBR-II core midplane. Based upon the maximum burnup of 1.4 a/o estimated by EBR-II personnel, the average burnup for the 54 fuel pellets was 1.25 a/o.

No evidence of  $^{85}\text{Kr}$  nor any other fission product was observed in the gas volume between the

Table 464-IV

## Tabulation of Radiographic Observation of Pellets in LASL-42B

Position No.*	Pellet No.	Test**			Consensus**	
		Neutron Radiograph	0° X-Ray	90° X-Ray	Condition	If Split, No. of Pieces
1	UC-8	OK	OK	OK	OK	
2	UC-9	OK	OK	OK	OK	
3	UC-10	OK	OK	OK	OK	
4	UC-11	OK	OK	OK	OK	
5	101	OK	OK	OK	OK	
6	102	OK	OK	OK	OK	
7	103	OK	OK	OK	OK	
8	104	OK	OK	OK	OK	
9	105	OK	OK	OK	OK	
10	99	OK	OK	OK	OK	
11	290	OK	OK	OK	OK	
12	259	OK	OK	OK	OK	
13	260	S	OK	S (L)	S	2
14	309	OK	OK	OK	OK	
15	316	OK	S (L)	S (L)	S	4
16	328	OK	OK	S (N)	S	2
17	332	OK	OK	S (N)	S	2
18	343	OK	OK	S (N)	S	2
19	109	OK	OK	OK	OK	
20	113	S	OK	S (N)	S	2
21	114	S	S (N)	S (N)	S	4
22	310	S	OK	S (N)	S	2
23	311	OK	OK	OK	OK	
24	313	S	S (N)	OK	S	2
25	314	S	OK	OK	S	2
26	315	S	S (N)	OK	S	2
27	318	S	S (B)	S (N)	S	4
28	320	S	S (L)	OK	S	2
29	321	OK	OK	OK	OK	
30	25	S	OK	S (N)	S	2
31	27	S	S (N)	OK	S	2
32	28	OK	S (B)	OK	S	2
33	30	S	S (N)	OK	S	2
34	31	OK	S (L)	S (N)	S	4
35	32	OK	OK	S (N)	S	2
36	33	OK (chip)	S (L)	OK	S	2
37	34	OK	S (N)	OK	S	2
38	323	OK	S (N)	OK	S	2
39	325	S	S (N)	OK	S	2
40	326	S	OK	S (N)	S	2
41	327	S	OK	OK	S	2
42	329	OK	OK	OK	OK	
43	330	OK	S (N)	OK	S	2
44	333	OK	S (N)	OK	S	2
45	335	S	OK	S (N)	S	2
46	116	OK	S (N)	OK	S	2
47	289	S	S (B)	S (N)	S	4
48	291	OK	OK	OK	OK	
49	171	S	S (N)	OK	S	2
50	261	OK	OK	S (R)	S	2
51	269	OK	S (R)	OK	S	2
52	270	OK	OK	OK	OK	
53	272	OK	OK	OK	OK	
54	106	OK	S (N)	OK	S	2
55	107	OK	OK	OK	OK	
56	161	OK	OK	OK	OK	
57	162	OK	OK	OK	OK	
58	?	OK	OK	OK	OK	

\*Position numbered from bottom up.

\*\*Key: OK - pellet intact; S - split longitudinally;  
(L) - annular gap on left; (R) - annular gap on  
right; (B) - annular gap on left and right;  
(N) - no annular gap.

\*\*\*Note: Pellets in positions 15, 21, 27, 34, and 47 were split into four pieces. For pellet 21 no annular gap was observed. As in all split pellets, gaps between the pieces were observed.

4 UC intact; 20 (U,Pu)C intact;  
34 (U,Pu)C split.

Table 464-V  
Length of Pellets in LASL-42B

Position No.	Pellet No.	Preirradiation Length (in.)	Postirradiation Length (in.)	Difference (mils)
1	UC-8			
2	UC-9			
3	UC-10			
4	UC-11			
5	101	0.282	0.282	0
6	102	0.252	0.253	+1
7	103	0.252	0.251	-1
8	104	0.252	0.253	+1
9	105	0.253	0.252	-1
10	99	0.251	0.251	0
11	290	0.252	0.252	0
12	259	0.251	0.252	+1
13	260	0.252	0.255	+3
14	309	0.250	0.252	+2
15	316	0.251	0.252	+1
16	328	0.252	0.255	+3
17	332	0.250	0.246	-4
18	343	0.252	0.254	+2
19	109	0.252	0.252	0
20	113	0.251	0.251	0
21	114	0.250	0.250	0
22	310	0.251	0.256	+5
23	311	0.252	0.255	+3
24	313	0.251	0.254	+3
25	314	0.253	0.254	+1
26	315	0.252	0.254	+2
27	318	0.253	0.255	+2
28	320	0.252	0.254	+2
29	321	0.252	0.256	+4
30	25	0.246	0.248	+2
31	27	0.246	0.249	+3
32	28	0.245	0.247	+2
33	30	0.244	0.248	+4
34	31	0.245	0.246	+1
35	32	0.243	0.244	+1
36	33	0.246	0.245	-1
37	34	0.245	0.246	+1
38	323	0.253	0.256	+3
39	325	0.252	0.254	+2
40	326	0.252	0.254	+2
41	327	0.252	0.254	+2
42	329	0.252	0.254	+2
43	330	0.251	0.253	+2
44	333	0.250	0.252	+2
45	335	0.251	0.252	+1
46	116	0.250	0.250	0
47	289	0.250	0.252	+2
48	291	0.252	0.254	+2
49	171	0.251	0.252	+1
50	261	0.254	0.254	0
51	269	0.254	0.254	0
52	270	0.254	0.254	0
53	272	0.254	0.253	-1
54	106	0.251	0.250	-1
55	107	0.253	0.252	-1
56	161	0.251	0.251	0
57	162	0.252	0.252	0
58	?	(0.250)	0.250	(0)
	Total	13.570	13.631	

inner and outer containers. Evidence of the three fuel chips observed in lower UC regions in the neutron radiographs was observed in the gamma scans. UC pellet interfaces were not detected in the gamma scans.

#### 5. Conclusions

1. The outer Type 304 stainless steel and the inner Type 316 stainless steel clads of LASL-42B appear to be intact.
2. There are no chips present in the inner sodium-fuel annulus that would appear to inhibit fuel expansion.
3. It could not be determined if there were any chips in the spaces between split pellets that would inhibit fuel expansion.
4. Based upon the average linear expansion rate of the fuel, the fuel would be restrained by the cladding at about 18 a/o burnup. Based upon observed linear expansions measured on individual fuel pellets in the center of the stack of about 2 mils per pellet, the fuel would be restrained at approximately 10 a/o burnup.
5. The probable presence of sodium in the space between split pellets will lower maximum fuel temperatures. Hence, swelling should be reduced to a lower rate.
6. LASL-42B is capable of undergoing further irradiation.

#### VI. GAMMA SCANNING AND RELATED STUDIES (D. M. Holm, W. M. Sanders, B. M. Moore, B. K. Barnes)

##### A. General

Gamma scanning is a nondestructive technique for obtaining information on the distribution of fission products and activation products in fuel elements. A new advanced semiconductor detector system has been constructed for this purpose.

Information on the gamma-ray spectra of fission products from fast fission of plutonium is limited when compared to the data available on uranium fission. To extend the basic data, a program for studying fission product gamma-ray spectra following the fast neutron-induced fission of plutonium is underway. An unshielded uranium metal critical assembly (Hydro)<sup>4</sup> serves as a source of neutrons for irradiating the plutonium.

#### B. Current Results

##### 1. Gamma Scanning

A uranium carbide fuel element (LASL-42B) has been examined by gamma scanning of the unsectioned element inside a secondary container. Axial activity of the fuel section was measured by gamma scanning with a slit collimator along the length of the fuel element. Individual fuel sections can be discerned from the multiscale scans, as shown by the two large dips in Fig. 464-10. In these multiscale scans, data were accumulated for 2 sec and the sample was moved in 0.003-in. increments between data points. From the multiscale scans, the complete length of the fuel was also measured. An accuracy of about 0.002 in. is easily obtained from these scans. To date, no anomalies in this fuel element have been detected.

As part of a cooperative agreement with the ASTM E-10 Committee, a 3 x 3-in. NaI detector assembly has been set up and a series of absolute decay rate determinations on a standard sample containing <sup>140</sup>La has been made. The results of those experiments have been received, and they are in very good agreement with the results obtained by the ORNL laboratories.

##### 2. Gamma-Ray Spectra of Short-Lived Fission Products from Fast Fission of Plutonium

All equipment is installed for the experiments on the fast fission of plutonium.

Experiments performed at the critical assembly site indicate that the neutron shielding for the 12 x 8-in. NaI detector is adequate. With the Hydro critical assembly running in the kilowatt range, there is no indication of either <sup>24</sup>Na or <sup>22</sup>Na activity. In the experiments on the fast fission of <sup>239</sup>Pu, Hydro will be at least a decade lower in power than during these tests.

The diode photocell used in the irradiation end station to indicate when the <sup>239</sup>Pu sample is present was tested with Hydro running in the kilowatt range and performed as it should. However, the life of the diode may be shortened in the high neutron and gamma field when Hydro is running.

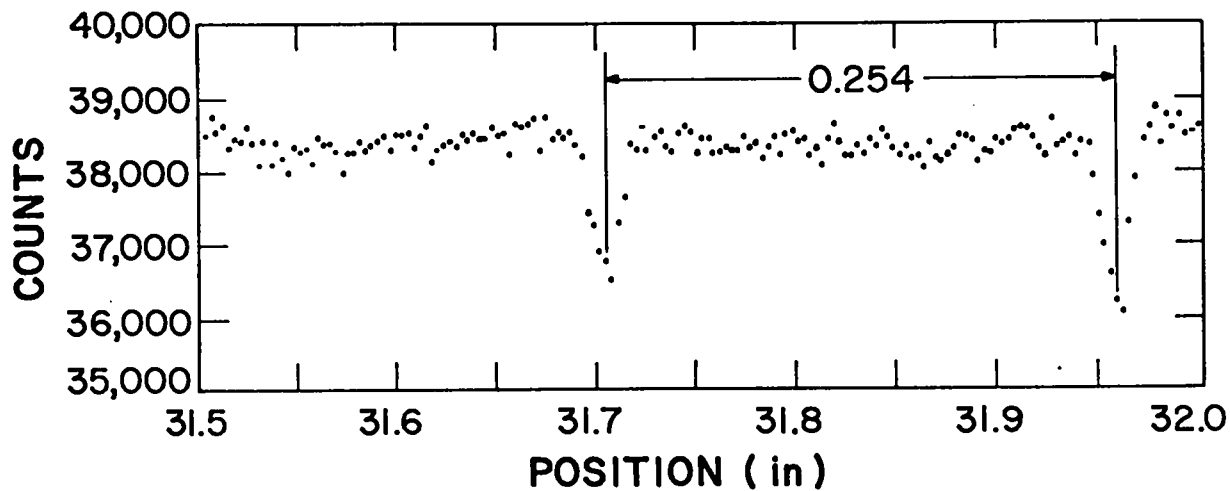


Fig. 464-10. Multiscaler scan of LASL-42B section showing pellet interfaces.

VII. SODIUM-BOND HEAT TRANSFER STUDIES  
(J. O. Barner, K. Meier)

A. General

The purpose of this project is to evaluate methods for determining the effects of fuel-pin defects on heat transfer properties of the sodium bond. Such defects could arise in a number of ways. For example, a void in the sodium bond could: (1) be present before insertion in the reactor, (2) come from dewetting of the pellet due to change in composition as fission products are formed, (3) form from a hot spot on the pellet and consequent local vaporization of the sodium, and/or (4) be produced from desorbed or fission-product gases. Of these, probably the most serious defect would be the presence of fission gas bubbles in the bond region.

There appear to be three methods of obtaining the high heat fluxes necessary for "defect analysis": (1) in-pile experiments, (2) out-of-pile experiments utilizing a central, high-heat-flux heater, (3) out-of-pile experiments utilizing an induction heat source with the heat flow direction reversed. These three methods are all receiving consideration for use in sodium-bond heat transfer studies.

B. Current Results

Design, construction, and testing of portions of the apparatus for out-of-pile testing of sodium

bonds utilizing a central, high-heat-flux heater are underway. The bubble injection apparatus was fabricated and assembled. A solenoid device was built to move the bubble injection tube down away from the bubble after injection into the sodium bond.

Equipment for studying bubble behavior in sodium annulus at 100°C was assembled. This contains a glass tube mockup of capsule cladding, a UC cylinder around the graphite rod heater, and sodium in the annulus between the UC cylinder and the glass tube. The bubble injection apparatus was incorporated into this equipment, and tests have begun. No meaningful results have yet been obtained because of impurities in the sodium and on the walls of the capsule mockup.

The status of other components of the high-heat-flux test apparatus is as follows:

- a. The transition section has been fabricated. Assembly has begun.
- b. Design work has been completed on the thermocouple rotor. The 40 thermocouples will be spring-loaded to ensure contact against the cladding. Drafting work has started.
- c. The drive train has been designed. This consists of a slo-syn motor, preset indexer, and gear which rotate the thermocouple rotor.
- d. Design and drafting work have begun on the

outer structure which houses the slip ring assembly, thermocouple rotor, and the test section. A thermal stress problem exists in the structure. An analysis of the problem has started.

## VIII. ANALYTICAL CHEMISTRY

### A. General

Specific analytical techniques have been developed and evaluated to cope with the problems encountered in the investigation of fuel/clad compatibility. The results of many of these special analyses are given in several sections of the report in Project 464. A brief summary of some of the techniques, and the problems to which they were applied, is given below.

### B. Current Results

#### 1. Spectroanalysis of Sodium (O. R. Simi, R. T. Phelps)

The semiquantitative spectrochemical method used to analyze sodium for impurity elements was tested in a hot cell facility. Two portions of a nonradioactive sodium sample were analyzed by remote manipulation operations according to the following steps. In Cell 12 (Solution Processing), the sample was dissolved in Dowanol EB and excess 6N hydrochloric acid was added. The solution was evaporated to dryness in a closed system with provision for absorption of acid fumes. The NaCl was packaged in a vial. In Cell 10 (Balance), a weighed amount of the NaCl was put into a Wig-L-Bug vial containing graphite-internal standard mixture. In Cell 16 (Spectrochemical Analysis), the sample vial was shaken on a Wig-L-Bug, electrode portions were taken, and the sample was arced. Spectra were recorded on S.A.-3 photographic plates by use of a 3.4-meter Ebert-mounting spectrograph equipped with a 15,000 line-per-in. grating. Standards were also arced and their spectra were recorded on the plates with those of the samples.

The results of the analysis are listed in Table 464-VI. The control sample, Na-7110, (a portion of the same sodium metal treated in Cell 12) was prepared outside the cells with the same reagents that were used in the cells and was arced in Cell 16. A range of concentrations is given for some elements when the individual results among the

Table 464-VI

Analysis of a Na Sample Using Hot Cell Facilities

Element	Na-1	Na-2	Na-7110
Mg	1-20	10	0.3
Al	5-30	20-30	1
Si	20-60	30-60	15
Ca	30-100	30	50
Ti	1-3	5-50	< 1
Cr	3-70	15-70	< 3
Mn	2-10	2-10	< 0.3
Fe	40-200	100-300	5
Ni	1-30	3-20	1
Cu	3-5	5	3
Mo	2-5	2-5	< 1
Ag	0.3	0.3	< 0.3
Sn	< 3-10	3	< 3
Pb	< 3-3	3	< 3

Note: The elements Be, B, V, Co, Zn, Sr, Cd, Ba, and Bi were not detected. Na-1 and Na-2 were converted to NaCl in Cell 12. Na-7110 was converted to NaCl and loaded into electrodes outside the cells.

four replicates are not uniform enough to report as an average. It is considered that contamination of the sample with some of the impurity elements (mainly Al, Si, Cr, Fe, and Ni) has occurred. Because uranium samples have been analyzed without contamination using Cells 10 and 16, the probable source of contamination is Cell 12.

Additional sodium samples will be tested in Cell 12 after further cleaning of the cell. This cell, which is also used for general solution processing, may not be suitable for spectrochemical analysis because of contamination resulting from corrosion of various metal parts.

#### 2. Electron Microprobe Examinations (E. A. Hakkila, H. L. Barker)

A reaction product at the surface of a sintered (U,Pu)C pellet that had contacted a V-Ti-Cr capsule was identified as V-Ti-Pu. Precipitates in grain boundaries in the (U,Pu)C were essentially free of carbon and contained more plutonium and less uranium than the matrix.

#### 3. Miscellaneous Analytical Support (W. W. Wilson, N. L. Koski, L. E. Thorn, R. G. Hurley, W. B. Hutchinson, G. R. Waterbury)

Controlled-potential coulometric and combustion-gravimetric methods were applied without difficulties

to measurement of U, Pu, and C in two pretest (U,Pu)C samples. The coulometric titrations of uranium and plutonium had a relative standard deviation of 0.2 to 0.3 per cent, and the combustion-gravimetric method for determining carbon had a precision ( $1 \sigma$ ) of 0.5 relative per cent.

A potentiometric titration method, having a relative standard deviation of 0.05 per cent, was applied to the assay of plutonium metal to be used in the preparation of mixed carbides. Spectrophotometric methods were used to measure Ta, W, and N in this Pu metal and also in a (U,Pu)C. The precision ( $1 \sigma$ ) of each spectrophotometric method was 2 relative per cent.

X-ray fluorescence spectrometry was very satisfactory in rapidly identifying a suspect alloy as V-Ti.

An inert-gas-fusion method, having a relative standard deviation of 10 per cent, was applied without difficulty to the measurement of oxygen in four samples of zirconium metal from a sodium hot trap. Oxygen analyses were also performed on five V-Ti, two V-Ti-Cr alloys, and two vanadium coupons that had been tested in molten sodium at 450 to 650°C for 500 h; one plutonium metal and two (U,Pu)C samples were also analyzed for oxygen.

A combustion-micromanometric method was used in measuring carbon in the plutonium metal. The precision ( $1 \sigma$ ) of the method in determining low concentrations of carbon was 10 relative per cent. No difficulties were experienced.

Samples of zirconium and various vanadium alloys for corrosion tests were analyzed for carbon and nitrogen. Sodium metal was analyzed for C, N, and H. Alloy steel samples were analyzed for carbon as an aid to identification. Established methods were used for this work.

#### IX. REFERENCES

1. C. S. Campbell and C. Tyzack, "A Preliminary Model for the Carburization of Stainless Steel at High Temperatures in Sodium Containing Carbon at Unit Activity," IAEA, Alkali Metal Coolants, Vienna (1967).
2. W. J. Anderson and G. V. Sneesby, "Carburization of Austenitic Stainless Steel in Liquid Sodium," Report NAA-SR-5282, Atomic International, 1960.
3. C. Wells, W. Batz, and R. F. Mehl, AIME Trans. 188, 553 (1950).

4. William Bernard, "Hydro - A Small, Water-Cooled, and Water-Reflected Neutron Source," Report LA-3374, Los Alamos Scientific Laboratory, March 14, 1966.

PROJECT 466

FAST REACTOR METALLIC FUEL STUDIES

Persons in Charge: R. D. Baker  
D. B. Hall  
Principal Investigators: W. J. Maraman  
R. H. Perkins

---

I. INTRODUCTION

The objective of this program is the development of metal fuels for fast reactor application. Much of the primary effort is placed on preparation and fabrication development of the U-Pu-Zr alloys. Supporting effort is directed toward areas of physics and system evaluation, determining of physical and chemical properties of the fuel, and studying fuel-cladding interactions.

Irradiation testing is an essential part of the evaluation of a potential fuel alloy for fast reactor application. A knowledge of its intrinsic swelling rate as a function of alloy composition, metallurgical history, irradiation temperature, and total burnup must be obtained. The fission gas release rates and the limits of lattice-retained gas as a function of the above parameters are also required. In addition, the compatibility of fuels and cladding during irradiation at temperatures of interest to the LMFBR program must be determined.

II. FUEL PREPARATION AND FABRICATION  
(D. R. Harbur, B. N. Robbins, A. K. Murdock,  
E. L. Grady)

A. General

The initial goals of this project are to prepare high purity, homogeneous U-15Pu-6Zr to U-15Pu-15Zr alloys, to fabricate these alloys into fuel pins of the EBR-II size and to fully characterize these pins. An alloy preparation and casting method for making high purity extrusion billets has been developed. The extrusion billets are prepared by induction melting of the three elements in a NbC-coated graphite crucible at 1400°C, mechanically

stirring the melt for 30 min followed by pouring into an aluminum mold at an ambient temperature. Emphasis is now being placed upon the fabrication of these billets into fuel pins with large length to diameter ratios. Characterization of these extruded alloys has been initiated.

B. Current Results

A new  $Y_2O_3$  coating which can be easily applied to a graphite or metal surface has been developed with Acheson Colloids Co. The coating is applied by spraying the colloidal  $Y_2O_3$  in  $K_2SiO_3$  solution (Acheson Colloids Co. Number EC 3327X) onto the desired surface. Once applied, the coating has excellent thermal shock resistance, good abrasion properties and is un-wetted by the molten U-Pu-Zr alloys. This  $Y_2O_3$  coating on a graphite crucible can be used for casting U-Pu-Zr alloys provided that the addition of about 100 ppm of silicon and oxygen can be tolerated. Attempts to develop similar coatings with NbC and ZrC have not yet been successful.

The development of an extrusion process for fabricating this alloy is essentially complete. Using a relatively low-pressure die system of 50 T capacity, the alloys are easily extruded in the alpha phase temperature region at 570°C. Extrusion ratios as high as 9 to 1 have been realized. The extrusion die, die body, punch and ram are made of M-2 tool steel hardened to 60-64 Rc. The lubricant used is  $WS_2$ -commercially available in a pressurized spray can under the trade name "Tungspray."

Installation of the dry box system for the swaging machine is nearly complete, and process development with this machine will be carried out during the next quarter.

X-ray diffractometer studies have shown that the as-extruded alloys exhibit a high degree of preferred orientation. This observation is supported by metallography and thermal cycling experiments. Thermal cycling experiments are being made with U-15Pu-12Zr alloy rods in the as-extruded condition. Three separate thermal cycles are being used (1) 500° (α phase) - 650°C (β phase) (2) 500° (α phase) - 750°C (γ phase) and (3) 630° (β phase) - 750°C (γ phase). After 200 thermal cycles the diameters of the specimens (originally 0.163 in.) increased, whereas the lengths and densities of the specimens (originally 0.75 in. long) decreased. Figure 466-1 shows the behavior of this material during the various thermal cycles. Metallographic examination of

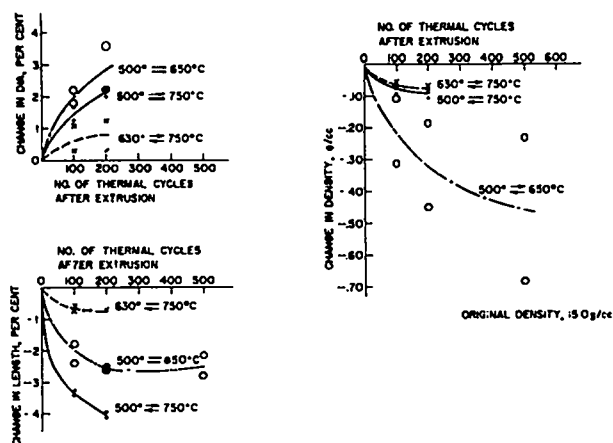


Fig. 466-1. Physical Changes in As-Extruded U-15Pu-12Zr Alloy Due to Thermal Cycling.

these specimens after 100 thermal cycles showed all of the specimens to have a completely recrystallized-equiaxed grain structure. It appears, however, that the anisotropic growth pattern continues to 200 thermal cycles. After 200 thermal cycles, the diameters of the specimens cycled between the α and β phase were out of round by a maximum of 0.010 in. During the same period, the length of one specimen continued to decrease slightly whereas the length of another specimen started to increase. Between 200 and 500 thermal cycles the preferred orientation was eliminated in the specimens cycled between the α and β phase.

The density decreases of the specimens cycled between the α and γ phases or the β and γ phases were quite uniform, appearing to level out at a 0.06 to 0.10 g/cc decrease from the as-extruded

density of 15.0 g/cc. Density decreases of 0.07 and 0.09 g/cc for two specimens from the same lot were observed after simply holding them for 17 days at 750° and 650°C, respectively. It is believed that the density decreases of the above specimens were caused by a redistribution of phases due to homogenization in the γ phase temperature region.

A catastrophic density decrease occurred in the specimens cycled between the α and β phases. After 500 thermal cycles, the density decreases were 0.23 to 0.68 g/cc. Both specimens tested had developed longitudinal cracks which were visible on the surfaces. A 0.030 in. diameter hole had opened up in the center of the specimen which had the greater density decrease. It is quite probable that this hole was a former shrinkage cavity formed during casting that closed during extrusion. The change in diameter, length, and density for a specimen held for 17 days at 500°C was negligible. Metallographic and microprobe data are being gathered on all of the thermal cycling specimens after 100 and 500 thermal cycles. The extent of ion transfer due to a thermal gradient along the length of a U-Pu-Zr rod is being determined. One end of the 1-in.-long, 0.178-in.-diam rod is in the γ phase temperature region while the other end of the rod is in the α phase temperature region.

The tensile properties of several U-Pu-Zr alloys are given in Table 466-I. The highest room temperature tensile strength of the extruded material is 97,000 psi for the U-15Pu-6Zr alloy, decreasing to a value of 70,000 psi for the U-15Pu-10Zr alloy and again increasing to 84,000 psi for the U-15Pu-13.5Zr alloy. All of these alloys tested were high purity containing 125, 70, and 180 ppm oxygen, respectively. The maximum tensile strength exhibited by the U-15Pu-12.2Zr alloy in the as-cast condition was 61,000 psi. Tensile strength values as much as 17,000 psi lower than this value were obtained, but small cavities were always evident at the fracture surface. These small cavities were a result of centerline porosity which occurred during the casting operation. The U-15Pu-10Zr alloy behaved in a brittle manner up to 300°C. At 350°C the alloy showed some ductility and became quite plastic at 400°C, having an elongation of 53% over the 2-in. gage section of the tensile bar. The U-15Pu-6Zr alloy was quite plastic at 290°C, elongating 11%

during a creep test at 5660 psi. The creep data between 290° and 500°C for two of the U-Pu-Zr alloys are given in Table 466-II. All of the tensile/creep test bars were reduced to a tapered point at the fracture interface even though the entire 2-in. gage section was carefully maintained at the test temperature. This observation coupled with the short

temperature spread between a brittle mode of fracture and a completely plastic behavior suggests that the grain boundaries are becoming plastic at the higher temperature resulting in grain boundary creep.

Three high purity alloys have been cast and extruded and are being machined into samples for further characterization.

Table 466-I  
Tensile Properties of U-Pu-Zr Alloys<sup>(a)</sup>

Alloy Composition, Nominal w/o			Temp	U.T.S.	Y <sub>s</sub> , S <sub>s</sub> <sup>(b)</sup>	Elongation	Fabrication History	E
U	Pu	Zr	(°C)	(psi)	(psi)	(%)		psi x 10 <sup>6</sup>
75	15	10	25	70,000	-	Nil	As-Extruded	2.2
			300	39,000	-	Nil	As-Extruded	2.1
			350	44,000	44,000	3	As-Extruded	0.9
			400	14,000	10,000	53	As-Extruded	0.4
73.3	15	11.7	25	76,000	-	Nil	As-Extruded	2.3
			100	80,000	-	Nil	As-Extruded	2.2
71.5	15	13.5	25	84,000	-	Nil	As-Extruded	1.0
79	15	6	25	97,000	-	Nil	As-Extruded	2.5
72.8	15	12.2	25	61,000	-	Nil	As-Cast	1.4

(a) Tensile test performed at a strain rate of 0.015 in./in./min.

(b) Yield strength at 0.2% offset.

Table 466-II  
Time (in minutes) to Attain 2% Strain in U-Pu-Zr Alloys  
In the As-Extruded Condition

Alloy Composition, Nominal w/o			Stress psi	Temperature, °C			
U	Pu	Zr		290	350	400	500
75	15	10	2,000	-	-	-	20
			3,000	-	-	-	5
			8,000	-	-	30	rupture
			10,000	-	-	9	"
			11,000	-	-	3	"
			20,000	-	300	rupture	"
			30,000	-	20	"	"
79	15	6	40,000	-	9	"	"
			1,000	-	-	-	0.3
			5,000	30	rupture	rupture	rupture
			6,000	9	"	"	"

### III. METAL FUEL COMPATIBILITY TESTING (J. A. Horak)

#### A. General

The purpose of this task is to study the compatibility of potential fast reactor metallic fuels (e.g., U-Pu-Zr, and other alloys) with potential cladding materials (e.g., Type 316 stainless steel). This will be accomplished by studying the mechanisms and kinetics of reactions between the fuels and cladding both in-pile and out-of-pile at temperatures of interest to LMFBR designers. The emphasis will be on out-of-pile studies with neutron irradiation being added as an experimental variable. To attempt to understand some of the reactions which will occur between the complex candidate fuel and cladding alloys, some experiments will be performed to study the reactions between the pure components of these alloys (e.g., U vs Fe).

#### B. Current Results

Eighteen diffusion couples of U-5F<sub>s</sub> versus Type 304L stainless steel have been prepared for irradiation by bonding at 600°C in a helium atmosphere for 1/2 h. Three diffusion couples and 0.31 g of sodium have been loaded into each of six primary irradiation containers. The three diffusion couples that constitute each irradiation assembly have been sodium-bonded to the primary container by centrifuging for 30 min at a temperature of 300°C.

These couples will be irradiated with the U-5F<sub>s</sub> fuel specimens to determine the effect of neutron irradiation on diffusion in cladding and fuel that is held at constant temperature during irradiation. The first irradiation is planned for a fuel/clad interface temperature of 600°C. This is 50°C higher than the present fuel surface temperature in EBR-II while it is operating at 50 MW; however, it will provide valuable information on the diffusion rates that will occur when EBR-II goes to its design power of 62.5 MW and the fuel surface temperature is increased by approximately 25°C.

In addition, 24 out-of-pile fuel specimens of U-15Pu-12.5Zr and 48 cladding specimens of Type 316 stainless steel have been prepared and are awaiting insertion into the fuel loading box for bonding of the fuel and clad and sodium-bonding of the diffusion couples to the primary container.

### IV. IRRADIATION EFFECTS STUDIES (J. A. Horak, R. L. Cubitt, D. C. Kirkpatrick)

#### A. General

All long-term irradiations of metal fuel to date have had the effects of thermal cycling (due to reactor shutdowns and changes in power level) imposed upon the effects due to irradiation. Some of the detrimental effects to the fuel caused by this thermal cycling are:

1. The internal stresses produced by the volume changes associated with the alpha-gamma phase transformation in uranium-base alloys could be the source of microcracking.
2. Upon cooling, as alpha grains nucleate and grow from the existing gamma grains, the fission products (those that are insoluble and/or above their solubility limits) are swept ahead of the new alpha grains and end up in the alpha grain boundaries. The reverse process occurs on heating. The agglomeration of these elements produces a brittle and/or weak phase (usually intermetallic) resulting in a decrease in the mechanical strength and ductility of the fuel. This phase could exhibit a lower corrosion resistance to hot sodium than that typical of the parent fuel.
3. Possibly even more important is the relocation of fission gases during thermal cycling; the agglomeration of fission gases during repeated phase transformations could be responsible for the extensive swelling and cracking observed in many of the fuel alloys irradiated to date.

It is evident that thermal cycling of unirradiated material does not provide the information necessary to separate the effects due to irradiation from those due to combined irradiation and thermal cycling.

One of the prime objectives of this program is to determine the effects of irradiation in the absence of thermal cycling. Irradiations will be conducted in the Omega West Reactor where controlled temperature instrumented facilities are available. Parallel experiments will involve thermal cycling to assess accurately the effects of thermal cycling during irradiation on the properties to be studied.

## B. Current Results

The OWR irradiation cell was reinserted into the core of the reactor on February 10, 1969. All of the controls, alarms, heaters, and associated circuitry were operated to check out the facility and prepare it for installation of an experimental insert the following week. Subsequent to these operations the cell was withdrawn from the core and placed in a standby position.

On February 17, 1969, the cell was reinserted into the core and an experimental insert installed in the cell. The insert contained stainless steel components to measure the gamma ray heating with an experimental insert in the cell. Determination of the gamma ray heating in the cell is necessary to determine the amount of fission heating that can be generated in the cell without exceeding the heat dissipation capability of the cell which is 10 kW.

The gamma ray heating in the specimen was determined as a function of reactor power level with stagnant nitrogen as the control gas and with a mixture of 50% helium and 50% nitrogen flowing at a rate of 50 cm<sup>3</sup>/min as the control gas. The gamma ray heating in the specimen was 0.35 kW per MW of reactor power, or a total of 2.8 kW of gamma heat at the normal reactor operating power of 8 MW. Therefore, a total of 7 kW of fission heat and electrical heat can be generated within an experimental insert without exceeding the heat dissipation capability of the irradiation cell. Calculations indicate that 1400 W of fission heat is generated in each U-5F<sub>s</sub> specimen that is 52% enriched and is 1-1/2 in. long by 0.144 in. diameter. In addition, 525 W are generated in each fuel-clad diffusion assembly. Hence, three fuel specimens and three diffusion specimens can be irradiated in the cell and still permit the application of 1.5 kW of electrical heat for control and for minimization of temperature gradients in the fuel and diffusion specimens.

Calculations also indicate that 650 W are generated in each 1 in. long U-15Pu-12.2Zr alloy fuel specimen and 370 W in each diffusion couple assembly. Hence, six fuel and three diffusion couple specimens can be irradiated, and 2 kW of electrical heat can be used for control without exceeding the 10 kW heat dissipating capability of the cell.

During this experiment, studies were also made of the effectiveness of various gas mixtures (helium and nitrogen) in controlling the temperature in the specimen. The electrical power required to hold the specimen at temperature as a function of the helium content of the heat control gas was determined. The time required for a change in gas composition to result in a temperature change in the specimen and the time required for a change in electrical heater power to result in a temperature change in the specimen were studied. The temperature decrease experienced by the specimen as the result of a reactor scram and the time required for the temperature to stabilize to the preset value after a scram were determined.

V. ANALYTICAL CHEMISTRY (W. Hutchinson, W. Wilson, N. Koski, L. Thorn, W. Baughman, R. Hurley, and G. Waterbury)

A modified inert-gas-fusion method was applied without difficulty to measurement of oxygen in sixteen U-Pu-Zr alloys. The standard deviation of this method is 9 relative percent over the oxygen concentration range between 50 and 410 ppm found in these samples.

A combustion-micromanometric method performed satisfactorily in measuring carbon in nine U-Pu-Zr alloys. For the carbon concentration range between 200 ppm and 0.42%, the precision (1  $\sigma$ ) was 10 relative percent. For the simultaneous determination of carbon and hydrogen in four U-Pu-Zr alloys, a combustion-gravimetric method was applied. At the low concentration ranges found, the standard deviation of the method was 10 ppm in measuring carbon and 5 ppm in measuring hydrogen.

Controlled-potential coulometric methods were used in measuring uranium and plutonium in ten U-Pu-Zr alloys. The relative standard deviations were 0.2 to 0.3% in measuring either element. No difficulties were experienced.

Spectrophotometric methods were applied to determination of zirconium in twenty-three U-Pu-Zr alloys; Ta, Fe, Ga, Th, W, and N in four of these alloys; and Nb in two alloys. The relative standard deviations were 1 percent in measuring zirconium and 2 percent in measuring the seven impurity elements listed.

An x-ray fluorescence spectrometric method was used to determine yttrium in four U-Pu-Zr alloys.

The yttrium concentrations were less than the 400 ppm lower limit of reliable measurement by this method.

Spectrochemical methods were used for the semi-quantitative analysis of five samples of U-Pu-Zr alloys.

PROJECT 465

REACTOR PHYSICS

Person in Charge: D. B. Hall  
Principal Investigator: G. H. Best

---

I. INTRODUCTION

Basic to the evaluation of various fast breeder concepts and proposals are the analytical techniques and physical data used in the analyses. Valid comparisons between different concepts and proposals depend on minimization of differences in results due to methods of analysis. To this end, the Los Alamos Scientific Laboratory is cooperating with other AEC laboratories and contractors in the development of evaluated cross-section data and associated processing codes. In addition, the Laboratory is working on the development and maintenance of digital computer programs pertinent to the nuclear analysis of fast breeder concepts. Finally, the Laboratory is evaluating the performance characteristics of various fast breeder reactor concepts.

II. CROSS-SECTION PROCUREMENT, EVALUATION AND TESTING (M. E. Battat, R. J. LaBauve, A. C. Niethammer, R. E. Seamon)

A. General

Accurate predictions of reactor design parameters, such as critical mass, sodium worth, and spectral response, require the development and maintenance of up-to-date basic microscopic nuclear data files. To meet this need, a national cooperative program is in progress to prepare an evaluated nuclear data file (ENDF/B). The large amount of experimental data which is becoming available, together with the theoretical data, makes the maintenance of ENDF/B a continuing task. In addition, a large effort is needed in evaluating and testing the microscopic data prior to use in reactor calculations.

B. Data Testing

New nuclides added to the MC<sup>2</sup> library tape are <sup>6</sup>Li, <sup>7</sup>Li, <sup>1</sup>H, <sup>2</sup>D, Zr, <sup>185</sup>Re, <sup>187</sup>Re, <sup>63</sup>Cu, <sup>65</sup>Cu, Cu, and He. Natural gallium data (atomic mass 69.72) is being processed from Livermore Radiation Laboratory data and added to the library cross section tape. The data received included reaction types in ENDF/B files 3, 4, and 5. MC<sup>2</sup> problems run with the Hansen-Roach 16-group energy structure<sup>1</sup> using the gallium data have not been successful, so more test runs are being made to determine the source of error.

C. Processing Codes

1. SINTAB. A code is being written for generating multigroup cross sections from the ENDF/B thermal data. In the first version of this code, SINTAB, only single table cross sections will be generated, using a transport correction for an anisotropic approximation. SINTAB will consist mainly of the codes FLANGE2, used for the generation of the inelastic kernel, and THERM2, used for collapsing the thermal cross sections to a broad group structure, in an overlay arrangement. Cross sections for nonscattering isotopes needed for input to THERM2 will be obtained from MC<sup>2</sup>, as will all nonthermal cross sections for all materials. A schematic representation of SINTAB is shown in Fig. 465-1.

2. FLANGE2. Fine-group flux spectra in the energy range  $0.001 < E < 1.0$  eV have been calculated with thermal data obtained from the ENDF/B tapes using FLANGE2 and with thermal data derived from other sources. The input for THERM2, the code which generates the flux spectrum, consists of absorber data from MC<sup>2</sup>, capture and total scatter cross

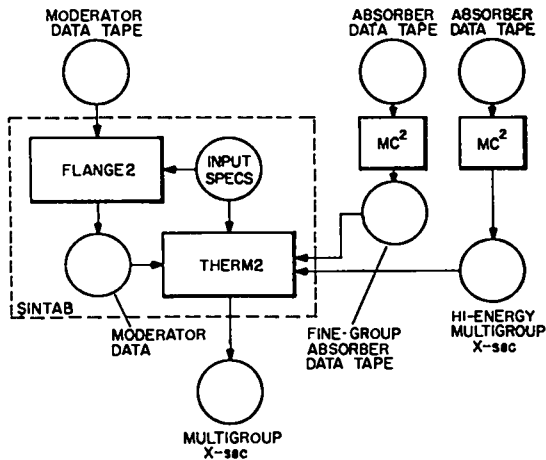


Fig. 465-1. Schematic representation of SINTAB.

sections from FLANGE2 for the moderator <sup>12</sup>C, and an inelastic scattering kernel calculated by one of the thermal group collapsing codes FLANGE2, SUMMIT, or GLEN. At a given temperature, the same moderator data was used regardless of how the scattering kernel was calculated. Results are available for 296, 500, 1000, and 1200°K for FLANGE2 and SUMMIT and for 296 and 500°K for GLEN. Representative results are shown in Figs. 465-2 through 465-4. The flux spectra calculated using the FLANGE2 kernels at four temperatures are shown in Fig. 465-2. In Figs. 465-3 and 465-4, the flux spectra at 296 and 500°K

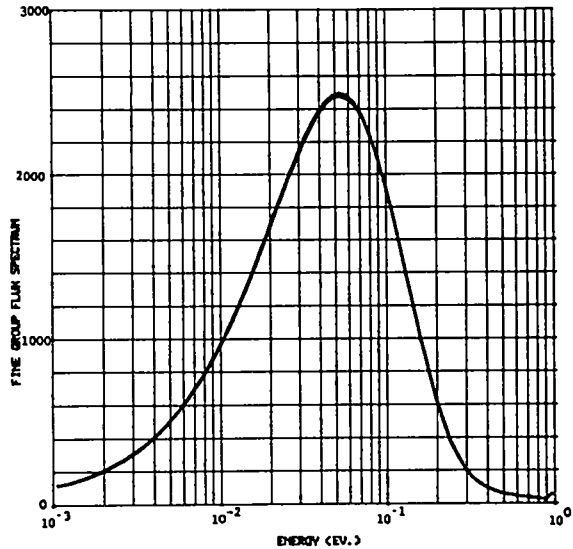


Fig. 465-3. Flux spectra at 296°K for calculations made with FLANGE2, GLEN-TOR, and SUMMIT.

are shown for calculations made with the three kernels. At 296°K, the curve for the FLANGE2 spectrum lies between the curves for the GLEN and SUMMIT spectra, the maximum difference between the spectra amounting to 1.3% at 0.04 eV. At 500°K, the SUMMIT curve lies below the other two by less than 1% at 0.05 eV.

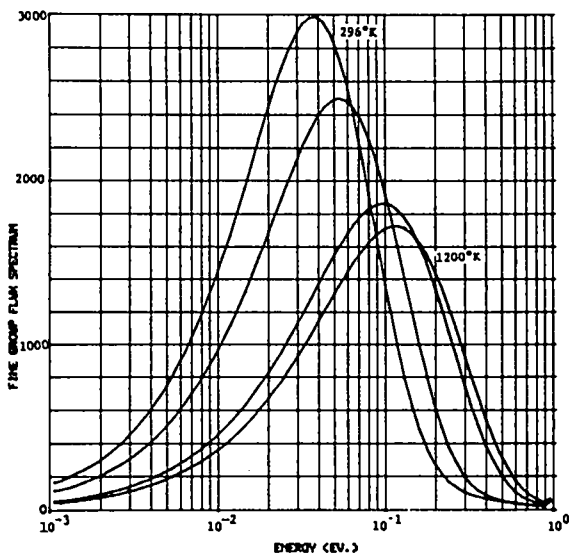


Fig. 465-2. Flux spectra calculated using FLANGE2 kernels.

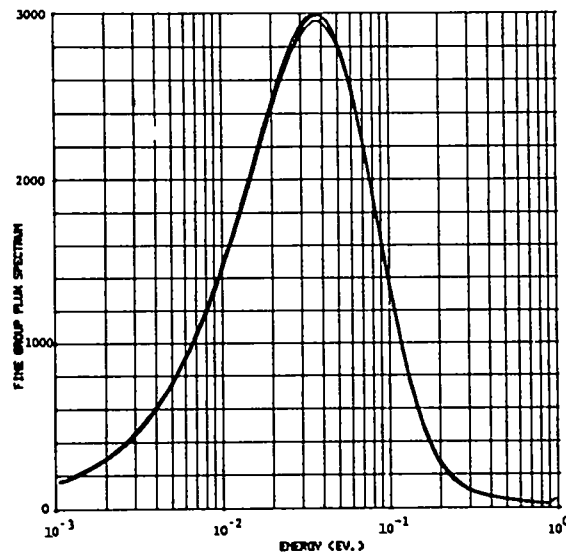


Fig. 465-4. Flux spectra at 500°K for calculations made with FLANGE2, GLEN-TOR, and SUMMIT.

3. ETOE. Test computer runs using extended core storage (ECS) file simulation have effectively reduced the peripheral processor time required for this code, especially when using ECS as a scratch file. A sample problem showed a reduction from 5.08 to 3.20 min peripheral processor time, with no significant change in the central processor time. The time required to read data tapes to ECS and to use ECS for data storage was approximately equal to the time required to read directly from the tape file.

4. LAPH. The Los Alamos photon production code, LAPH, now calculates photon production cross sections using gamma transition probabilities and neutron cross sections, as well as the photon production by capture and fission using neutron cross sections read either from cards or the ENDF/B library tape. The neutron cross sections are averaged over each fine-group interval. These portions of the code have all been checked by hand calculations. Work is in progress on debugging those parts of the code which account for photon production by neutrons at energies above those for which there are level de-excitation schemes (MT = 15 and = 110 on the ENDF/B tape). It has been verified that the code calculates photon production matrices for several zones and several materials within each zone.

For each material, the LAPH code uses files 3 and 15 on the ENDF/B tape. These files contain a small fraction of the total information stored for each material, and large amounts of peripheral processor time were being spent in reading past the unneeded information. A code, ETOL (ENDF/B to LAPH), has been written to prepare a library tape containing only files 3 and 15 for each material. The peripheral processor time required by LAPH using the abbreviated library tape has been reduced by more than a factor of ten. The original ENDF/B tape did not contain information for MT = 110. This information has been retrieved from another tape, is available on punched cards, and has been edited onto the abbreviated library tape for LAPH.

### III. REACTOR ANALYSIS METHODS AND CONCEPT EVALUATIONS

#### A. General

A continuing task in fast reactor analysis and evaluation is the improvement of computer programs and the development of new computational methods. In addition to new methods, advances are constantly being made in computer technology which make possible the extension of existing calculational techniques.

#### B. Variational Principles Applied to Transport Problems (R. E. Alcouffe)

One method for improving the functional method for obtaining transverse leakage corrections when performing one-dimensional transport calculations on two-dimensional small fast systems is to improve the trial function representation of the solution. An attempt to improve the trial function representation of Ref. 2 is to represent the two-dimensional angular flux as

$$\phi(r, z, \xi, \omega, E) = \frac{\psi(r, \xi, \omega)}{[\psi]_R} \frac{\chi(z, \xi, E)}{[\chi]_{kin}} a_{kin},$$

for the ranges  $E_{k+1} \leq E \leq E_k$ ,

$$\xi_n \leq \xi \leq \xi_{n+1},$$

and

$$z_1 \leq z \leq z_{i+1}$$

where

$$\psi(r, \xi, \omega) = \int_0^\infty \psi(r, \xi, \omega, E) dE$$

$$[\psi]_R = \frac{1}{4\pi} \int_0^R r dr \int_{-1}^1 d\xi \int_0^{2\pi} d\omega \psi(r, \xi, \omega)$$

$$[\chi]_{kin} = \int_{E_{k+1}}^{E_k} dE \int_{\xi_n}^{\xi_{n+1}} d\xi \int_{z_i}^{z_{i+1}} dz \chi(z, \xi, E)$$

The quantities  $\psi(r, z, \omega, E)$  and  $\chi(z, \xi, E)$  are assumed to come from previous calculations in the radial and axial directions, respectively.

The addition of information through the quantity  $\chi(z, \xi, E)$  was done with the expectation that this would improve the energy spectrum information. The equations derived from these trial functions are similar to those in Ref. 2. However, the resulting calculations showed no improvement in the eigenvalue for the examples given in Ref. 3.

### C. Preparation and Maintenance of Code Packages

1. Multiple User Experiment (MUX) (B. M. Carmichael). A system of remote terminals for the CDC 6600 called the Multiple User Experiment (MUX) is being developed by the Computing Division of LASL. The basic remote terminal device is the Teletype Corporation Model 35 Teletype. A distinct advantage of this type of terminal is that the cost is of the same order of magnitude as that of an electronic desk calculator.

A variety of computer problems have been run using the MUX terminals set up at the Central Computer Facility of the Laboratory.

With proper procedures, the debugging phase on problems can be performed much more efficiently through MUX than otherwise. In general, one should divide problems into increments requiring short execution times and minimum storage during the debugging phase in order to obtain rapid service through MUX. The system is well adapted to output sampling of problems for checking results. By such sampling, one can verify results before releasing the output to the high-speed printers for full printing.

Large production codes can be called off tape using MUX. For problems requiring extensive input, the input for a reference problem is read off cards in the usual way and stored on tape. Then MUX can be used for modifying such input to perform parameter studies.

2. Burnup Codes (R. D. O'Dell, T. J. Hiron). Two additions were made to 2DB<sup>4,5</sup> which are useful in connection with the burnup portion of the code. The first calculates the instantaneous power fraction for each zone in the reactor, both before and after the burnup step. This feature allows the power shift to be observed over a single burnup step, and the total change to be observed over the

lifetime of the reactor. The second addition to the code provides for the calculation of the average burnup rate for each zone, in MWd/T, for each burnup step of the reactor lifetime. This parameter is useful in determining the burnup distribution of the fuel and could be used as a criterion for making changes in the fuel management schedule.

The LASL CDC-6600 version of 2DB has been submitted to the Argonne Code Center with a brief memorandum summarizing the input instructions for this version of the code. The LASL version will appear in the Code Abstracts under the same abstract number (325) as the original Battelle-Northwest version.

A subroutine, REFUEL, has been added to 2DB to form a single burnup-refueling code, PHENIX, which will account for the flux shift over the reactor lifetime. The refueling option gives a nearly exact treatment of the fuel discharge at any time for the different refueling fractions. The code searches on the control poison to give the desired initial eigenvalue, performs the burnup over the given time step, calculates the final eigenvalue after the burnup using a straight  $k_{eff}$  calculation, and calculates the discharged atom densities for the given burnup step and the refueled atom densities of all fuel isotopes for the next burnup step, for any fuel management schedule. This single code for fuel-cycle studies will greatly simplify the detailed burnup analysis of any reactor and provide accurate results for input to economics codes.

The separate refueling program ATDENS<sup>3</sup> was modified to summarize the results of all burnup intervals in a single burnup analysis. These results include the charges and discharges of all fuel isotopes for all burnup intervals, which are punched out on cards in the correct format for input to the fuel-cycle economics code LAREC.

3. Linked Codes (A. F. McGirt). Work is continuing in the development of linked code packages which will facilitate the solution of complicated reactor problems by automating much of the handling of the input data. The DPC code, which prepares input for the two-dimensional neutron transport theory code 2DF was rewritten, incorporating many of the FORTRAN-IV programming features such as

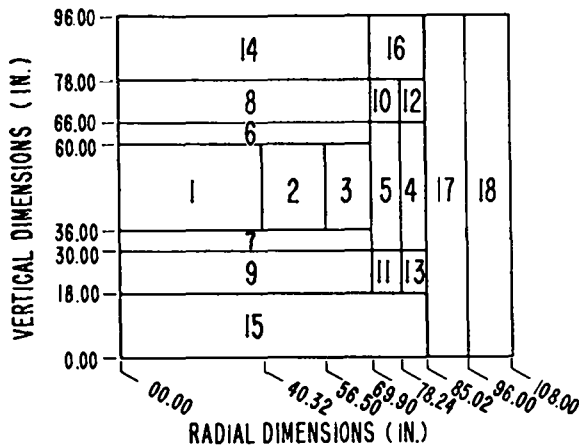
variable dimensioning. This task was made somewhat easier by the use of a FORTRAN-IV subroutine package ASAP, which helps to eliminate many of the book-keeping chores normally associated with the use of adjustable dimensions. The ASAP package also includes debugging aids such as array dumping and optional error trace printout.

The revised version of DPC is being linked to 2DF to form an independent computational package with simple input requirements. The complete DPC-2DF linked code package should be fully operational soon.

4. FATDTF (A. C. Niethammer). FATDTF, a code designed to calculate the regular and adjoint DTF-IV problems simultaneously with a perturbation calculation, is being tested. Problems are being run using the DTF-IV angular distribution option. Criticality and central reactivity calculations will be run for each of the 63 materials presently on the MC<sup>2</sup> library tape.

D. Fast Reactor Design Analysis (R. D. O'Dell, T. J. Hirons)

In conjunction with the detailed burnup analysis of the 1000-MWe mixed-oxide LMFBR,<sup>6</sup> studies have been conducted in an attempt to answer the question:



- |                              |                             |
|------------------------------|-----------------------------|
| 1. CORE ZONE 1               | 10. UPPER RADIAL BLANKET    |
| 2. CORE ZONE 2               | 11. LOWER RADIAL BLANKET    |
| 3. CORE ZONE 3               | 12. VOID                    |
| 4. RADIAL BLANKET OUTER      | 13. VOID                    |
| 5. RADIAL BLANKET INNER      | 14. UPPER AXIAL REFLECTOR   |
| 6. UPPER AXIAL BLANKET INNER | 15. LOWER AXIAL REFLECTOR   |
| 7. LOWER AXIAL BLANKET INNER | 16. UPPER RADIAL REFLECTOR  |
| 8. UPPER AXIAL BLANKET OUTER | 17. THERMAL SHIELD          |
| 9. LOWER AXIAL BLANKET OUTER | 18. RADIAL SODIUM REFLECTOR |

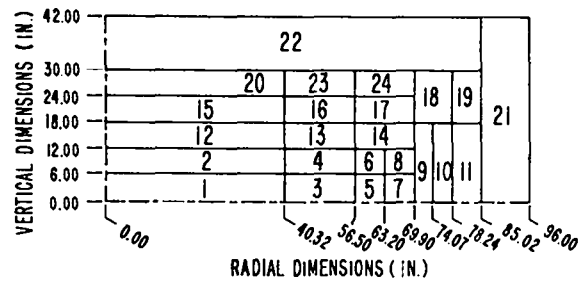
Fig. 465-5. 18-region whole-core model.

To what extent can the calculational model be simplified without unduly affecting the fuel-cycle analysis?

The variation of fuel-cycle parameters (e.g., breeding ratio and fuel-discharge rate) with five model characteristics has been studied. These characteristics are the amount of region detail used in describing the reactor, the maintenance of criticality during the burnup step, the flux or power shift over the reactor lifetime, the initial fissile content, and the boron distribution during the burnup lifetime.

Two reactor models were selected to determine the effect of region detail on the fuel-cycle parameters: One was the 18-region whole-core model (Fig. 465-5), and the other was the 24-region half-core model with axial temperature asymmetry neglected (Fig. 465-6). The same group constants were used for both models. A comparison of results indicated no significant differences (>1%) in any of the fuel-cycle parameters.

The second area of study was the effect of maintaining criticality on fuel-cycle parameters. One burnup analysis was performed with the reactor just critical after refueling and 2-3% subcritical at the end of the burnup step. Another analysis was performed with the reactor supercritical after refueling and just critical at the end of the burnup step.



- |                           |                           |
|---------------------------|---------------------------|
| 1. CORE ZONE 1 INNER      | 13. AXIAL BLANKET INNER 2 |
| 2. CORE ZONE 1 OUTER      | 14. AXIAL BLANKET INNER 3 |
| 3. CORE ZONE 2 INNER      | 15. AXIAL BLANKET MID 1   |
| 4. CORE ZONE 2 OUTER      | 16. AXIAL BLANKET MID 2   |
| 5. CORE ZONE 3A           | 17. AXIAL BLANKET MID 3   |
| 6. CORE ZONE 3B           | 18. UPPER RADIAL BLANKET  |
| 7. CORE ZONE 3C           | 19. VOID                  |
| 8. CORE ZONE 3D           | 20. AXIAL BLANKET OUTER 1 |
| 9. RADIAL BLANKET INNER   | 21. THERMAL SHIELD        |
| 10. RADIAL BLANKET MID    | 22. AXIAL REFLECTOR       |
| 11. RADIAL BLANKET OUTER  | 23. AXIAL BLANKET OUTER 2 |
| 12. AXIAL BLANKET INNER 1 | 24. AXIAL BLANKET OUTER 3 |

Fig. 465-6. 24-region half-core model.

The fuel-cycle parameters from these two analyses agreed to within 1%, except for the  $^{239}\text{Pu}$  discharge from the inner axial blankets, where the difference was about 2.5%.

The third study involved the effect of flux shift over the reactor lifetime on the calculated discharges. One fuel-cycle analysis was performed in which differences in the zone- and group-averaged fluxes over the lifetime were neglected. A second analysis was conducted with a first-order correction for the relative flux shifts. Between these two analyses, appreciable differences in results occurred in the  $^{239}\text{Pu}$  discharge from the axial blankets. In these blankets, differences of up to 7.4% were produced, and the total accumulated  $^{239}\text{Pu}$  discharge from the center third of the axial blanket over the first 12 refueling intervals differed by nearly 4%.

In the fourth study, the initial fissile content of the mixed-oxide LMFBR was varied to determine the amount of initial excess reactivity which must be built in to ensure that the system will remain critical throughout its burnup history. This criterion is particularly important if a fixed refueling schedule is to be followed. Preliminary burnup calculations were first made to approximate the overall reactivity loss of the reactor in reaching the equilibrium cycle. Based on these results, three burnup analyses were performed in which the initial plutonium content of the three core zones was increased by 12, 14, and 16%. These studies were carried out using the 18-region whole-core model and no flux shift correction. Results of the analyses indicated that each 2% increase in the initial plutonium content is worth approximately 1% additional reactivity in the clean reactor. In order to maintain criticality over the burnup history, approximately the +16%-plutonium initial core loading would be required. As the initial plutonium content is increased, the U/Pu ratio is decreased, and the boron content required to maintain criticality is greater. These effects combine to produce a lower overall breeding ratio.

When a power reactor is initially loaded, the control rods can be adjusted in several ways to achieve the desired degree of criticality. Two burnup studies were made to determine the effect of boron distribution on the fuel-cycle parameters. In

the first analysis, an equal percentage change in the boron content, based on the boron densities at the end of the previous burnup interval, was made for all zones to obtain the proper criticality adjustment. Since the boron burnup is much greater in regions nearer the center of the reactor, this method led to a poison distribution that was heavily weighted toward the outer core zone and the blanket regions during the latter burnup intervals. In the second burnup analysis, the boron distribution at the beginning of each burnup interval was maintained at some fraction of the initial poison loading. This method gave a spatially uniform boron content throughout the burnup history. Both analyses were carried out over the first 16 burnup intervals using the 18-region whole-core model with no flux shift correction. The breeding ratios and fissile discharge rates were higher for the uniform boron approach, and this method of treating the control rods is more realistic. The boron tilting effect obtained from the first analysis resulted in significantly reduced contributions to the breeding ratio from the outer core zone and the blanket regions, and this method is not physically realistic because of the limited number of control rods in these regions.

#### REFERENCES

1. G. E. Hansen and W. H. Roach, "Six and Sixteen Group Cross-Sections for Fast and Intermediate Critical Assemblies," LAMS-2543, Los Alamos Scientific Laboratory (1961).
2. "Quarterly Status Report on the Advanced Plutonium Fuels Program, July 1 to September 30, 1968," LA-4073-MS, Los Alamos Scientific Laboratory (1968).
3. "Quarterly Status Report on the Advanced Plutonium Fuels Program, October 1 to December 31 1968," LA-4114-MS, Los Alamos Scientific Laboratory (1969).
4. W. W. Little, Jr. and R. W. Hardie, "2DB, a Two-Dimensional Diffusion-Burnup Code for Fast Reactor Analysis," BNWL-640, Battelle Northwest Laboratory (1968).
5. W. W. Little, Jr. and R. W. Hardie, "2DB User's Manual," BNWL-831, Battelle Northwest Laboratory (1968).
6. "Liquid Metal Fast Breeder Reactor Design Study (1000 MWe  $\text{UO}_2\text{-PuO}_2$  Fueled Plant)," GEAP-4418, General Electric (1963).

PROJECT 471

OTHER ADVANCED SYSTEMS - RESEARCH AND DEVELOPMENT

Person in Charge: D. B. Hall  
Principal Investigator: G. H. Best

I. PULSED REACTOR NEUTRONICS (G. C. Hopkins)

In a repetitively pulsed neutron facility excited by some form of accelerator, it is desirable to have the maximum neutron intensity compatible with pulse width requirements for high resolution. Several combinations of parameters were investigated, including the addition of synchronously pulsed reactivity.

The basic reactor system under study is a small fast assembly fueled with either  $^{239}\text{Pu}$  or  $^{233}\text{U}$ . The relationship of the pulse characteristics is shown graphically in Fig. 471-1, and typical values of reactor and pulse parameters are listed in Table 471-I, where  $\Lambda$  is the neutron generation time,  $k_1$  is the reactivity during the pulse,  $k_2$  is the off-pulse reactivity,  $t_p$  is the pulse width,  $T$  is the cycle duration,  $(S/N)_n$  is the ratio of the maximum to the minimum values of the neutron density,  $(S/N)_p$  is the ratio of the average pulse power to the average background power, and peak  $n$  is the peak neutron density.

For simplicity, the monoenergetic point kinetics equations were used, with six delayed neutron groups, but neglecting feedback. This program produces survey comparisons of responses resulting from

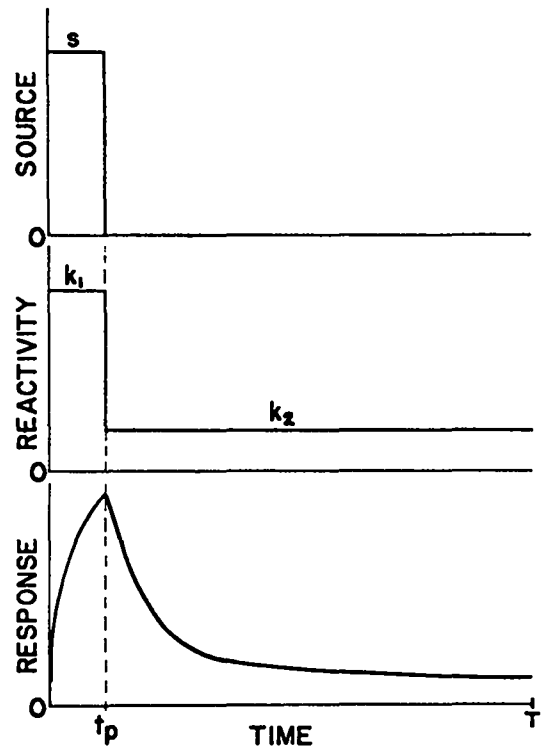


Fig. 471-1. Relation of input source pulse, reactivity pulse, and neutron output.

various combinations of parameters, in a short amount of computing time.

TABLE 471-I  
PARAMETER VARIATION RESULTS  
( $S = 1 \times 10^{17}$  neutrons/sec)

Fuel	$\Lambda$ ( $10^{-9}$ sec)	$k_1$	$k_2$	$t_p$ ( $10^{-6}$ sec)	$T$ (sec)	$(S/N)_n$	$(S/N)_p$	Peak $n$	
$^{239}\text{Pu}$	5.0	0.990	0.990	5.0	0.005	5,056	2954	$4.1 \times 10^{10}$	
		0.990	0.980			10,618	7187	$4.1 \times 10^{10}$	
		0.999	0.990			6,305	2920	$1.6 \times 10^{11}$	
		0.980	0.980			13,373	7137	$1.6 \times 10^{11}$	
		0.990	0.990			26,248	575	$7.5 \times 10^{10}$	
$^{233}\text{U}$	6.0	↓	↓	1.0	0.001	5,247	406	$7.5 \times 10^{10}$	
				1.0		0.005	6,410	2694	$1.8 \times 10^{11}$
				5.0		6,481	2328	$2.3 \times 10^{11}$	
	6.0	↓	↓	↓	↓	4,718	2129	$1.6 \times 10^{11}$	

The Laplace transform-residue method was used to obtain the time-dependent neutron response, after first noniteratively calculating the initial conditions, since there were no steady-state conditions.

For cases involving only step changes in the reactivity and source, the kinetics equations applicable over that portion of each cycle where  $\rho$  and  $\bar{S}$  are constant are

$$\frac{dN(t)}{dt} = \frac{\rho - \beta}{\Lambda} N(t) + \sum_i \lambda_i C_i(t) + \bar{S} \quad (1)$$

and

$$\frac{dC_i(t)}{dt} = \frac{\beta_i}{\Lambda} N(t) - \lambda_i C_i(t), \quad (2)$$

where the standard nomenclature applies.

Since  $\rho$  and  $\bar{S}$  change only once during the cycle, only two sets of Eqs. 1 and 2 are required, with the end values from the first portion of each cycle serving as the initial values for the second portion.

Applying the Laplace transform to Eqs. 1 and 2 results in the following equation set for the first portion of the cycle,  $t = 0$  to  $t = t_p$ ,

$$a_1 N_0 + \sum_i b_i C_i^0 + S_1 = N_0^i \quad (3)$$

$$d_i N_0 + \sum_j e_{ij} C_j^0 + S_i^i = C_i^{0'} \quad (4)$$

where

$$a_1 = \sum_{i=1}^8 \frac{r_i \prod_{j=1}^6 (r_i + \lambda_j)}{\prod_{j \neq i}^8 (r_i - r_j)} e^{r_i t_p} \quad (5)$$

$$b_j = \sum_{i=1}^8 \frac{r_i \lambda_j \prod_{k \neq j}^6 (r_i + \lambda_k)}{\prod_{k \neq i}^8 (r_i - r_k)} e^{r_i t_p} \quad (6)$$

$$S_1 = \sum_{i=1}^8 \frac{\bar{S} \prod_{j=1}^6 (r_i + \lambda_j)}{\prod_{j \neq i}^8 (r_i - r_j)} e^{r_i t_p} \quad (7)$$

$$d_i = \frac{\beta_i}{\Lambda} \sum_{j=1}^9 \frac{r_j \prod_{k=1}^6 (r_j + \lambda_k)}{\prod_{k \neq j}^9 (r_j - r_k)} e^{r_j t_p} \quad (8)$$

$$e_{ik} = \frac{\beta_i}{\Lambda} \sum_{j=1}^9 \frac{r_j \lambda_k \prod_{m \neq k}^6 (r_j + \lambda_m)}{\prod_{m \neq j}^9 (r_j - r_m)} e^{r_j t_p} + \delta_{ik} e^{-\lambda_i t_p} \quad (9)$$

$$S_i^i = \frac{\beta_i}{\Lambda} \sum_{j=1}^9 \frac{\bar{S} \prod_{k=1}^6 (r_j + \lambda_k)}{\prod_{k \neq j}^9 (r_j - r_k)} e^{r_j t_p} \quad (10)$$

and the  $r_i$  are the roots obtained from the characteristic equation of the system matrix of the Laplace transformed Eqs. 1 and 2.  $N_0^i$  and  $C_i^{0'}$  are the values of the neutron density and precursors, respectively, at  $t = t_p$ .

An equation set similar to Eqs. 3 through 10 exists for the second portion of the cycle,  $t = t_p$  to  $t = T$ , with  $N_0$  replaced by  $N_0^i$ ,  $C_i^0$  by  $C_i^{0'}$ , and  $t_p$  by  $(T - t_p)$ . The resulting two sets of simultaneous equations are then solved for  $N_0$  and  $C_i^0$ . The time-dependent response is obtained from Eqs. 3 and 4, using desired values of  $t$  in place of  $t_p$ .

Some of the results obtained, seen by comparing cases in Table 471-I, are:

1. Synchronously adding reactivity in phase with source pulse improves the peak  $n$  by a factor of 4, decreases  $(S/N)_p$  by about 2%, and increases  $(S/N)_n$  by about 25%.
2. Achieving an even lower reactivity during off-pulse considerably improves the S/N ratios.

3. Decreasing  $t_p$  results in a substantial increase in  $(S/N)_n$ , but at the expense of a decreased  $(S/N)_p$  and peak  $n$ .
4. A shorter generation time slightly increases  $(S/N)_p$  and slightly decreases  $(S/N)_n$  and peak  $n$ .
5. Although shorter generation times are possible with  $^{233}\text{U}$ ,  $^{239}\text{Pu}$  gives better S/N ratios and peak  $n$ .

These survey results can aid the experimenter in determining specifications based on his particular design requirements.

## II. $^3\text{He}$ ACTIVATION (D. M. Holm, W. M. Sanders, B. K. Barnes)

### A. General

Carbon and oxygen impurities in high-purity materials are being studied by means of charged-particle activation and spectroscopy. These impurities are of interest because of the effect they have on the properties of the materials. In addition, for crystalline materials, charged-particle channeling gives information about the location of the impurities in the crystal structure.

Before the impurities in the body of the material can be studied, it is necessary to determine their amounts on the surface and how to remove them or distinguish them from impurities in the body. A method of abrading and etching the samples before bombardment has been developed which is very effective in cleaning off the surface contaminants. Work on charged-particle channeling has started.

In order to calibrate the results on surface contaminants, surface films of oxygen on tantalum were studied. Anodizing of tantalum provides surface oxygen films of controlled and known thickness. The thickness of the surface layer varies directly with the anodizing voltage.<sup>1</sup>

### B. Current Results

The study of body oxygen and carbon by observing protons from the  $^{12}\text{C}(^3\text{He},p)^{14}\text{N}$  and  $^{16}\text{O}(^3\text{He},p)^{18}\text{F}$  reactions has been very successful. A preliminary problem was separating the reaction protons from the Coulomb-scattered  $^3\text{He}$  particles. Figure 471-2 shows a charged-particle spectrum taken at  $160^\circ$  with a surface barrier semiconductor detector with 8-MeV

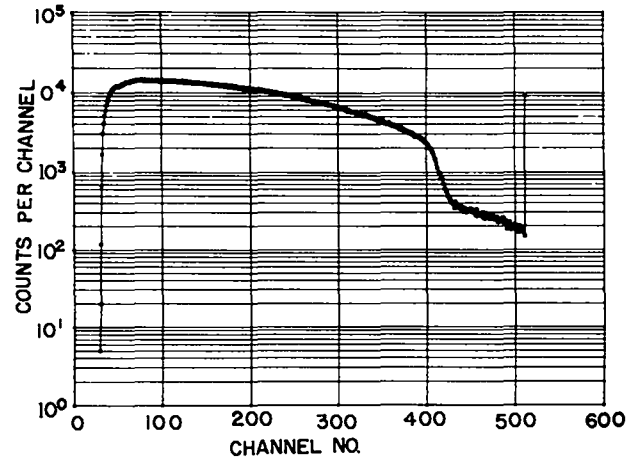


Fig. 471-2. Charged-particle spectrum with 8-MeV  $^3\text{He}$  particles incident on an anodized tantalum target.

$^3\text{He}$  particles incident on an anodized tantalum target. All features of interest are washed out by the large number of  $^3\text{He}$  particles Coulomb scattered by the tantalum. The elastically backscattered  $^3\text{He}$  ions can be degraded in energy below the electronic thresholds by placing absorber foils between the detector and the target. With a suitable absorber, only the less ionizing protons from the  $(^3\text{He},p)$  reactions have sufficient energy after traversing the foils to be recorded by the detector system.

Figure 471-3 is a spectrum made under the same conditions as Fig. 471-2, but with a 0.001-in. aluminum foil in front of the detector to screen out the scattered  $^3\text{He}$  particles; the large count rate at low energies is due to  $^3\text{He}$  particles. Figure 471-4 is

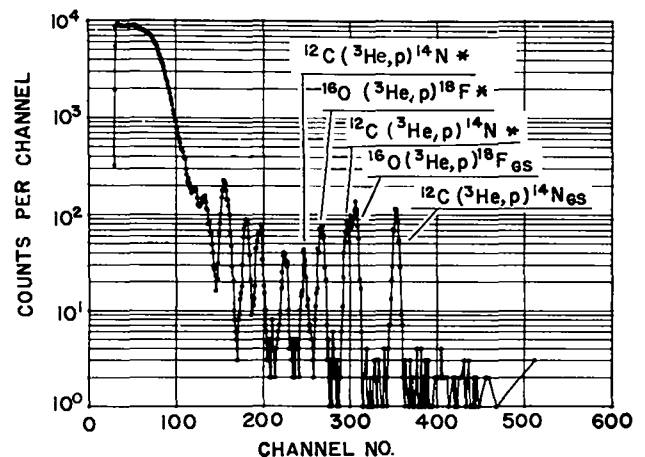


Fig. 471-3. Charged particle spectrum with 8-MeV  $^3\text{He}$  particles incident on an anodized tantalum target, with a 0.001-in. aluminum foil in front of the detector.

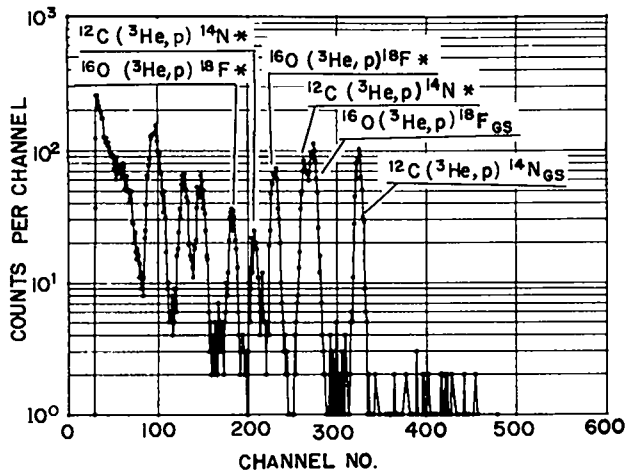


Fig. 471-4. Charged-particle spectrum with 8-MeV  $^3\text{He}$  particles incident on an anodized tantalum target, with two 0.001-in. aluminum foils in front of the detector.

similar, but with two 0.001-in. foils in front of the detector; the  $^3\text{He}$  count rate is significantly reduced. It is clear that the scattered  $^3\text{He}$  particles can readily be absorbed, leaving a good spectrum of the high-energy protons produced in the nuclear reactions.

Figure 471-5 shows a charged-particle spectrum from an anodized tantalum target bombarded by 6.5-MeV  $^3\text{He}$  particles. This target was anodized at 40 V. The tantalum discs were anodized at voltages up to 160 V in a dilute  $\text{H}_2\text{SO}_4$  solution, after being bright dipped in a solution consisting of 55 parts 95%  $\text{H}_2\text{SO}_4$ , 25 parts 70%  $\text{HNO}_3$ , and 20 parts 48% HF. Extrapolation of available data<sup>1</sup> indicates that anodizing at 40 V gives a surface layer of  $84 \mu\text{g}/\text{cm}^2$  oxygen.

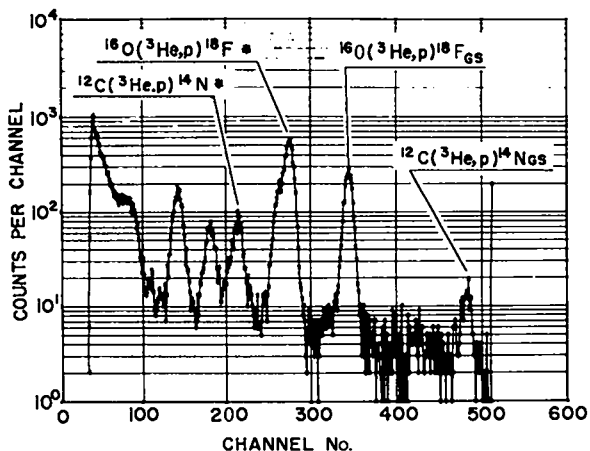


Fig. 471-5. Charged-particle spectrum from an anodized tantalum target bombarded by 6.5-MeV  $^3\text{He}$  particles.

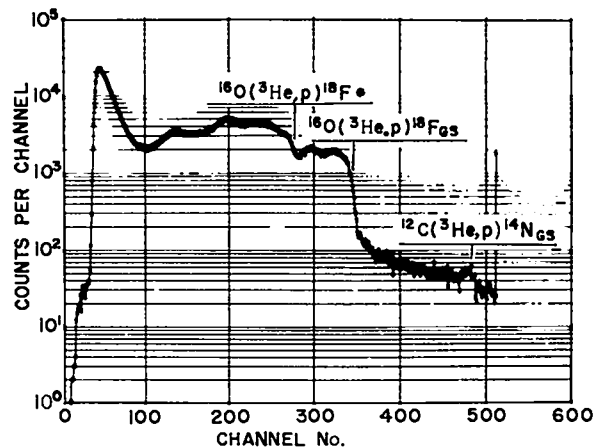


Fig. 471-6. Charged-particle spectrum from a thick tantalum oxide target bombarded by 6.5-MeV  $^3\text{He}$  ions.

The charged-particle spectrum of Fig. 471-6 is similar to that of Fig. 471-5, but it was obtained from a tantalum oxide target thicker than the range of the 6.5-MeV  $^3\text{He}$  ions. It is believed that some of the additional peaks that appear in Fig. 471-6 are caused by resonances in the oxygen cross section. Therefore, the excitation function (cross section versus  $^3\text{He}$  energy) is being measured to determine these resonances. It is important to know this excitation function so that erroneous results will not be obtained by irradiating a sample at a resonance energy.

Figure 471-7 is a charged-particle spectrum from a semiconductor detector as obtained during bombardment of a germanium sample which had been exposed to the atmosphere for about five months and had no surface treatment prior to irradiation. Significant full-energy proton peaks are seen from

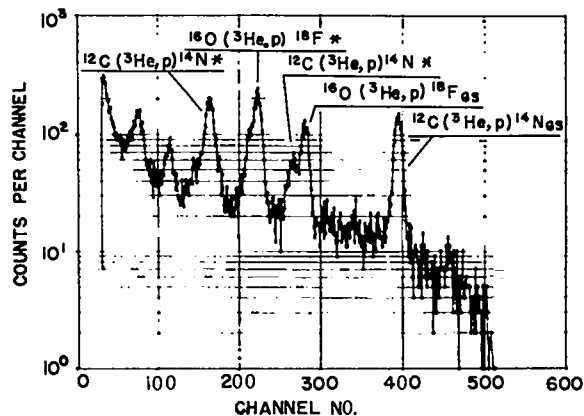


Fig. 471-7. Charged-particle spectrum obtained during bombardment of a germanium sample with no surface treatment.

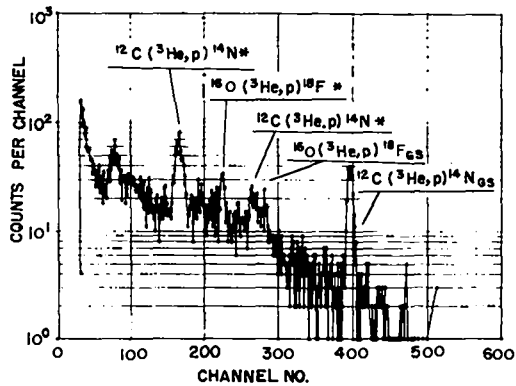


Fig. 471-8. Charged-particle spectrum obtained during bombardment of a germanium sample after lapping and etching.

carbon and oxygen activations. Figure 471-8 is a similar charged-particle spectrum from the same sample after lapping and etching with CP-4 acid etching solution (3 parts  $\text{HNO}_3$  and 1 part HF). A 95% reduction in activity was obtained after this treatment. The spectrum in Fig. 471-8 was taken with four times as much integrated beam as that in Fig. 471-7.

Surface contaminants can be removed from germanium crystals by abrading and etching. The samples are neutralized with water after each etch, and some of the water remains on the germanium. To remove the water prior to irradiation, the samples are placed in a high-vacuum system for up to one hour following the water wash.

#### REFERENCE

1. F. Kover and M. J. Musselin, Thin Solid Films **2**, 211 (1968).

SPECIAL DISTRIBUTION

Atomic Energy Commission, Washington

Division of Research

D. K. Stevens

Division of Naval Reactors

R. H. Steele

Division of Reactor Development and Technology

L. J. Colby

G. W. Cunningham

D. E. Erb

Nicholas Grossman

W. H. Hannum (2)

K. E. Horton

J. R. Humphreys

R. E. Pahler

J. M. Simmons (2)

E. E. Sinclair

Bernard Singer

C. E. Weber

G. W. Wensch

M. J. Whitman

Division of Space Nuclear Systems

G. K. Dicker

F. C. Schwenk

Idaho Operations Office

DeWitt Moss

Ames Laboratory, ISU

O. N. Carlson

W. L. Larsen

M. Smutz

Argonne National Laboratory

F. G. Foote

Sherman Greenberg

J. H. Kittel

W. B. Loewenstein

R. E. Machery

M. V. Nevitt

Idaho Falls, Idaho

D. W. Cissell

R. C. Robertson

Atomics International

R. W. Dickinson, Director (2)

Liquid Metals Information Center

J. L. Ballif

Babcock & Wilcox Co.

C. Baroch

J. H. MacMillan

Battelle Memorial Institute

D. L. Keller

S. J. Paprocki

Brookhaven National Laboratory

D. H. Gurinsky

C. Klamut

Combustion Engineering, Inc.

S. Christopher

Donald W. Douglas Laboratories

R. W. Andelin

General Electric Co., Cincinnati, Ohio

V. P. Calkins

General Electric Co., Sunnyvale, California

R. E. Skavdahl

Gulf General Atomic, Inc.

E. C. Creutz

Idaho Nuclear Corporation

W. C. Francis

IIT Research Institute

R. Van Tyne

Lawrence Radiation Laboratory

Leo Brewer

J. S. Kane

A. J. Rothman

LMFBR Program Office

Alfred Amorosi

D. K. Butler (Physics)

L. R. Kelman (Fuels & Materials)

J. M. McKee (Sodium Technology)

Mound Laboratory

R. G. Grove

NASA, Lewis Research Center

J. J. Lombardo

Naval Research Laboratory

L. E. Steele

Oak Ridge National Laboratory

G. M. Adamson

J. E. Cunningham

J. H. Frye, Jr.

C. J. McHargue

P. Patriarca

O. Sisman

M. S. Wechsler

J. R. Weil

Pacific Northwest Laboratory

F. W. Albaugh

E. A. Evans

V. J. Rutkauskas

W. R. Wykoff

FFTF Project

E. R. Astley

B. M. Johnson

D. W. Shannon (2)

U. S. Department of Interior

Bureau of Mines, Albany, Oregon

H. Kato

United Nuclear Corporation

A. Strasser

Westinghouse, Advanced Research Division

E. C. Bishop

Westinghouse, Bettis Atomic Power Laboratory

E. J. Kreigh